Fundamental Excitations of Nonconservative Quantum Fluids

Samuel Norman Alperin

Department of Applied Mathematics and Theoretical Physics

University of Cambridge

Supervisor: Prof. Natalia G. Berloff

This dissertation is submitted for the degree of

Doctor of Philosophy

Christ's College July 2021

Declaration

I hereby declare that except where specific reference is made to the work of others, the contents of this dissertation are original and have not been submitted in whole or in part for consideration for any other degree or qualification in this, or any other university.

Samuel Norman Alperin

July 2021

Fundamental Excitations of

Nonconservative Quantum Fluids

Samuel Norman Alperin

Abstract

The study of Bose-Einstein condensates (BECs) has represented a core subject of physics for decades. Recently however, experiments have demonstrated a fundamentally distinct, inherently nonequilibriated class of BEC from photonic quasiparticles known as exciton-polaritons (polaritons). These photonic condensates are free to gain or lose energy as a part of their dynamics, and are thus not constrained to tend towards thermodynamic equilibrium. This greatly increases their pattern forming capabilities, but in turn severely complicates their theoretical treatment. The dynamical theory of these nonconservative condensates is an emerging field which resides at the intersection of the theories of nonequilibrium pattern formation, nonlinear wave dynamics and condensed matter theory. In this thesis I describe several contributions to this theory of *nonconservative* quantum hydrodynamics, and towards the argument that it truly represents a paradigmatic departure from the now mature theory of equilibrium quantum hydrodynamics.

The polariton is formed in an optical cavity: cavity photons excite and superpose with excitons in a solid state sample to form bosonic light-matter quasiparticles. However, photons are trapped in the cavity for finite times, and are thus continually lost. A key characteristic of the polariton condensate is thus that to be created or sustained, they must be fed by an optical pump, which can take on any incident geometry, and which can be resonant or nonresonant with the natural frequency of the optical cavity. As a result, understanding the dynamical and structural implications of different forcing scenarios is fundamentally important for these systems, and exploring these scenarios is a major theme of this work.

In the first part of the thesis I focus on the role of pumping geometry on the dynamical behaviours and structural forms that can emerge. First, I show that an annular pumping geometry can lead to the spontaneous formation of stable multiply charged vortices, fundamental topological structures which have long been sought but are understood to be dynamically unstable even when imprinted and externally trapped in equilibrium BECs. The spontaneous formation is shown to come from the excitation of ring dark solitons in the early condensation, which are in this scenario dynamically unstable to breakup into vortices. I then show how the closed geometry of the forcing causes the stable binding of like-signed vortices via particle flux forces. It is shown that the topological charge limit on a multiply charged vortex formed this way is set by a Kelvin-Helmholtz instability, the first example of such an instability in a nonconservative condensate system. The acoustic properties of the multiply charged vortex are also considered, as they are found to emit topological charge dependent density waves. Links to analogue gravity and the process of quasinormal ringing are made.

I then elucidate the importance of the temporal symmetries imposed by the pump forcing. In particular, I show that the combination of non-resonant and resonant forcing generically leads to a fundamental breathing behaviour resulting from frustration between the incommensurate $\mathrm{U}(1)$ phase symmetry of nonresonant forcing and the $\mathbb{Z}_n$ symmetry of n^{th} order resonant forcing. The most severe frustration is that between the $\mathrm{U}(1)$ and $\mathbb{Z}_2$ symmetries, a case which I thus give special attention. In particular, I introduce a new solitary structure in this regime,

a breathing ring dark soliton which represents a fundamental localized excitation of the extended condensate under this maximal phase frustration, forming spontaneously during the condensation process in a nonequilibrium analogue of the Kibble-Zurek mechanism. I also study the instability of vortices in this regime, which I show are unstable to self-slicing into dark solitons (Ising domain walls), the opposite transformation known to equilibria condensates, in which dark solitons are unstable to breakup into vortices via snake-instability. I then study the pattern forming abilities in a condensate with a radially dependent degree of phase-bistability, introducing a family of breather patterns which spontaneously break rotational symmetry in favor of polygonal spatial symmetries, the order of which can be tuned.

Finally, the inherent nonequilibration of the polariton condensate makes it a natural setting to consider the problem of turbulence. I introduce a process by which tuning the distances between a grid of pump spots allows for the formation of a nondecaying turbulent state of tunable average inter-vortex spacing. I show that this allows for the continuous tuning of quantum turbulence from the well known regime of superfluid turbulence (well separated vortices) into that of strong turbulence (separation of the order of a healing length), and into the theoretical regime of quantum weak turbulence, in which vortices have mean separations below the healing length and cores become destructured. I also discuss the possibility of observing the signatures of turbulence in polariton condensate experiments.

Acknowledgements

I am eternally grateful to Prof. Natalia Berloff for being such a wonderful supervisor, whose expertise and support have been invaluable. From the bottom of my heart I thank my family, who had to survive all of my childhood science experiments. Finally, I acknowledge Rebecca for her emotional support, as well as for always providing candid stylistic criticisms of my figures.

With all my love, for R.

Table of contents

List of figures

Chapter 1

Preliminaries

1.1 Introductory Remarks

As far as can be told, everything we experience can be described by fundamental quantum particles. These are divided into two classes, fermions and bosons. While no two fermions are able to occupy the same quantum state, bosons have no such restriction. Nearly a century ago, based on the quantum statistical theory Bose and Einstein predicted a special state of bosonic gases. This *condensate* phase would occur when the gas is cooled so that the bosons simultaneously occupy the ground state, so that the macroscopic many-particle quantum system becomes spontaneously coherent and can be described by a single effective wavefunction. Since the first successful experimental creations of Bose-Einstein condensates (BECs) from atomic vapours a quarter-century ago, the field has exploded into a major component of contemporary physics research. Due to their macroscopic exhibition of quantum phenomena they have allowed for the creation and probing of new physical regimes, as well as the engineering of macroscopic physical simulations of atomic-scale quantum many body processes [1].

Given the importance of BECs to physicists as a tool used to study and engineer quantum systems, in addition to the inherent interest in their fundamental physics, there is a large and varied literature focused on their fundamental excitations. While much BEC related research takes place in the regime in which quantum fluctuations play an important role [2], there is also a huge interest in the hydrodynamical regime, in which the mean field theory applies and the BEC can be modelled by a semiclassical field equation. In particular, a great deal of effort has gone into the discovery and characterisation of self-localized excitations such as quantized vortices. While still an intensely active area of research, this field has over the years reached a stage of maturity.

Their is a current trend in condensed matter physics intent on moving the scope of our understanding beyond near-equilibrium physics. This has required paradigmatic shifts in our thinking, but continues to promise correspondingly weighty rewards. In the context of quantum gases, this has been represented by the experimental achievement of the condensation of the inherently far-from-equilibrium quasiparticle excitations of solid state photonic systems. These fundamentally distinct condensates do not conserve particle number, instead gaining and losing particles as a part of their complicated dynamics. This thesis presents some contributions to the theory of the hydrodynamics of these nonconservative quantum fluids, and introduces some fundamental excitations which are novel to such systems.

The purpose of this introductory chapter is to familiarize the reader with the context out of which the central motivations and methods of this work have emerged. I thus begin with a brief discussion of dilute *equilibrium* BECs. Besides contextualizing the history of BEC research, this serves two purposes. First, the equilibrium BEC is a much simpler system in which to introduce some important concepts. Second, a review of equilibrium BEC phenomena serves as a foil against which we will introduce nonequilibrium phenomena.

I will then provide an introduction to the physics of exciton-polariton condensates, the prototypical physical case of the nonconservative quantum fluid. These are condensates of hybridized light-matter which live inside of optical cavities. These BECs are characterized by a strange combination of properties stemming from both constituents, and really represent an *interstitial* physical regime, residing somewhere between the limiting behaviours represented the equilibrium BEC on the one side, and on the other the highly nonequilibriated pattern-forming systems seen in nonlinear optical cavities. According to the intuition gained from the literature on atomic BECs, some of the behaviours that I will discuss in polaritonic BECs may seem counterintuitive at first, but I hope to make clear throughout this work that they are not actually so counterintuitive when viewed from the perspective of classical optics.

Following this introductory chapter, the thesis structured in the following way.

In Chapter 2 I address the problem of breathers in exciton-polariton condensates. Specifically, I introduce two classes of solitonic breathers, which are shown to naturally emerge from systems fed by both resonant and nonresonant forcing. The first class is of annular breathers which may form spontaneously in homogeneous condensates and which are solitonic in the typical sense, being self-localized and free to move about in response to interactions. The second excitations are pinned, but exhibit spontaneous rotational symmetry breaking into polygon-symmetric breathers, which makes for the emergence of a naturally quantized rotational degree of freedom. These fundamental, localized breathers are important examples of the types dynamical structures which cannot exist in an equilibrium quantum fluid. This chapter is made from the (reordered) combination of two articles, one published as a rapid communication in Phys. Rev. A [3] and one currently under review at Phys. Rev. Lett [4].

In Chapter 3 I show that multiply charged vortices are a natural topological excitation of the exciton-polariton condensate, when spatially separated from the forcing which sustains it. The multiply charged vortex is a structure which has long been sought in quantum fluidic systems, but without much success: in an equilibrium BEC the multiply charged vortex is dynamically unstable. The properties of these new structures are then studied. Interestingly, I show that their maximum vorticity is limited by a Kelvin-Helmholtz instability, a textbook instability in classical and quantum fluid dynamics which had not yet been observed in a nonconservative system. This chapter represents the results of an article published in Optica [5].

In Chapter 4 I will discuss turbulent systems of many vortices. Turbulence has not yet been observed in any polariton condensate experiments; with numerical experiments I will demonstrate two methods of generating turbulence in such a system, and show that the density of vorticity can be tuned continuously into the theoretical regime of weak quantum turbulence. I will also discuss some unpublished experimental results from Dr. Daniele Sanvitto and his Advanced Photonics Group in Lecce, which I argue show the signatures of turbulence.

1.2 Condensation of Dilute Bose Gases

1.2.1 A Rough Sketch

Fermions, the class of particles having half-integer spin, are antisymmetric under the operation of particle exchange, and no two of these particles may occupy the same quantum state. Bosons, which have integer spin and are symmetric under such exchanges, have no such restriction and may share occupation of the same state. Thus at low temperatures, the ground state can in theory be shared by many or all of the constituent particles.

At higher temperatures, these quantum effects have vanishing effect on the statistical behaviour of a dilute gas. For an intuitive idea of this, it is helpful to refer to the matter-wave picture of de Broglie. The de Broglie wavelength λ_{dB} of a particle of mass m at temperature T is written as

$$\lambda_T = \sqrt{\frac{2\pi\hbar}{mkT}} \tag{1.1}$$

where k is the Boltzmann constant and $\hbar$ the Planck constant. At nonvanishing temperatures and atomic masses this lengthscale is microscopic, so that the constituent bosons are well described as classical point-particles. As an order-of-magnitude calculation, we would then expect the onset of any quantum effects to occur when the temperature of the gas is lowered such that the lengthscale of the de Broglie matter-waves become comparable to the lengthscale of the interparticle spacing. In this case the individual wavefunctions, all (or in part for finite temperatures) sharing the ground state and overlapping in space may become spontaneously coherent.

This estimate of the transition temperature turns out to be fairly good, and for typical alkali gas experiments this temperature is on the order of 100nK. This is *very* cold, in fact colder than interstellar space, but is achievable in experiments via a combination of laser and evaporative cooling. Though is exists in different iterations, the most common version of laser cooling works by trapping the gas with lasers incident from all directions, which are redshifted from the peak absorption frequency of the particles. Thus due to the Doppler effect, the chance of absorption is increased when a particle is moving against the propagating optical field. Invoking the geometry of the laser trap, it is clear that every particle motion is counter to a field, and thus the particle motions are, on average, reduced, reducing the temperature. The development of this technique was a major technical achievement, which was acknowledged by the 1997 Nobel prize in Physics. The evaporate cooling in turn works by allowing the higher-energy particles to leak from the trap, lowering the average energy of the system.

The details of these cooling processes are not, themselves, important for the subject of this thesis, nor are the absolute temperatures of the condensation of alkali gases. However, it is important to provide the reader with an idea of the experimental challenges involved in the creation and study of a BEC of atomic gases, if not to inspire tremendous respect for those who do such experiments, then to provide some idea of experimental constraints; coaxing bosonic gases into the BEC phase is difficult enough without fancy trapping geometries, etc.

The other significant point made so far, for our purposes, is the relationship between the mass of the condensing particles and the BEC transition temperature. Soon we will discuss bosonic quasiparticles with ultralight effective masses, which then allows for condensation to take place at temperatures approaching room temperature.

1.2.2 Mean Field Theory

The quintessential, perhaps *defining* property of a quantum fluid is its ability to be described macroscopically by a classical field (the so called *mean field*.) In such a treatment, the physics occurring at lengthscales smaller than that of the mean inter-particle spacing are lumped together (or more properly *integrated out*) into an effective long-wavelength interaction. This process thus takes an unapproachably high-dimensional quantum many-body problem and replaces it with a classical field. The fact that this works for a particular system is not trivial. Formally, the mean field approximation works well when the lengthscale of the microscopic interactions is much smaller than that of the mean interparticle spacing, so that the interparticle interactions can be treatable as delta functions when viewed from the lengthscale of the ensemble. In typical dilute alkali gases used in the laboratory, the scattering lengths are indeed significantly smaller than the average interparticle spacings, while temperatures can be lowered such that the lengthscale of the de

Broglie matter-wavelengths are comparable to the interparticle spacing. Thus the mean field treatment is well justified here, and indeed works extraordinarily well.

A fairly intuitive derivation of the mean field equation of the BEC of typical dilute alkali gases turns out to be reasonably simple, and quite robust because of the conditions given above. However, the derivation is more a matter of technical machinations than it is worth for the purposes of this thesis, which as we will discuss later is based on less rigorously supported phenomenological models. Here we are more interested in the dynamical phenomena which *follow* from the form of the mean field equation, we will simply state the result of the mean field treatment of the dilute atomic BEC, the famous Gross-Pitaesvkii equation (GPE). For the reader interested in the derivation, I recommend the pedogogical treatment presented by [6]. For those left unsatisfied by a "physics proof", there is the much longer but mathematically rigorous derivation of Lieb and colleagues [7], which proves that the GPE indeed follows asymptotically from first principles.

Interestingly, the Gross-Pitaesvkii equation was first developed as a mean field description of superfluid helium, a system which is by no means dilute. Superfluid ^{4}He was understood very early on to have to do with Bose-Einstein condensation (the isotope ^{4}He is bosonic). However, the liquid helium is very far from our diluteness condition of the mean field theory, and due to the nature of the strong interactions between helium atoms, even at very low temperatures the condensate fraction tends to be quite low. Despite the Gross-Pitaevskii equation originating as a model for helium, it is much more theoretically justified as a model for dilute, *weakly interacting* condensed gases; all in all, helium represents a much more theoretically difficult problem, as the microscopic degrees of freedom are not so willing to be integrated out.

Only a few years after the experimental achievement of alkali gas BECs by the Boulder and MIT groups, the soon-to-be Nobel laureate Anthony Leggett wrote about the relationship between the dilute BEC and superfluid helium [1], making clear that the two represent entirely different physical regimes despite their common underlying physics [8]. While superfluid helium represents the historical *beginning* of the field of quantum fluid dynamics, the *direct* historical and *conceptual* precursor to the subject of this thesis is the weakly interacting condensate of dilute gases. Thus there will be no review of helium here, and every mention of the equilibrium BEC should be read to refer to that of dilute gases.

Without further ado, the time dependent GPE of a BEC trapped with external potential $V(\mathbf{r})$, particle mass m, and effective particle-particle interaction strength g takes the form

$$i\partial_t \Psi(\mathbf{r},t) = \left(\frac{\hbar^2}{2m}\nabla^2 + V(\mathbf{r}) + g|\Psi(\mathbf{r},t)|^2\right)\Psi(\mathbf{r},t) \tag{1.2}$$

where we denote $\partial_t = \frac{\partial}{\partial t}$, and write the Laplacian operator as ∇^2 (these notations will remain consistent throughout).

This might seem to be a extraordinarily simple equation for such a complex physical scenario, with very many microscopic degrees of freedom having been integrated out. However, this simple equation has stood up against what is now a quarter century of experimental data probing a range of macroscopic dynamical phenomena, from vortex structure and soliton instabilities to traped cloud profiles [**?**]. Indeed, the hydrodynamic regime of the the dilute BEC is well described by the GPE, and while other interesting physical regimes can and are probed, their hydrodynamics represents a large and significant component of the nature of these condensates. Some have actually found the high degree to which experiments tend to match the GPE to be surprising. Leggett, only a few years after the Boulder/MIT experiments gave the opinion that the robustness of the GPE seemed to be *too* good and must have to do with some unknown symmetry related to the harmonic

[1] The essay of Leggett presents a wonderfully written historiography of quantum fluid physics, and is worth reading.

trapping typically used in experiments [8]. As time has gone on however, other trapping geometries have been engineered without apparent anomalies. Regardless of whether or not there may exist some yet-to-be-known quantum anomaly in some extreme yet-to-be-probed regime, it remains true that the GPE represents an excellent description of a large physical regime and captures a great deal of important physics. We will see later that much of the GPE and its physics is actually quite generic, and has applications far beyond BECs, which given its erasure of any structural distinctions in the short-wavelength physics, should not be entirely surprising.

1.2.3 Dark and Grey Solitons

We begin by considering the form of the condensate density profile near an infinite wall potential, which tends to uniformity away from the wall. At the wall the potential is infinite and the density must vanish, and thus very *close* to the wall the effective particle interaction potential dominates the structure. *Far* from the wall the potential energy is null and the kinetic term dominates. The lengthscale of the transition from the density null to uniformity, called the *healing length*, is thus defined as the lengthscale at which the interaction energy and the kinetic energies are equal. Denoting the healing length as ξ, we can thus write

$$\xi = \frac{\hbar}{\sqrt{2mg}}\rho^{-\frac{1}{2}} \tag{1.3}$$

where we define the condensate density $\rho = |\Psi|^2$. This length is of fundamental importance, representing the shortest distance over which the condensate can "fully vary". This is thus considered the smallest relevant lengthscale in the dynamical theories within the mean field treatment. In experiments this length is typically *significantly* larger than that of the mean interparticle spacing, and thus even at this minimum dynamical lengthscale we do not have to worry about the physical applicability of the mean field treatment.

The exact solution to the density profile of the condensate with one wall boundary follows almost as easily as the determination of its characteristic lengthscale, following the method of [6]. A time-independent solution to the one-dimensional GPE can be written in the form $\Psi(r,t) = \sqrt{\rho(r)}\exp(i\mu t)$, where $\rho(r)$ is the time independent wavefunction density and where we define the chemical potential μ, which is merely the constant of the phase evolution. The one-dimensional, time-independent GPE in Cartesian coordinates is written as

$$\mu\psi(r) = \frac{\hbar^2}{2m}\frac{d^2\psi(r)}{dr^2} + g|\psi(r)|^2\psi(r). \tag{1.4}$$

Obviously, for a uniform condensate profile the differential term of Eq. 1.4 vanishes, so that $\mu = g|\rho_0|$ where ρ_0 is the unperturbed condensate wavefunction density (fully healed). Entering this into Eq. 1.4 we get the second order ordinary differential equation (ODE)

$$\frac{d^2\psi(r)}{dr^2} = \frac{2mg}{\hbar^2}\left(|\psi(r)|^2 - |\rho_0|\right)\psi(r), \tag{1.5}$$

which can be solved exactly by recognizing a first integral, inverse scattering transform methods, or by the Lie algebraic method of similarity transformations [9]. Again defining the wall at $r = 0$ and healing in the positive r direction, the solution can be easily confirmed to take the form

$$\psi(r) = \sqrt{\rho_0}\tanh\left(\frac{r}{\sqrt{2}\xi}\right). \tag{1.6}$$

It is worth noting that this solution also holds when we allow the condensate to heal along both the positive and negative r directions. In this case the result is a density "dip" with width characterized only by ξ, within an otherwise uniform condensate of density ρ_0. However there is also phase structure, with a discontinuity (π phase jump) at the density minimum. Such a solution is thus topological in nature, and given the phase-symmetry of the GPE, is necessary to simultaneously allow for two ground state solutions which have adopted opposite phase, whether by phase imprinting or spontaneously during the condensation process.

This structure is quite fundamental to many systems, and is known under several names which emphasise different aspects of its nature. Emphasising the density zero and qualitatively solitonic character [2] the structure is called a *dark* soliton. Emphasising the phase discontinuity it is called a *kink*, or a *domain wall* as the structure separates two degenerate ground state solutions with opposed phase. While this analytical solution is only exact in the one-dimensional problem, it is an important and fundamental conceptual structure and will be useful in generating the anzatz used in variational methods when tackling more difficult scenarios beyond atomic BECs.

The dark soliton is the simple, stationary case of a more generic class of structures derived in 1971 by Tsuzuki [10]. This wider class of exact solutions includes the so-called *grey* solitons, which are characterized by density depressions which do not reach zero, and which move at a velocity set by both their depth and the healing length. The derivation of the general solution is again more tedious than illuminating for our purposes, so we will just state it. The grey/dark solitons take the form [10, 11]

$$\psi(r) = \sqrt{\rho_0}\left(i\frac{v_{ds}}{c_s} + \sqrt{1-\frac{v_{ds}^2}{c_s^2}}\tanh\left(\frac{r-r_{ds}}{\xi}\sqrt{1-\frac{v_{ds}^2}{c_s^2}}\right)\right). \qquad (1.7)$$

[2] Historically, a self localized structure was only called a soliton if its collisions resulted in unchanged forms, aside from a phase factor. More recently, the terminology has loosened: now just about any self-localized structure is called a soliton. The distinction is important in some contexts, but not here. I will thus conform to the more recent (circa 1990's) literature and call structures solitons which do not meet the historical definition.

denoting the speed of sound in the condensate as $c_s = \sqrt{\frac{\hbar}{\xi m}}$, and the position and constant velocity of the soliton along the r axis as r_{ds} and v_{ds} respectively. It was also shown in the original work of Tzuzuki that the velocity of the grey soliton is simply that of the speed of sound at the density minimum ρ_{ds}, so that

$$\frac{v_{ds}^2}{c_s^2} = \frac{\rho_{ds}}{\rho_0}. \tag{1.8}$$

Thus when deep, the gray soliton moves slowly, tending towards the stationary limit of the dark soliton. Sustained in their localized form by the balance of dispersion and nonlinearity, these are effectively massive and are thus particle-like in nature [6]. However, it can be shown variationally that the effective inertial mass and thus the kinetic energy of the soliton increases as it is slowed/deepened. In this way the soliton has an effectively *negative* mass [10, 12**?**]. In contrast, the shallow soliton approaches the limit of the vanishing density perturbation travelling at the local speed of sound and are thus sound-like in nature.

While these structures represent exact solutions in one dimensional space, this does not generally mean that they are stable, especially in higher dimensional spaces. First, there is the issue of the negative mass: it is more energetically favorable for the soliton to accelerate and become shallow, until reaching the speed of sound at vanishing depth – this is to say that the solitons are unstable to dissipating acoustically. Further, the reader may have noticed that the form of the dark soliton solution given in Eq. 1.6 assumed the realness of the wavefunction. This was without loss of generality: ψ could have been imaginary, or for that matter fixed to any diametric axis in the complex plane. However it is very important to note that unless the wavefunction is continually constrained to that subset of the phase space, perturbations may break the condition. Therefore the dark soliton, which is characterized by a topological defect (phase discontinuity), is not in fact topologically protected, as in the full complex plane the defect may be smoothly mended. In particular, in two dimensions, dark solitons are unstable to the so called *snake instability*, in which they couple to the extra spatial degree of freedom and buckle into pairs of vortices of opposite charge which are linked by a grey soliton; the vortex/antivortex pair may then annihilate while maintaining net topological charge (total vorticity of the system). This process has been studied a great deal in theory and has been observed directly in experiments [13, 14].

Again, these solitons are highly fundamental, and there is a huge literature on them. Much of that literature predates the realization of dilute atomic BECs, having been a very important part of understanding the dynamical phenomena of laser systems. Here the important point is to communicate the basic idea of their structure as well as the difficulties of instability in higher dimensions, which will be important context when we get to the chapter on breathing solitons.

1.2.4 Vortices

The quantization of vorticity in the BEC follows directly from the single valued nature of the wavefunction. This is seen clearly by rewriting the generic wavefunction as the Ψ as the product of an amplitude and a phase term, the so called *Madelung transformation* $\Psi = \sqrt{\rho}\exp(i\phi)$. Inserting the transformed wavefunction into the GPE (Eq. 1.2) and separating real and imaginary terms, we get two equations, and introducing the velocity field as $\mathbf{v} = \frac{\hbar}{m}\nabla\phi$, these are written as

$$\partial_t \rho + \nabla \cdot (\mathbf{v}\rho) = 0 \tag{1.9}$$

$$m\partial_t \mathbf{v} = -\nabla\left(\frac{mv^2}{2} - \frac{\hbar^2}{2m\sqrt{\rho}}\nabla^2(\sqrt{\rho}) + g\rho + V(\mathbf{r})\right). \tag{1.10}$$

The first equation is a statement of continuity, while the second takes a form analogous to the integrated Euler equation of classical fluid dynamics. Due to their fluid-dynamical form, these equations are generally referred to as the *quantum hydrodynamical* form of the GPE [15]. It follows trivially from the scalar form of the velocity potential that for simply-connected[3] velocity field $\mathbf{v}$,

$$\nabla \times \mathbf{v} = \nabla \cdot (\frac{\hbar}{m}\nabla\phi) = 0. \tag{1.11}$$

The field is thus irrotational. This is a deeply fundamental constraint on the dynamics of the quantum fluid, telling us that any rotational flows require phase singularities at which the condensate must vanish such that simple-connectedness is lost. These singularities, about which the phase smoothly cycles by an integer multiple of 2π, are known as quantum vortices. At the vortex singularity, the density necessarily vanishes, making the condensate topologically nontrivial. The topological charge is a conserved quantity in the equilibrium condensate, and thus the individual quantum vortex is protected against dissipation by its topological charge - a vortex must be destroyed by annihilation with a vortex of opposite topological charge.

The density profile of a single quantum vortex in an otherwise uniform condensate is rotationally symmetric, and is thus characterised only by its topological charge and radial structure. Writing the GPE in radial coordinates and inserting the anzats $\Psi(r,\phi) = \sqrt{\rho(r)}\exp(i\ell\phi)$ for topological charge ℓ results in the following equation for the radial amplitude $f = \sqrt{\rho(r)}$

$$f^{''} + \frac{f^{'}}{r} + \left(1 - \frac{\ell^2}{r^2} - f\right) f = 0 \tag{1.12}$$

The solutions are not amenable to being written in closed form, but can be solved numerically, as shown in Fig. 1.1. Alternatively, there has also been work done on Padé approximations for these profiles [16]. We will see an equation very

[3] The property maintaining that any loop in the space can be smoothly contracted to a point.

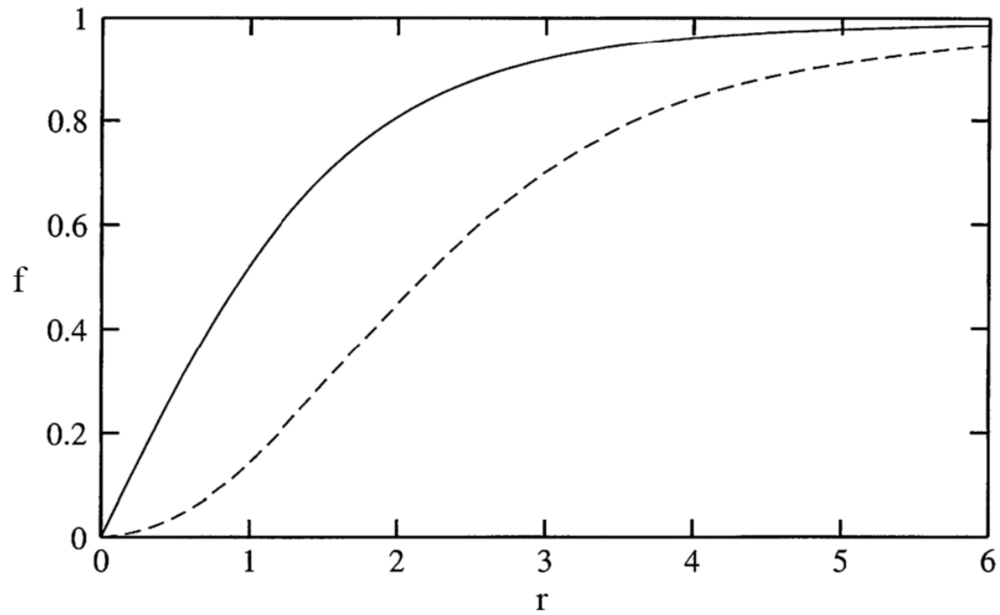

Fig. 1.1 Numerical solution of Eq. 1.12, for $\ell = 1$ (solid) and $\ell = 2$ (dashed). Image from the textbook of Pitaevskii and Stringari [17].

close in form to Eq. 1.12 in the chapter on multiply charged vortices in polariton condensates.

An important quality of the quantized vortex is its reaction to the surrounding fluid flow. From Eq. 1.10 it can be shown that (simply as a potential flow problem) the flows obey Kelvin's theorem and thus there is no drag force in the flow about a body [6]. As a result, the vortex simply travels with the local condensate flow. In a system of two vortices, each moves according to the flows created by the other, resulting in the so-called superfluid Magnus force. Far from the density null at the vortex center, the vortex can be considered as a simple and well defined phase structure without density structure, which generates flows according to the equally simple Biot-Savart law familiar from elementary electrodynamics. However, when vortices are not well separated, the problem becomes much more difficult [18].

While a vortex with unit topological charge has strong protection against dissipation due to the topological charge conservation constraint, a vortex singularity with higher than unit vorticity may indeed break into unit vortices while

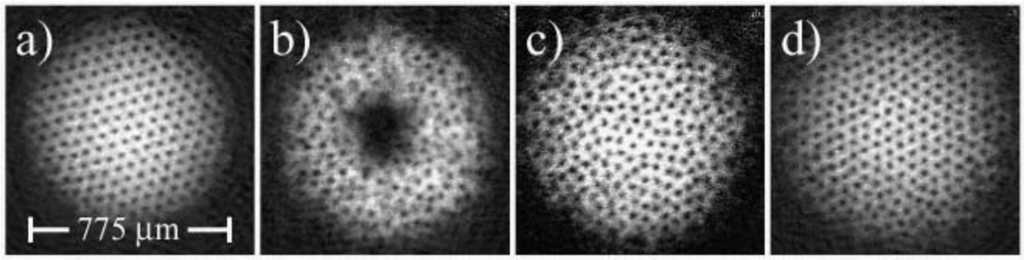

Fig. 1.2 Experimental images of rapidly rotated condensate (a), which is given an evaporative boost in rotation after which some vorticity concentrates (b) until decaying back into the stable lattice configuration (c,d). Image taken from [21].

conserving the topological charge, and thus there is no topological protection against such decay [19–21]. Indeed, multiply charged vortices are energetically unfavorable and dynamically unstable: the typical scenario of a rapidly rotated BEC in a harmonic trap thus involves the formation of the so-called Abrikosov lattice of unit vortices [22]. A great deal of theoretical and experimental work has gone into the hope of forcing the stability of "giant" vortices with higher-than-unit vorticity [23–28]. The best studied approach is that of the BEC in a rapidly rotated trap, where rotation is performed by slightly distorting the trap (by weakly breaking rotational symmetry) and rotating the symmetry axis. Such a process can induce high vorticity in a condensate, with vorticity on the order of hundreds of units in some experiments. However, it has been shown theoretically [23, 24, 29] and supported by direct in experimental observation that in harmonic traps the Abrikosov lattice is always energetically favorable to the concentration of vorticity in a shared, central core [30]. Theory does however predict [23, 24] that in an infinite wall potential, the rapidly rotated condensate in a trap of fixed radius cannot expand to accommodate the Abrikosov lattice of a high enough total vorticity; the condensate instead "creeps up" the wall, concentrating in a ring profile due to the centrifugal force from the rotation. In the limit of very high rotation speeds, the condensate thus tends to an effective ring profile, in which there is no density near the core (thus the problem of higher order vortex stability is circumvented by the condensate not being simply connected in the first place) [31]. While this works in theory, in reality the process is highly nontrivial and only the short-lived, partial concentration of vorticity has been achieved, as shown in Fig. 1.2 [21]. We will discuss this again in the chapter on multiply charged vortices.

1.2.5 Profile in a Trap

The density profile of a condensate in a trap which varies gradually (relative to the healing length) can be solved by making what is known as the Thomas-Fermi approximation. Starting from the stationary GPE and at this point setting units such that $\frac{\hbar}{2m} = 1$, we define the slowly varying external potential V_{ext} and make the Madelung transformation to yield

$$\nabla \cdot (\rho \mathbf{v}) = 0 \tag{1.13}$$

$$\mu = \rho + v^2 + V_{ext} - \frac{1}{\sqrt{\rho}} \nabla^2 \sqrt{\rho}. \tag{1.14}$$

As we have defined the external potential to vary slowly , we expect the condensate density to vary smoothly as well, so that we can neglect the so-called *quantum pressure* term $\frac{1}{\sqrt{\rho}} \nabla^2 \sqrt{\rho}$. We can then solve the problem exactly, with the solution $\rho = \mu - V_{ext}$ for $\mu - V_{ext} \geq 0$ and $\rho = 0$ otherwise, and $\mathbf{v} = 0$. The approximation works very well for the bulk of the condensate, and less well near the edges. Variational methods and asymptotic expansions can show exactly how well this simple solution holds up for a particular external potential (see [6]), but the exact profile of a trapped BEC is not of significant interest here. Rather, it is a nice way of demonstrating that the equilibrium condensate supports nonuniform steady state solutions with zero velocity; this will not be the case for polariton condensates.

1.2.6 Remark on Symmetries

One of the wonderful properties of the Gross-Pitaevskii equation is that it is highly symmetric. The full symmetry group of the GPE in two dimensional space is the Lorentz group SO(2,1) [32]. For the purpose of this thesis, the most important symmetry is that of particle conservation [4]. It is hard to stress how simplifying this assumption is; without restricting the system to tend towards equilibrium a system is much more free in its dynamics. For example, we will see that the spontaneous rotation of nonconservative condensates is allowed by the gain processes of a nonconservative system, and that breathing structures can exist indefinitely. However, while freeing, the nonequilibriation is also complicating: for example while in an equilibrium nonlinear field such as is described by the GPE, solitons may exist via the balance of dispersion and nonlinearity as demonstrated by the exact solutions to the dark and grey solitons problems in 1D. In a nonequilibrium system such as is the subject of this thesis, such structures can only exist when they balance dispersion, nonlinearity, gain, and loss. This makes analytical soliton descriptions difficult at best, especially in more than one spatial dimension.

1.3 Exciton-Polariton Condensates

1.3.1 Exciton-Polaritons

The exciton-polariton condensate is the object of interest in this thesis, and will be introduced here. The "polariton" is actually a *class* of quasiparticles which form when an optical oscillator and a matter oscillator sync through their interactions, so that they become effectively merged into hybrid eigenstates (the polariton) which take on both light-like and matter-like properties. The exciton-polariton is

[4] There have been experiments in which particles are allowed to flow in and out of the system, as in [2, 33], but these are highly-engineered exceptions

thus the superposed excitation of a cavity photon (the optical oscillator) and an exciton (the matter oscillator).

A variety of solid state samples have been used with various properties. However, we will describe the first and most common sample, the semiconductor microcavity. This cavity generally takes on a Fabry-Perot geometry, an optically transparent material sandwiched by two distributed Bragg reflectors (DBRs). These reflectors are photonic crystal heterostructures composed of thin layers of materials with differing refractive indices. These reflectors serve to confine photons which enter the cavity, yielding trapped cavity photons which are two-dimensional and thus have an effective rest-mass (about four orders of magnitude lighter than that of the electron) in the plane in which they are confined. The dispersion relation of the cavity photon takes the form

$$E_{ph}(k_{\|}) = \sqrt{E_{\perp}^2 + \frac{\hbar^2 c^2 k_{\|}^2}{n^2}} \tag{1.15}$$

in which n is the refractive index, and $E_{\perp}$ is the energy of the photon whose propagation axis aligns with the confinement axis, which can be written as $\frac{\hbar c \pi N}{nL}$ where N is the integer cavity mode number and L is the length of the cavity. The transverse wavevector $\mathbf{k}_{\|}$ is the off-axis component of the photon wavevector, and from the form of Eq. 1.15, gives us a sort of effective kinetic energy. Of course, cavity photons cannot remain trapped indefinitely, simply from the fact that no reflector is perfectly reflective. Thus after a time characterized by the quality of the reflectors, the cavity photon mode decays through the emission of a free photon from the cavity with the same momentum as the cavity photon. Thus to sustain a cavity photon mode, a supply of new photons must be pumped into the cavity.

Optically active excitons are easily excitable in direct-bandgap semiconductors; in an indirect bandgap semiconductor such as silicon, the excitons are not amenable to strong optical coupling. A typical indirect bandgap semiconductor

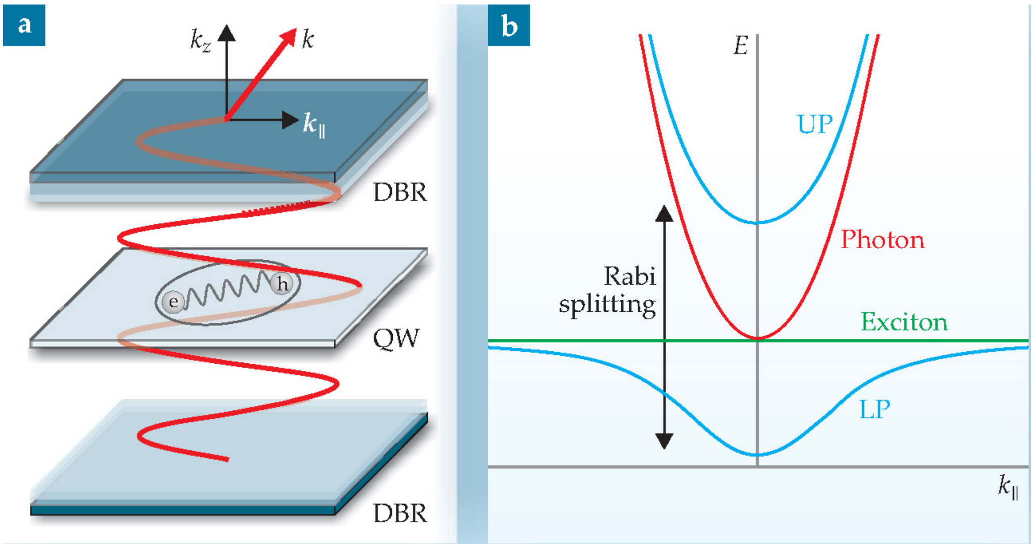

Fig. 1.3 (a) Schematic of typical microcavity and (b). Dispersion curves of cavity modes, including upper and lower polariton branches. Image taken from [36].

used in exciton-polariton experiments is Gallium Arsenide (GaAs). To match the confinement of the cavity photons, the active semiconductor is typically sandwiched between layers of higher bandgap energy semiconductors to form a quantum well (QW), confining excitons to the plane. These microstructures, including the cavity and the quantum well, can be grown very precisely in the laboratory as a single object [34, 35], so that the optical confinement plane lines up exactly with the quantum well confinement plane. This allows for the strong coupling between the quantum well excitons and the cavity photons, which is, critically, characterized by the *reversibility* of that coupling. It is this reversability which allows for the back-and-forth excitation (of an exciton) and emission (of a cavity photon) to repeat many times before the photon eventually leaks from the cavity. When the timescale of this repeated transfer of energy between exciton and cavity photon is small compared to the lifetimes of uncoupled excitations, the coupled excitations can be treated as distinct quasiparticles.

The Hamiltonian for the coupled system can be written as

$$H_{pol} = H_{ph} + H_{exc} + H_{int} = \sum_{\mathbf{k}} E_{ph}(\mathbf{k}) a^{\dagger}_{\mathbf{k}} a_{\mathbf{k}} + \sum_{\mathbf{k}} E_{exc}(\mathbf{k}) b^{\dagger}_{\mathbf{k}} b_{\mathbf{k}} + \hbar\Omega(a^{\dagger}_{\mathbf{k}} b_{\mathbf{k}} + b^{\dagger}_{\mathbf{k}} a_{\mathbf{k}}) \tag{1.16}$$

in which $a^{\dagger}_{\mathbf{k}}$ and $a_{\mathbf{k}}$ are the photon creation and annihilation operators, and $b^{\dagger}_{\mathbf{k}}$ and $b_{\mathbf{k}}$ are those of the exciton, and where Ω is the Rabi frequency. This Hamiltonian can be diagonalized to yield the eigenstates [37]

$$E_{LP}(k_{\|}) = \frac{1}{2}\left(E_{ph} + E_{exc} - \sqrt{4\hbar^2\Omega^2 + (E_{exc} - E_{ph})^2}\right) \tag{1.17}$$

$$E_{UP}(k_{\|}) = \frac{1}{2}\left(E_{ph} + E_{exc} + \sqrt{4\hbar^2\Omega^2 + (E_{exc} - E_{ph})^2},\right) \tag{1.18}$$

which are the so called *lower polariton* and *upper polariton* branches. A schematic of the upper and lower polariton dispersion curves in relation to those of the exciton and cavity photon dispersion curves is shown in Fig. 1.3. Clearly, for high transverse momentum the upper and lower polariton branches tend towards being cavity-photonic or excitonic in nature, respectively. For a more detailed description of the quantum theory of exciton-polaritons themselves, including the process of the diagonalisation of Eq. 1.16, and of the theory of the related scattering processes, see [37, 38] and the references therein.

1.3.2 Pumping

A sustained population of polaritons must balance the consistent loss of particles due to the finite reflectivity of the cavity with the input of new particles via "pumping". The losses can be tuned simply by changing the quality and number of dielectric Bragg mirrors in the microcavity. This tuning of loss rate can even be engineered to have a spatial structure, but the results of this thesis will not rely on such difficult manufacturing processes.

We will, however, rely on the two types of pumping: resonant and nonresonant. In both cases, we will consider pumping by a laser [5]. In the case of the nonresonant pumping, the laser feeds the cavity with photons which are far from the exciton absorption energies. These photons therefore have to undergo many scattering processes before exciting polaritons, a process by which the pumping of the polaritons become effectively incoherent, with the phase structure of the input laser being lost by the time it couples to the excitons. In contrast, resonant pumping uses a laser which is, as the name suggests, at a frequency resonant with the cavity and which directly excites excitons. This imprints the phase information from the coherent laser pump on the polaritons formed by this mechanism. Both first and second order resonant frequencies (at 1:1 and 1:2 resonance with the cavity) have been successfully used in experiments to form polariton condensates [39].

Very recently, experimentalists have achieved the simultaneous, independently controlled pumping of polaritons with resonant and nonresonant lasers [39]. In these experiments, chemical etching of a GaAs substrate allowed for the resonant excitation from the back side of the cavity, which prevented backscattering while allowing synchronization. This technique makes it possible to independently vary the pumping intensity distributions of resonant and non-resonant excitations. In experiment, $2:1$ resonance can be achieved with the same apparatus used for the combined nonresonant and $1:1$ resonant pumping (for example [39]), but tuning it to the twice the frequency of the condensate, which is within the laser capabilities [6]. This will be important for the results presented in Chapter 2.

[5]In principle the quasiparticles can be pumped electronically, but this remains highly difficult for experimental reasons, and will not be discussed further.

[6]Private correspondences with Prof. Pavlos Savvidis (University of Crete) and Dr. Hamid Ohadi (St. Andrews University).

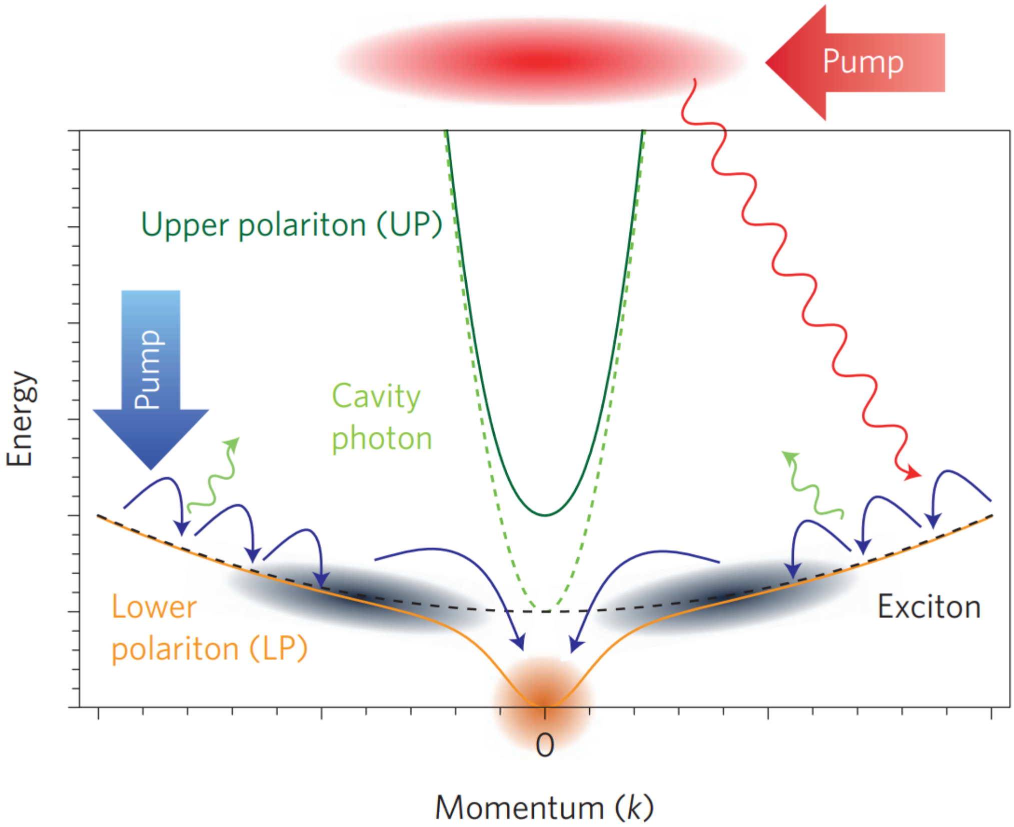

Fig. 1.4 Illustration of resonant pumping process (blue) and nonresonant pumping process (red). Image taken from [37].

1.3.3 Nonequilibrium Condensation

Excitons are bound pairs of electrons and holes, both of which are fermions. However at lengthscales much larger than the typical analogue Bohr radius of the bound pairs, the two half-integer spins add to an integer, yielding an effective boson. Thus at low enough polariton densities, the quasiparticles are separated on average by large enough distances to be effectively bosonic (the effectively integer spin of the exciton plus the "actually" integer spin of the photon component obviously yields an integer).

The exciton-polariton (from this point "polariton") inherits key properties from both its constituents, which can be independently engineered in the laboratory [37]. In particular, the hybridized quasiparticles combine the strong nonlinear interactions of their matter component with an ultralight effective mass coming from their photonic part.

Being bosonic at low densities, polaritons are in theory candidates for condensation. However, the proper thermodynamic defintion of Bose-Einstein condensation requires that the condensed particles be in thermodynamic equilibrium [6, 17], and even at ultralow temperatures the dilute gas of polaritons is consistently losing particles, as constituent cavity photons decay via free-photon emission. Thus to sustain the polariton population, photons must be fed into the cavity. This scenario clearly precludes the quasiparticle gas from ever truly reaching thermodynamic equilibrium, although experimental improvements in cavity quality continue to bring us closer.

Further, the nature of microcavity experiments are such that the states are confined to two spatial dimensions. At face value this should be problematic, as the spontaneous breaking of continuous symmetries is forbidden at finite temperature for homogeneous systems with fewer than three spatial dimensions: by the rigorous proofs of Mermin and Wagner [41], of Hohenberg [42], and of Coleman [43]: in such systems true long-range order is precluded by low-wavelength divergences at nonzero temperatures. Still, these rigorous results have not prevented the experimental condensation of dilute gases confined to effectively two spatial dimensions, most likely due to the nonuniformity of actual physical systems (for a discussion of the condensation of 2D systems see [44]).

Regardless of these concerns, a strikingly *condensate-like* state, characterized by the spontaneous coherence of the polariton gas at the threshold temperature/density does indeed occur in experiment, as first seen by [40]. Recalling the relation between mass and condensation threshold from the section on equilibrium BECs, this process occurs at relatively high temperatures - a balmy 5K in the landmark first experiment, allowing for the use of standard liquid-helium cryogenic

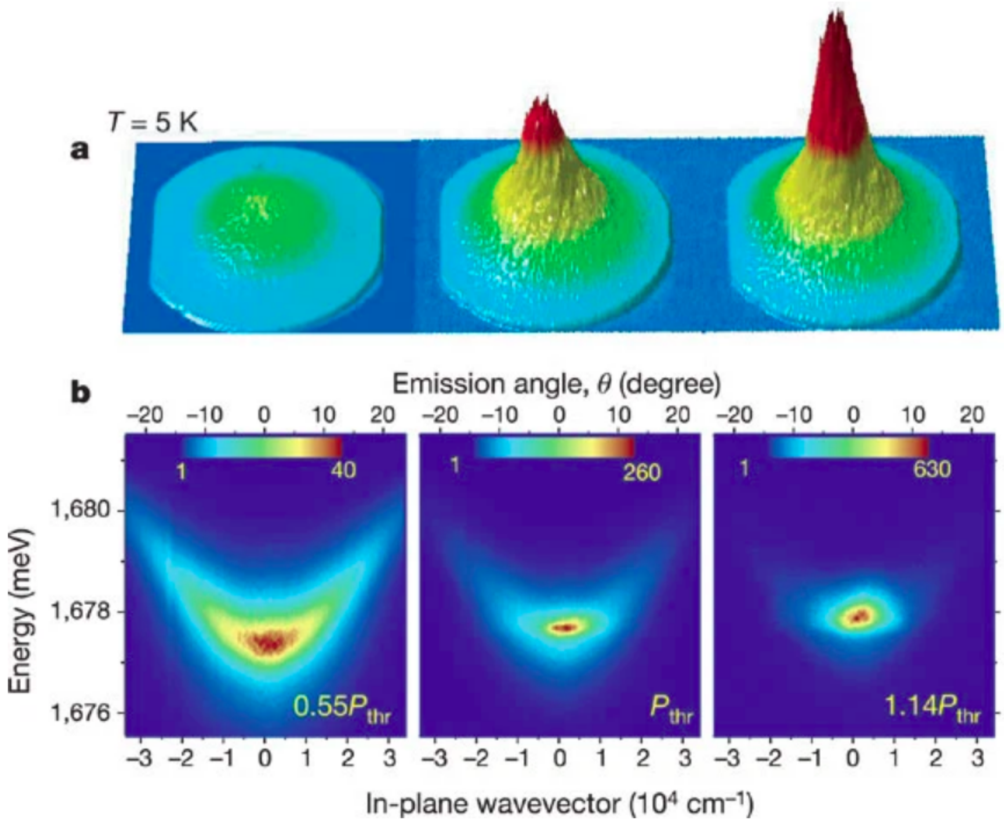

Fig. 1.5 (a) Far field emission below (left), at (middle) and above (right) the pumping threshold. (b) The same data, showing a slice of the far-field emission (horizontal axis) and the energy (vertical axis). At and above the threshold, the energy rapidly drops to the minimum, and the spread in emission wavevectors also decreases rapidly. Image taken from [40].

equipment [40] [7]. The far field emission from that experiment is shown in Fig. 1.5: holding the temperature fixed, the pump power of the (nonresonant) incident laser is increased, in turn increasing the density of microcavity polaritons. When the threshold polariton density is achieved, condensation occurs (recall the role of density in the order-of-magnitude relationship 1.1): the energy distribution of emitted photons drops dramatically to the ground state energy, and the transverse momentum distribution likewise collapses. Perhaps most importantly, Michelson interferometry of the emission reveals a sudden and again, dramatic, increase in

[7] While I do not discuss organic samples here, it is worth noting that with them the condensation temperatures can go up to *room temperature*, which truly is an extraordinary difference from the frigid temperatures needed for atomic BECs.

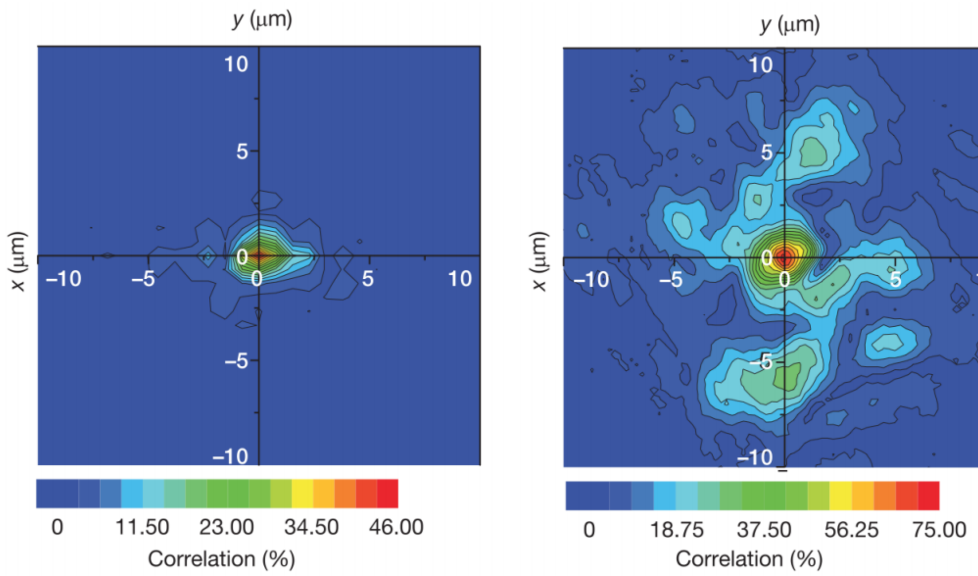

Fig. 1.6 Experimental measurement of first order correlations $g^{(1)}(x,x^{'})$, below (left) and above (right) threshold pump intensity. Image taken from [40].

the spatial coherence of the emitted light. The first order correlation function is defined as $g^{(1)}(x,x^{'}) = \psi^{*}(x)\psi(x^{'})/\sqrt{\psi^{*}(x)\psi(x)\psi^{*}(x^{'})\psi(x^{'})}$, and is a commonly used metric for the degree of spatial coherence; Fig. 1.6 shows the first order correlations below (left) and above (right) threshold, revealing a large increase in the spatial extent of the correlations.

1.3.4 An Interparadigmatic Regime

Given that Bose-Einstein condensation only properly occurs at thermal equilibrium, there has been some debate in the literature about the nature of the condensate-like coherent state of polaritons, given their fundamental nonequilibriation. Clearly, from the first experiment [40] and from those which have followed, the polariton gas undergoes a sudden transition to a condensate-like state, a coherent state at the ground state energy - at a threshold orders of magnitude lower than that required for the achievement of coherence through lasing, which can be had in the same microcavity systems. Thus while the polariton state in [40] is fundamentally distinct from condensate states in equilibrium systems, it is also fundamentally distinct from those seen in lasers, which require population inversion and are much more highly nonequilibriated. However, like laser systems, a direct readout of the wavefunction is possible optically, unlike in atomic BEC systems in which wavefunctions must be reconstructed from measurements taken after the release and rapid expansion of the trapped gas. Of course the polariton BEC comes with a different challenge, as the timescales of their dynamics are to quick for direct time resolved imaging, and thus experimentalists are currently restricted to either time-integrated wavefunction measurements or reconstructing time dynamics by taking one snapshot at a time over many iterations of the experiment.

Rather than lumping the physics of the polariton condensate into that of equilibrium BECs or of lasers, it is instead most advantageous to consider them as representing an interstitial regime, tending to the physics of equilibrium BECs in the limit of long polariton lifetimes, and tending to the physics of lasers in the limit of very short polariton lifetimes. This now appears to represent the mainstream view in the literature [45–47]. Thus while the polariton "condensate" is not properly a condensate in the strictest sense, I will follow the terminology of the literature and call it a condensate. Really this is just semantics, as all that matters to us is that the system undergoes a spontaneous coherence transition and presents us with interesting new physics.

Perhaps because those in the polariton community found themselves having to defend their condensates as such, there has not been as much work exploring the phenomena that are more akin to that of laser systems. This thesis certainly owes quite a lot to the old laser physics literature, and I hope to emphasize throughout this work that some of the behaviours of polariton condensates that appear to be unintuitive from the perspective of equilibrium condensate dynamics are more intuitive from the perspective of nonequilibrium pattern forming systems.

It is worth noting that even from the perspective of the polaritonic condensate as a system of heavily dressed photons, they have several advantages with respect

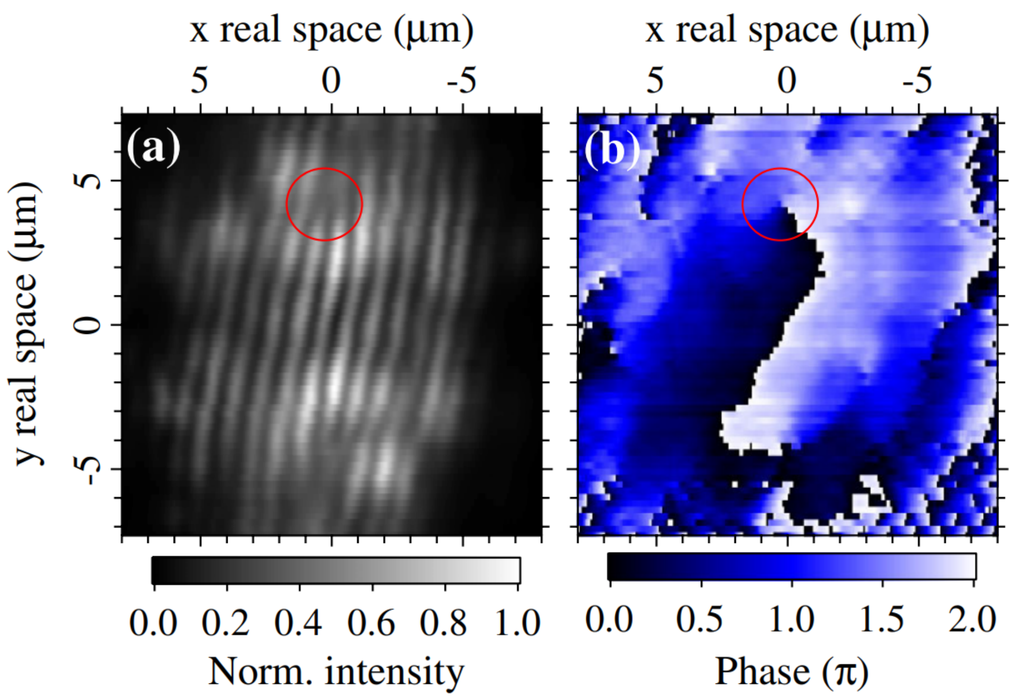

Fig. 1.7 Experimental observation of a vortex in a polariton condensate, showing the directly measured interferogram (a) and the reconstructed phase structure. Image taken from [49].

to other confined optical systems. One is their extraordinary nonlinear properties, which arise from their excitonic component. As one of the founders of the field wrote, polariton condensates open up an "optical playground" [48], and extremely low power thresholds, their unusually strong-nonlinearity given those low pump powers, high operating temperature, and their ability to be "printed" on widely accessible and well-studied semiconductors, they are widely regarded as the leading candidate for a practical, purely photonic transistor. Such a development would certainly change the landscape of computing, even without invoking *quantum* computing.

1.3.5 Superfluidity

Although Bose-Einstein condensates are typically associated with superfluidity, the later is an emergent phenomenon which neither necessitates nor implies the state of Bose-Einstein condensation. For example, in a Bose-Einstein condensate of noninteracting particles, the dispersion relation is quadratic and superfluidity does not take place - the latter takes place in the regime of *linear* dispersion [50]. On the other side of the spectrum, superfluid ^{3}He exhibits superfluidity, yet is composed of a fermionic species of helium. Superfluidity itself is a complicated and nuanced subject [51, 8, 50], and there was not certainty that it could be seen in a nonequilibrium system like the polariton condensate: like condensation itself, superfluidity is properly defined as an equilibrium property [48].

The core hallmark of superfluidity is the flow around an obstacle without drag. After being led up to by several strong signs of superfluidity in polariton condensates (the observation of vortices as in Fig. 1.7 [52], and of Bogoliubov excitations [53–55]), the drag-free flow past an obstacle was observed directly in exciton-polariton condensate experiments [56]. Soon after, the breakdown of superfluidity and associated nucleation of vortices at flows above the critical velocity was observed explicitly [57]. More recently, superfluidity in polariton condensates have been observed and studied at room temperature using organic microcavities [58], an enormous change from the extremely low temperatures typical of superfluid systems.

Thus, while the polariton condensate is not properly a superfluid due to its nonequilibriation, it exhibits strikingly superfluid-like behaviours. Thus the system is a superfluid in the same way as it is a condensate: effectively so, but with a nonequilibrium flavour.

1.3.6 Mean Field Theory

The mean field description of the polariton condensate is a significantly more difficult problem to approach from first principles than that of the dilute equilibrium condensate. As the state is always inherently out of thermal equilibrium, quantities such as chemical potential and temperature are not formally defined. A significant body of theoretical work has gone into the kinetic theory describing the relaxation of the "hot" particles excited by pumping [59–61], but it has also been lamented that such theories do not provide any description of the collective excitations that are expected in a quantum fluidic system [62]. Thus, the strategy adopted by the literature has been to use a phenomenological model, which couples a dissipative GPE to an equation based on the kinetic theory of the relaxation process, which describe the reservoir of uncondensed particles excited by pumping, using a kinetic Boltzmann treatment [63]. That work also represents an especially illuminating description of the problem of modeling polariton condensates. This approach has seen huge success, and has been highly descriptive and predictive of experimental observations.

In its currently accepted form, the mean field model of the exciton-polariton condensate takes the form of a complex Ginzburg-Landau equation (cGLE) coupled to a real reservoir equation representing the bath of hot excitons in the sample, nonresonantly excited by the spatially resolved laser pump profile $P(\mathbf{r})$ [47, 63, 45, 62]

$$i\hbar\partial_t\psi = -\frac{\hbar^2}{2m}(1-i\hat{\eta}N_R)\nabla^2\psi + U_0|\psi|^2\psi + g_R N_R\psi + \frac{i\hbar}{2}(R_R N_R - \gamma_C)\psi, \tag{1.19}$$

$$\partial_t N_R = P - (\gamma_R + R_R|\psi|^2)N_R, \tag{1.20}$$

in which ψ represents the condensate wavefunction, N_R and the exciton reservoir density. U_0 and g_R give the polariton-polariton and exciton-polariton interaction strengths, R_R and $\hat{\eta}$ represent the scattering and diffusion rates. The effective mass of the polariton is given by m. Finally, the loss rates of excitons and polaritons are described by γ_C and γ_R. To rewrite these equations in a nondimensional form more anemable to us, we apply the transforms $\psi \to \sqrt{\hbar R_R/2U_0 l_0^2}\psi$,$t \to 2l_0^2 t/\hbar R_R$, $r \to$

$\sqrt{\hbar l_0^2/(mR_R)}r$,$N_R \to N_R/l_0^2$,$P \to R_R P/2\hbar l_0^2$, and we define the nondimensionless parameters $g = 2g_R/R_R$, $b_0 = 2\gamma_R l_0^2/\hbar R_R$, $b_1 = R_R/U_0$,$\eta = \hat{\eta}/l_0^2$,$\gamma = \gamma_C l_0^2/R_R$, and $\gamma = \gamma_C l_0^2/R_R$, where we set $l_0 = 1\mu m$. This yields [64, 5]

$$i\partial_t \psi = -(1 - i\eta N_R)\nabla^2\psi + |\psi|^2\psi + gN_R\psi + i(N_R - \gamma)\psi \quad (1.21)$$

$$\partial_t N_R = P - (b_0 + b_1|\psi|^2)N_R, \quad (1.22)$$

which will be the basis of the work presented in this thesis. Again, Eq. 1.21 is a complex Ginzburg Landau equation (cGLE), claimed at least by Aronson and Kramer in their review on the subject, to be the most studied nonlinear equation in physics [65]. This in part comes from its generalising description of such a wide variety of physical systems, which itself comes from it being the minimal model of nonlinear systems near a Hopf bifurcation. In addition to Eq. 1.21, the Gross-Pitaesvkii equation of dilute atomic condensates and the real Ginzburg-Landau equation of degenerate optical parametric oscillators are all particular cases of the cGLE. The reader interested in surveys the cGLE might start with that of Aronson and Kramer or the relevant sections of the review by Cross and Hohenberg [66].

There is still, of course, a glaring difference between the well studied cGLE and our mean field model of the polariton system: the coupling to the reservoir. In the regime in which the reservoir reacts very quickly to the changes in the condensate wavefunction, it may be adiabatically eliminated. This is a procedure we make use of in the chapter on multiply charged vortices. However, this still does not reduce the model to the standard cGLE, as there remain saturable nonlinearities in several terms. Further, not every interesting behaviour takes place in the regime in which adiabatic elimination of the reservoir is justified. While in the case of multiply charged vortices the reservoir is stationary during the condensates dynamics of interest, in other scenarios the reservoir is changing dynamically along with the condensate dynamics. In particular, we will introduce novel breather excitations in the chapter on breathers, which require some delay in the reservoir dynamics relative to changes in the condensate wavefunction to remain stable.

Additionally, the pumping profiles in polariton BEC experiments are, as we have mentioned already, extraordinarily flexible: at the low optical powers typical of such experiments, beam engineering is fairly trivial with spatial light modulators, which can programmatically modulate the amplitude and phase of a beam [67]. Thus we have a really exciting degree of freedom to play with which has not been experimentally feasible in other systems: the spatial structure of the pump. This allows for, among other things, the approximate spatial separation of the reservoir from the condensate wavefunction, which *does* greatly simplify the theory, as we will make use of to describe multiply charged vortices. Finally, we note that the spatial extent of condensates can generally be made much smaller than the samples on which they reside, so that boundaries may be safely set to zero. This is the case throughout this thesis unless otherwise specified, and does have a nontrivial effect: in contrast to an infinitely extended condensate, a polariton condensate which tends to zero density must necessarily have quasiparticle flows at its edges.

Chapter 2

Breather Solutions

2.1 Introduction

The basic nonlinear excitations of Bose-Einstein condensates (BECs) are of significant fundamental interest, and have been studied in detail for decades [68–77]. However, relatively little is understood about their breather solutions [32]. In equilibrium BECs, there are significant fundamental restrictions on the formation and stability of breathers, due to their intrinsic tendency towards thermodynamic equilibrium. Solutions with sustained density oscillations can be constructed by the superposition of the ground state with one of the eigenstates of the Bogoliubov excitations, however, these simple periodic solutions are only persistent in the limit of zero amplitude so as to avoid damping via nonlinear spectral broadening, and in reality lose periodicity as modes are mixed [32]. Other simple breathing solutions have been constructed with the help of an explicitly periodic external potential in space [78] or an interaction term which is explicitly periodic in time [79]. In a non-periodic system, Pitaevskii and Rosch showed that in two spatial dimensions the nonlinear Schrodinger equation under harmonic trapping admits solutions in which the potential energy oscillates without damping, due explicitly to the SO(2,1) dynamical symmetry of that system [80, 81]. This latter phenomenon has recently been extended, with it being experimentally and theoretically shown that the SO(2,1) symmetric system also allows particular solutions which are periodic in the wavefunction evolution [32, 82, 83]. Specifically, it was shown that uniform condensates prepared in a disk and equilateral triangle box potentials, upon release from those box potentials, periodically reformed their initial states. While the phenomenon is striking, the breathers in this case are not solitonic, and their nature as global excitations precludes the possibility of an interacting system of these breathers.

In this chapter I introduce a novel, generic mechanism of breather formation in polaritonic BECs, from which a solitonic breather can emerge spontaneously as a fundamental excitation. Like vortices - but having no topological charge - these breathers are free to move and interact with and within their condensate background. I then proceed to construct a family of breathers with spontaneously adopted nontrivial discrete orders of rotational symmetry, which must be pinned but maintain their rotational degree of freedom, from which I demonstrate the spontaneous emergence of both crystalline and glassy orderings of lattices of polygonal breathers, depending on the degree of polygonal excitations at the lattice sites.

To get to this, we begin with the seemingly unrelated and apparently broader question of forcing symmetries.

2.2 Temporal Symmetry Breaking

To form and sustain a polariton condensate, the cavity in which it lives must be forced optically. These input photons may be either resonant or nonresonant with the natural frequency of the cavity. Thus, understanding the fundamental repercussions of the forcing scenario is among the most fundamental problems in the rapidly growing field of polaritonics.

Recent experiments have demonstrated that the exciton-polariton condensate can be simultaneously forced resonantly and nonresonantly, as discussed in the preliminary review chapter. In this chapter I will show that simultaneous forcing with nonresonant and n^{th} order resonant frequencies allows for a novel mechanism of breather formation, caused by a sort of frustration between the $\mathrm{U}(1)$ phase symmetry of nonresonantly forced systems and the $\mathbb{Z}_n$ symmetry of n^{th} order resonant forcing. After introducing the generic mechanism, we will explore its dynamical repercussions in extended systems in the particularly important case of $n = 2$. From this we construct a family of exotic breathers, the members of which spontaneously break rotational symmetry in favor of polygonal symmetry D_m in real space, with order m set by tunable system parameters.

2.2.1 Symmetry-Frustration and Breathing Modes

As discussed in the introductory chapter, the dynamics of the polariton condensate are well described by a generalized complex Ginzburg-Landau equation (cGLE) coupled to a real equation representing the reservoir of uncondensed particles. The reservoir is fed by the excitation of hot excitons by nonresonant pumping (see Fig. 1.3). However when pumping at resonance with the cavity, the wavefunction is forced directly and coherently. Forcing the generic cGLE at the resonance order n yields (at lowest order) the term $\bar{P}\psi^{*(n-1)}$, in which the forcing strength is represented by $\bar{P}$ [84]. Experiments have successfully implemented polariton condensates pumped simultaneously by nonresonant and resonant lasers with $n = 1$ order, and are possible with $n = 2$ with the same experimental apparatuses [39]. The phenomenological nontriviality of the physics of polariton condensates forced at the second order resonance, however, has not previously been noted, and as such as not yet been explored in experiment. Higher than second order resonances are not experimentally feasible, simply because the optical frequencies quickly become too high to work with. For some organic samples, which can see polariton condensation at room temperature [54], even second order resonances are likely not possible due to their already-higher operating frequencies. However the resonance of typical semiconductor microcavities are on the order of $800nm$, so that the second order resonance at about $400nm$ is entirely feasible. Luckily, the second order resonance is the most interesting: as we will see soon, it leads to the lowest order and thus the most *severe* degenerate symmetry breaking of the condensate phase.

In nondimensional form, we restate our model with the inclusion of the resonant forcing term, as [64, 45, 63, 47, 85]

$$\begin{aligned} i\partial_t \psi &= -(1-i\eta N_R)\nabla^2\psi + |\psi|^2\psi + gN_R\psi & (2.1)\\ &+ i(N_R-\gamma)\psi + iV\psi + i\bar{P}\psi^{*(n-1)} \\ \partial_t N_R &= P-(b_0+b_1|\psi|^2)N_R, & (2.2)\end{aligned}$$

in which g represents the polariton-exciton interaction strength, η is the energy relaxation [86, 46], γ represents the dissipation rate, b_0 is the polariton inverse lifetime, and b_1 scales with the rate of scattering between the condensate and the reservoir of uncondensed particles. The incoherent and resonant (at $n:1$ resonance with the condensate frequency) pump sources are described by the pumping intensities $P(\mathbf{r},t)$ and $\bar{P}(\mathbf{r},t)$, respectively [1].

We begin by focusing on the regime in which the reservoir dynamics react quickly to the condensate wavefunction ($\partial_t N_R \approx 0$), and in which the energy relaxation $\eta \ll 1$. For analytical tractability we fix the parameters $b_0 = b_1 = 1$ (which are still within the range of experimentally accessible values). From here we insert $N_R = P/(1+|\psi|^2)$ into Eq. 2.1; focusing first on the behavior of the

[1] Unless otherwise noted, simulations in this chapter use the fixed parameter values $b_0 = 1$, $b_1 = 1$, $\gamma = 0.3$, and $\eta = 0.3$. These are set to correspond to the experimental parameters of a dual excitation setup [39].

system in zero-dimensional space, the dynamics of the polariton condensate are reduced to the following complex ordinary differential equation:

$$i\dot{\psi} \quad = \quad \frac{(1-i\gamma)\,|\psi|^2+|\psi|^4-i\gamma+(g+i)P}{(|\psi|^2+1)/\psi}+i\bar{P}\psi^{*(n-1)}. \tag{2.3}$$

Making the Madelung transformation $\psi(t) \to \sqrt{\rho(t)}\exp(i\theta(t))$ and separating real and imaginary parts of the resulting equation and doing some fairly tedious manipulations, we can rewrite Eq. 2.3 as the following real, coupled ODEs:

$$\dot{\rho} \quad = \quad 2\frac{\bar{P}\cos(n\theta)\left(\rho^{\frac{n}{2}}+\rho^{\frac{n}{2}+1}\right)+(P-\gamma)\rho-\gamma\rho^2}{(1+\rho)}, \tag{2.4}$$

$$\dot{\theta} \quad = \quad \frac{\bar{P}\sin(n\theta)\left(\rho^{\frac{n}{2}-1}-\rho^{\frac{n}{2}}\right)-gP-\rho-\rho^2}{(1+\rho)}. \tag{2.5}$$

Physically, ρ represents the time dependent condensate wavefunction density and θ its phase. Eqs. 2.4-2.5 are not explicitly solvable; however, in the limit of small resonant pump strength $\bar{P}$, we can view solutions as perturbations of the steady states familiar to purely nonresonantly pumped condensates. Such nonzero steady states have constant phase evolution $\theta = \mu t$.

We are most interested in the maximal degenerate symmetry breaking case of $n = 2$. Substituting into Eq. 2.5 and setting $n = 2$ yields the small $\bar{P}$ approximation for the condensate density under simultaneous nonresonant and second order resonant forcing

$$\rho(t) \quad = \quad \frac{1}{2}\left(\sqrt{\zeta(t)^2-4(gP+\zeta(t))}-\zeta(t)-1\right) \tag{2.6}$$

in which $\zeta(t) = 1+\mu+\bar{P}\sin(2\mu t)$. From here, it is clear that for $\bar{P} = 0$, $\xi(t)$ reduces to $\mu+1$ and Eq. 2.6 returns the familiar steady state solution, with the

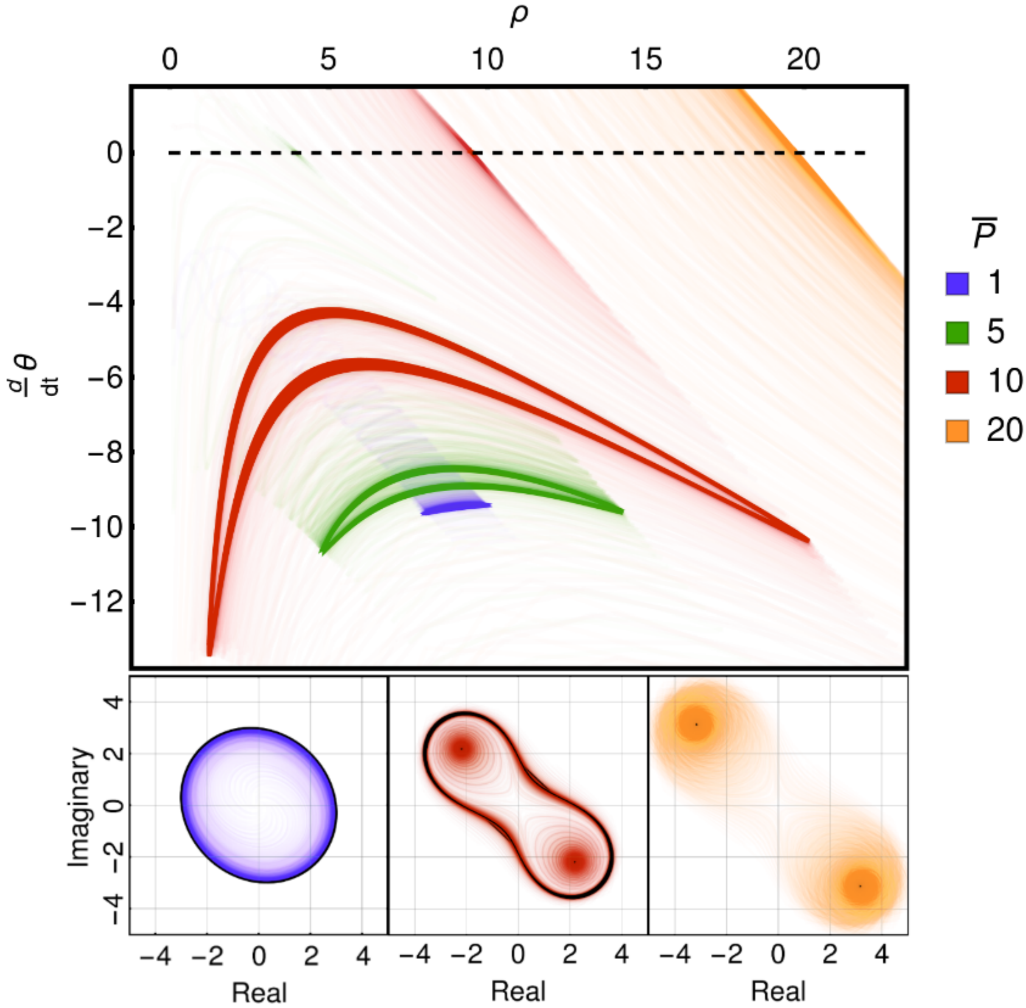

Fig. 2.1 Top: Trajectories of Eqs. 2.4-2.5 traced numerically in phase space from many initial conditions, for fixed parameters $\gamma = 1/2$, $P = 5$, $g = 1$ and various second order resonant pump strengths $\bar{P} = \{1, 5, 10, 20\}$. For clarity, the line of zero phase velocity is marked (dashed black)- the slanted linear phase trajectories through this line are those to the symmetry-broken fixed points along it. Bottom: To show the geometry of the symmetry breaking, the same phase trajectories are plotted in the complex plane (real and imaginary axes shown from ± 4.25). From both, we see the transition in behavior from small, nearly uniform oscillations driven by small resonant pumping (blue), to the dual fixed point attractors seen under high resonant forcing (orange). In between, both fixed points and large nonuniform density oscillations are seen (red).

fixed density set by the parameterization. However for $\bar{P} > 0$ oscillations take hold, with period given simply by

$$T = \pi/\mu, \tag{2.7}$$

and with amplitude scaling with $\bar{P}$. Later we will see that even in full 2D simulations of Eqs. 2.1-2.2, these simple predictions remain robust, even beyond the analytically supported regime of weak resonant pumping. In the other extreme that can be considered is the scenario of very strong resonant pumping. In this case we expect n fixed points -setting the left hand sides of Eqs. 2.1-2.2 to zero yields n θ solutions and one value for ρ. The uniform stationary solutions of Eqs. (2.1-2.2) with $n = 2$ and without noise satisfy

$$R^2 + g\tilde{P}/(1+\xi R^2) + \bar{P}\sin 2S = 0 \tag{2.8}$$

$$\tilde{P}/(1+\xi R^2) + \bar{P}\cos 2S - \gamma = 0 \tag{2.9}$$

where we used the Madelung transformation $\psi = R\exp[iS]$ and denoted $\tilde{P} = P/b_0, \xi = b_1/b_0$. Eliminating S gives

$$\bar{P}^2 = (R^2 + g\tilde{P}(1+\xi R^2)^{-1})^2 + (\gamma - \tilde{P}(1+\xi R^2)^{-1})^2. \tag{2.10}$$

For a given set of system parameters this equation can be solved to find $\rho = R^2$ with two expressions for S that differ by π. These are the phase locking solutions.

However, to probe the full range of behaviours between these extreme of weak and strong resonance, we must integrate Eqs. 2.4-2.5 numerically. Again fixing $n = 2$ and integrating for many initial conditions $\{\rho_i, \theta_i\}$, phase space trajectories are collected for varying resonant pump strength $\bar{P}$ (with other system parameters fixed), shown in Fig. 2.1 (top). In that figure the solution trajectories are traced out at low opacity for many initial conditions, so that the solutions which are tended to and/or are cycled many times become visible. The bottom panel of that figure shows some of the same accumulated trajectories, but in the complex plane as opposed to the phase space. In these spaces geometrical interpretations of the effect of resonant pumping, and the resulting density oscillations, become clear. As expected, for $\bar{P} = 0$ (not shown), there is a single fixed point attractor corresponding to a single point of nonzero phase velocity and nonzero density in the phase space, which corresponds to a circular trajectory in the complex plane; this is simply the plane wave solution. At the other extreme, high resonant forcing (orange) leads to a set of two fixed point attractors (resolved in the complex plane) at states with fixed density and null phase velocity (resolved in phase space).

These numerical results agree with analytical predictions, but now the interstitial regime between strong and weak resonant forcing is also resolved: as the resonant forcing strength is increased gradually from zero, the smooth *stretching* of the closed state trajectories in the complex plane is recorded, in the directions of the symmetry broken fixed points which then eventually form. Recalling that the resonant forcing terms in Eqs. 2.4-2.5 are $\bar{P}\cos(n\theta)$ and $\bar{P}\sin(n\theta)$, the n-fold stretching is geometrically clear: in the complex plane these terms are linear scaling operators acting along n axes separated by $2\pi/n$. Thus we should expect an n-fold stretching of the circular orbit as $\bar{P}$ is increased from zero, and for increasing $\bar{P}$ we should expect the density increasingly dependent on the phase with degeneracy n. Fig. 2.1 confirms these behaviors. For small resonant pumping, we see slight n-fold deformation of the orbit in the complex plane (blue), which becomes severely deformed (but with equal symmetry) as the resonant pumping is increased (red). That case also shows the overlap between the limit cycle and phase locked regimes. We note that the same procedure for any n^{th} order resonance yields the same fundamental result, but showing n-fold symmetry in the complex plane. We confirm this in numerical experiments for $n \in \{1...5\}$, although the higher-than-second-order resonances are, again, beyond current experimental capabilities.

Of course, the warping of the phase-space trajectories has more than a geometric effect: the non-circular closed path in the complex state space is trivially indicative of density oscillations in the wave function. Thus the orbit deformations can actually be considered as *driving* the density oscillations, and which fully characterize their wave-forms.

In this way, breathing is a result of frustration between the two natural states of competing symmetries, the $\mathrm{U}(1)$ symmetry of $\bar{P}=0$ (circular orbit in complex plane), and the $\mathbb{Z}_n$ symmetry of large $\bar{P}$ (n-fold fixed points), in a sort of temporal analogue of geometrical frustration.

2.3 The Breathing Ring Soliton

2.3.1 Introduction

So far we have established that under the simultaneous resonant and nonresonant forcing of a polariton condensate, there generically exists a regime of density oscillations in between the plane-wave and phase locked solutions. We now turn to the full, spatially extended (2D) system. The order of resonant pumping, and thus the geometry of the phase-symmetry breaking, is intimately connected with the types of stable topological defects that are allowed in a spatially extended system. In a phase symmetric system, all phases are equally stable, and thus stable topological defects must take the form of continuous helical phase gradations wrapped around zero dimensional singularities - this is the celebrated quantum vortex. In a system phase locked by strong $2^{nd}-$ order resonant forcing, there are two equally stable phases differing by π, so that stable one-dimensional topological defects naturally form between domains of opposite phase (domain walls or 'dark solitons'). For $n>2$, more phases become stable, quickly approximating the $\mathrm{U}(1)$ symmetry. Thus from the perspective of pattern formation, the $2^{nd}-$order resonant forcing is the most extreme case, as the associated $\mathbb{Z}_2$ symmetry is the starkest departure from $\mathrm{U}(1)$ while maintaining the necessary degeneracy. Thus while the our breathing mechanism applies to higher resonances, in the 2D case we will focus only the 2^{nd}−order resonant forcing.

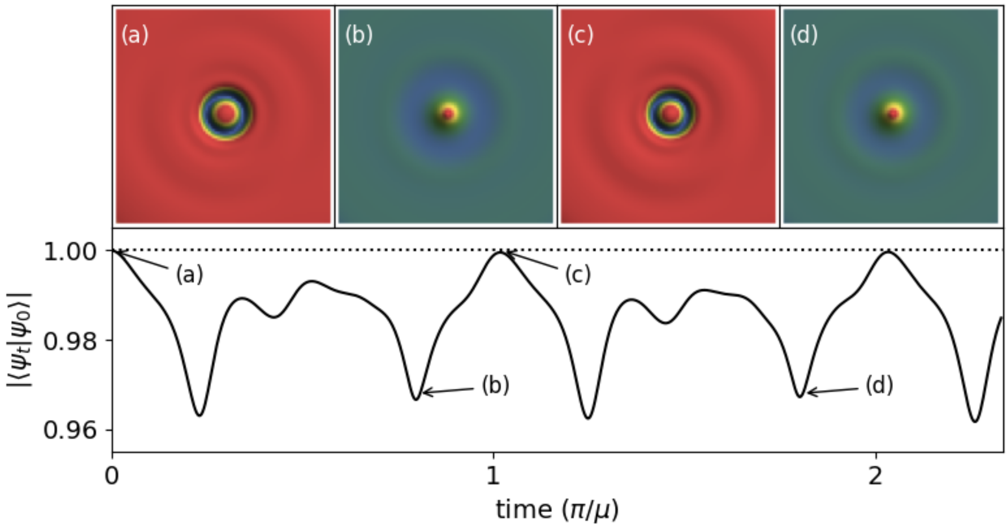

Fig. 2.2 Top: Close-up of density profile of a breathing ring soliton, over the course of one oscillation period. Computational domain extends beyond shown area beyond the pump radius, after which the condensate does tend to zero. Bottom: the overlap between the condensate wavefunction at fixed time show at (a) with the time dependent wavefunction, showing the periodicity of the breathing ring wavefunction. Time is shown in units of π/μ, the natural period of the symmetry-frustration oscillations from which the ring emerges.

We begin this by considering the condensate forced uniformly with nonresonant and 2^{nd}−order resonant (from this point “resonant") forcing. It was recently shown that ring-shaped breathers can form in such a system [3], and we now show that these result from the breathing mechanism described here. In full numerical integration of Eqs. 2.1-2.2, we prepare a uniform disk-shaped condensate pumped in such a manner, with resonant forcing high enough such that the regime of phase locking is achieved. By phase imprinting a perturbation, we observe the excitation of a breathing ring soliton, as shown in Fig. 2.2, which have the periodicity π/μ as predicted in the zero-dimensional problem. These structures may thus be interpreted as the localized excitations of the phase-locked state into the limit cycle in a phase space which, as in the zero-dimensional space, admits both simultaneously.

2.3.2 Temporal Structure

Before turning to the geometrical structure of the rings, it is worth turning at this point to their temporal structure. We know from 2.7 that there exists a natural frequency at which the condensate density is driven to oscillate in the regime of weak to moderate resonant forcing. Of course, the regime in which breathing rings are stable is one characterised by a constant, uniform background condensate resonantly driven into phase bistability. However, we recall Fig. 2.1, which showed the existence of not two but three distinct regimes of symmetry broken states: that with a limit cycle only (weak resonant forcing), that with fixed points only (strong resonant forcing), but also that with fixed points circumscribed by a limit cycle (moderate resonant forcing). Indeed, numerical experiments show that for too strong of resonant forcing breathing ring solitons are not supported - even a phase imprinted ring soliton shrinks into itself and disappears. Likewise, if the resonant pump is made to be too weak, the ring is not supported at all, with vortices dominating instead. Thus while the case of the breathing ring is of course much more complicated than the zero-dimensional picture represented by Fig. 2.1, it seems at least plausible to hypothesise the breathing ring as being a localised excitation of the limit cycle state, on a condensate background which in one of the phase-bistable fixed points. In this case, we would expect the period of the ring breather to match that of the natural frequency of the symmetry-frustration limit cycle, π/μ. As shown in Fig. 2.2, this is indeed the case: measuring μ numerically by sampling the phase evolution rate near the edge of the background condensate, there appears to be a close match between the natural period and the observed ring-breath period. Further, by plotting the overlap between the wavefunction of the condensate with a single ring at a fixed time (I have chosen the time when the dark ring reaches null density) with the wavefunction of that condensate in time, it is easy to see that the ring structure does indeed have a periodic wavefunction, returning to complete wavefunction overlap.

2.3.3 Physical Structure

While the existence of a closed form description of this dynamical structure is highly unlikely, some insight into its structure can be gained by treating the breathing behavior as a perturbation of a stationary solution. Using the Taylor expansion in the steady state expression for the reservoir density $N_R = \tilde{P}(1 + \xi|\psi|^2)^{-1} \approx \tilde{P} - \tilde{P}\xi|\psi|^2$. The dynamics of the condensate results from Eqs. (2.1-2.2) and reads

$$\partial_t \psi = (i + \eta\tilde{P})\nabla^2\psi - \kappa|\psi|^2\psi + \bar{P}\psi^* + [(g\tilde{P})i + \tilde{P} - \gamma]\psi, \tag{2.11}$$

where we denoted $\kappa = \tilde{P}\xi + (1 - g\tilde{P}\xi)i$.

Close to the condensation threshold and for sufficiently strong external resonant forcing, we can assume that $\eta\tilde{P} \ll 1$. Neglecting the corresponding terms, rescaling $\psi \to \Psi\sqrt{\bar{P}/\tilde{P}\xi}$, $t \to t/\bar{P}$, $\mathbf{x} \to \mathbf{x}/\sqrt{\bar{P}}$ and denoting $\chi = (1 - g\tilde{P}\xi)/\tilde{P}\xi$, $\alpha_1 = (\tilde{P} - \gamma)/\bar{P}$, and $\alpha_2 = g\tilde{P}/\bar{P}$, we rewrite Eq. 2.11 as

$$\partial_t \Psi_i = i\nabla^2\Psi - (1 + i\chi)|\Psi|^2\Psi + \Psi^* + (\alpha_1 - i\alpha_2)\Psi, \tag{2.12}$$

The uniform density is given by $|\Psi|^2 = 1+\alpha_1$. We rewrite the condensate wavefunction as the sum of real and imaginary components $\Psi = U + iV$, so that

$$\begin{aligned}
\partial_t U &= -\nabla^2 V - (U^2+V^2)U + \chi(U^2+V^2)V \quad (2.13)\\
&+ (1+\alpha_1)U + \alpha_2 V,\\
\partial_t V &= \nabla^2 U - (U^2+V^2)V - \chi(U^2+V^2)U \quad (2.14)\\
&- (1-\alpha_1)V - \alpha_2 U.
\end{aligned}$$

In the ring soliton $V \ll U$ and so $|\Psi|^2 \approx U^2 \approx 1+\alpha_1$ except for the small healing region that defines the radius of the ring, and $\partial_t V \approx 0$. Under these assumptions we solve Eq. 2.15 for $V \approx [\nabla^2 U - \{\chi(1+\alpha_1)+\alpha_2\}U]/2$ and substitute into Eq. 2.13 to get a real Swift-Hohenberg equation

$$\partial_t U = -\frac{1}{2}[\nabla^2+\Delta]^2 U - U^3 + (1+\alpha_1)U, \quad (2.15)$$

where we write $\Delta = -[\chi(1+\alpha_1)+\alpha_2]$.

The RSHE is a variational equation, and can be written in the gradient form $\partial_t U = -\partial\mathscr{F}/\partial U$ [66] where the potential $\mathscr{F}$ takes the form

$$\mathscr{F} = \int_0^{+\infty}\{\frac{1}{4}[(\nabla^2+\Delta)U]^2 - \frac{1}{4}(U^4-U_0^4) - \frac{1}{2}(1+a_1)(U^2-U_0^2) - \frac{1}{4}\Delta^2 U_0^2\}\,dr, \quad (2.16)$$

denoting the background contribution as $U_0 = \sqrt{1+\alpha_1 - 1/2\Delta^2}$.

In one dimension the Ising wall [2] takes the approximate form $U(r) = U_0 \tanh(r/w)$, where the width parameter w determines the healing length. Inserting this into $\mathscr{F}$ and evaluating the integral yields an analytical form for the potential energy. The Ising wall width w which minimizes this potential can be written as

[2]This terminology comes analogizing from spin models. In the Ising spin model, the order parameter is fixed to either $\uparrow$ or $\downarrow$, which is mathematically equivalent to an order parameter fixed to phases 0 and π. Thus here the Ising domain is that separating a π phase shift.

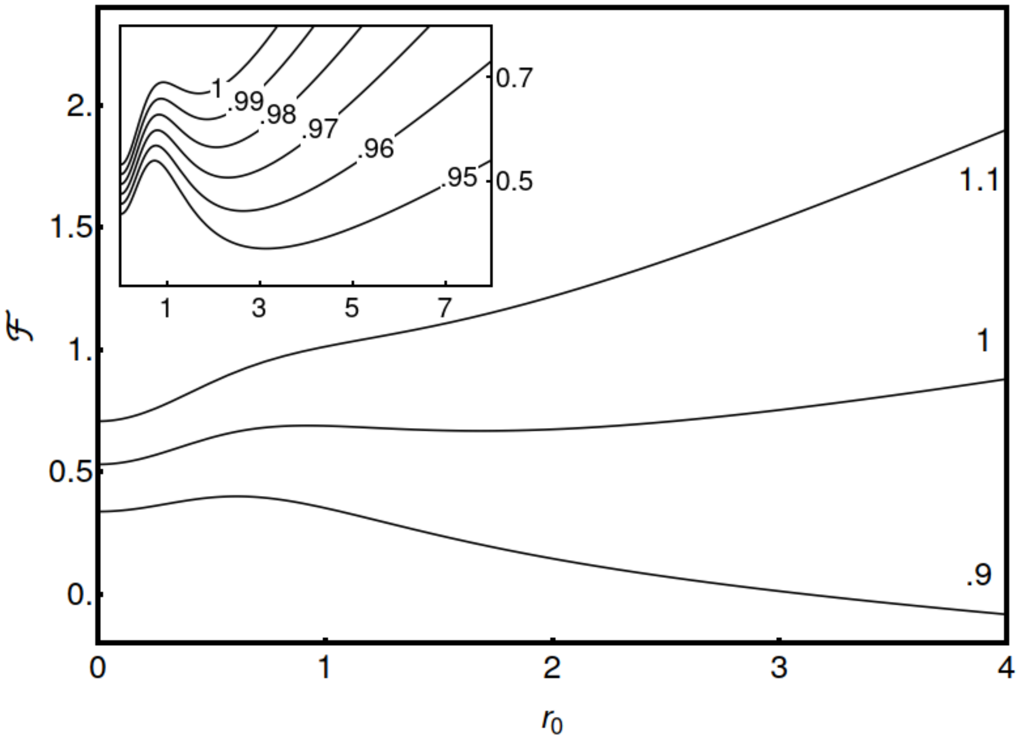

Fig. 2.3 The potential energy $\mathscr{F}$ as a function of the ring radius r_0, for several pump powers $P = \bar{P}$, for $g = 1$. The inset shows the same, for a smaller range of pump strength, for which there exist energy minima for finite ring radii.

$$w^2 = \frac{\sqrt{5}\Delta^2 + 12U_0^2}{\sqrt{5}U_0^2} - \frac{\Delta}{U_0^2}. \tag{2.17}$$

The circularly symmetric Ising wall can be approximated with the anzätz

$$U(r) = U_0(r+r_0)(r-r_0)/\sqrt{[(r+r_0)^2+w^2][(r-r_0)^2+w^2]}. \tag{2.18}$$

Substituting w and inserting the 2D ansatz (again taking care to remove the contribution of the homogenous background)), $\mathscr{F}$ is again exactly integrable, yielding an analytical formula for the potential energy of the ring soliton as a function of its radius and the system parameters. This potential takes the exact form

$$
\begin{aligned}
\mathscr{F} &= \frac{U_0^2}{1024 r_0^5 w^3 (r_0^2+w^2)^4}\Big(r_0 w(-27w^{12} - 4r_0^{12}(-45+96\Delta w^2 - 64V^2w^4) \\
&- r_0^2 w^{10}(229+32\Delta w^2+16V^2w^4) + 2r_0^4 w^8(-241-192\Delta w^2+56V^2w^4) \\
&+ 2r_0^6 w^6(127-608\Delta w^2+328V^2w^4) + r_0^{10}w^2(807-1312\Delta w^2+896V^2w^4) \\
&+ r_0^8 w^4(1545-1792\Delta w^2+1168V^2w^4)) + (r_0^2+w^2)^4(27w^6 - 4r_0^6(-45+96\Delta w^2-64V^2w^4) \\
&+ 2r_0^2w^4(65+16\Delta w^2+8V^2w^4) + r_0^4w^2(147+96\Delta w^2+128V^2w^4))\arctan(r_0/w)\Big) \qquad (2.19)
\end{aligned}
$$

For typical system parameters Figure 2.3 shows the potential energy $\mathscr{F}$ of the ring as a function of its radius, for several values of the pump power. This shows that under the approximation of the breathing ring soliton's radial oscillations as small perturbations a stationary solution, a significant amount of insight can be gleaned about the relationship between the pump strength and the behavior of the ring: too small, and the ring expands to infinity, but too large, the ring contracts to a point. As the inset shows, for a range of values in between, there exist finite ring radii which minimize the potential. Over this range, the minimizing radius decreases with increasing pump power. The steepness of the curve also decreases towards the large r_0 side as the pump is decreased, suggesting that as the pump strength is lowered, the range of r_0 over the ring oscillation should increase. While the relevant range of pump strengths differ between the analytical predictions and the full numerical experiments, the behavioral predictions of the analytical model are are entirely consistent with the numerical experiments.

2.3.4 Stability and Spontaneous Formation

We now consider the spontaneous formation of breathing rings. It is well understood that due to the finite noise (whether from quantum fluctuations in experiments or from numerical noise/truncation in simulations), the spontaneous coherence of a condensate during its early formation does not occur everywhere at the same time. Thus multiple regions of locally coherent condensate form independently first, and then "meet in the middle". In the case of a phase bistable system, these locally coherent regions may just as likely have opposite phase as equal phase, and in the former can this results in the spontaneous emergence of an Ising domain wall (the name of the dark soliton in the 2D space). In a phase bistable system Ising walls are topologically required to either end at the boundary of the condensate or to form closed loops that grow or shrink until they reach a characteristic radius, close to a point, or grow infinitely.

Similarly, in the case of the nonlinear optical resonator (as in [87]) such dark soliton rings have been observed to form spontaneously, and can be stable, minimizing the local potential energy, and thus remain stationary. Of course at the critical radius the rings in polariton condensates behave differently, as we have seen already. However, by the same mechanism of spontaneous coherence, we expect the spontaneous formation of breathing ring solitons in polariton condensates under suitable conditions.

In numerical experiments, the ring solitons are found to self-annihilate (i) in the fast reservoir regime $b_0 \gg \gamma$, (ii) in small reservoir detuning regime $g \ll 1$, (iii) in condensates made of long-lived polaritons. All these regimes are physically relevant to some experiments [88–90]. However, a slow reservoir evolution ($b_0 \lesssim \gamma$), for short-lived polaritons and a sufficiently large reservoir detuning (all of which correspond to values of typical GaAs microcavity experiments [40, 38, 91]) prevent the ring soliton from disappearing and lead to appearance of a ring breather: the dissipative decrease in the radius of the ring soliton is accompanied by the increase in the reservoir profile density in the ring core, which imposes a repulsive force in the outward direction to make the ring expand. The excitation is thus self-localized by an explicitly dynamical interaction.

The destabilizing mechanisms (i)-(iii) have similar effects on the existence and dynamics of the ring solitons, we concentrate on the effect of varying the polariton-exciton interaction strength (parametrized by g). The detuning between the cavity photon energy and the exciton resonance determines the relative photonic/excitonic character of the polariton and, therefore, its effective mass and the strength of the polariton-exciton interactions [47]. The detuning g can be further changed by the pumping geometry by considering trapped condensates separated from the pumps [92]. Finally, implanting protons into the quantum wells or into the top of distributed Bragg reflectors allows for an independent spatial control of both the exciton and the cavity photon energies, and, therefore, affects g [93] as well. By these mechanisms, the experimental ranges of our dimensionless parameter g can vary between $0.1-2$. We observe spontaneous ring formation in the entire physical range of that parameter, between 0.1 and 1.5. It is found that the pumping amplitudes for which ring formation is supported depends on the detuning, extending for a range of nearly P_{th} for the case $g=1$, and extending for a range of more than $2P_{\text{th}}$ for $g=0.1$. We note that the experimental range of values of η are unknown. However, we have observed ring formation for the range $0.001 \leq \eta \leq 1$.

In systems with low g, rings form ad infinitum creating a sustained state of ring turbulence. A time snapshot of condensate density in this regime is shown in Fig. 2.4(a). In the high g case, rings are formed only during the condensation process. They tend to interact attractively, and upon contact a pair of rings appear to either merge into one or annihilate each other. Eventually the decay of rings ends and a quasistationary state is reached with rings being pinned by the system disorder represented in our simulations by setting V_{ext} to white noise with amplitudes ranging between $\pm 0.005\rho_0$. However, we note that we see the same type of pinning behavior for $V_{ext}=0$, as even when the only disorder comes from the discretization of the fluid (the high energy limit of any numerical simulation, and

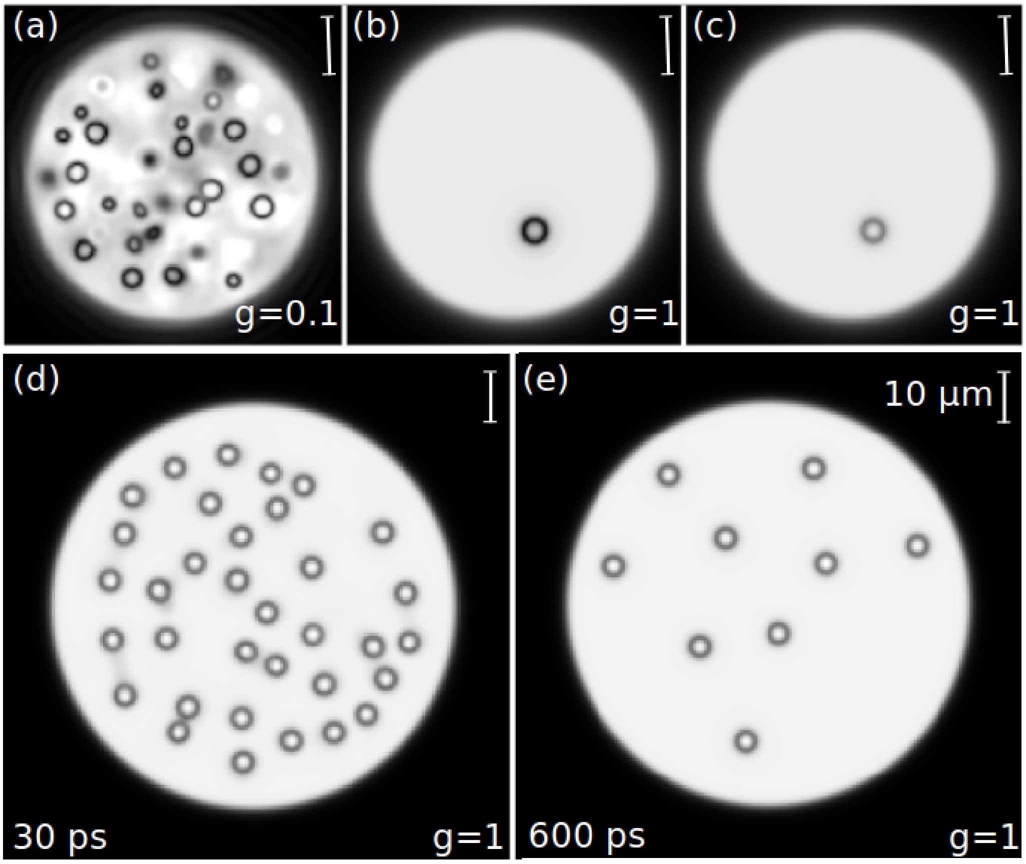

Fig. 2.4 Spontaneously formed breathing rings in exciton-polariton condensates for $P = \bar{P} = 5$, where P is the amplitude of the nonresonant pump, and $\bar{P}$ is that of a second-order resonant pump. Density contour plots of the condensate shown illustrate (a) a time- snapshot of ring turbulence; (b) a quasi-stationary state with a single ring; (c) time-averaging of (b) over many ring oscillations; (d-e) different stages of the condensate evolution averaged over the time-scale of the ring oscillation. White disk-shaped region is given by the uniform-disk shaped pump profiles, beyond which the condensate quickly tends to zero density.

of any physical many body system), structures that are far enough apart interact so negligibly that they remain stationary, pinned by slightly less negligible disorder (at least up to timescales relevant to experimental observation). This is demonstrated with time snapshots of the condensate density, shown in Fig. 2.4(d,e). Figure 2.4 shows a time snapshot of a spontaneously formed breathing ring soliton after the system has reached its final, quasistationary state (b), as well as a time integrated image of that state (c). Further we note that we find the rings to be stable against finite noise. Thus we predict that long-lived breathing ring solitons are directly observable, and that their ring shaped character, radii, locations and numbers are directly measurable as well. Again, state of the art experiments have recently become capable of the simultaneous resonant and nonresonant pumping needed to observe these novel and fundamental excitations [39]; experiments have simply not probed the second-order resonant regime owing to a perception that the physics would not be distinct from that of first order resonance experiments.

2.3.5 As a Probe of Critical Phenomena

The mechanism by which breathing ring solitons have been shown to form for high g resembles Kibble-Zurek (KZ) mechanism of defect formation in equilibrium systems [94, 95]. The KZ mechanism was first understood in the context of the phase transitions in the early Universe [96–98], and later in liquid 4He and 3He, liquid crystals, superconductors [99–102], equilibrium Bose-Einstein condensates [103, 104]. The similarities and differences between the KZ transition and pattern formation in nonequilibrium systems are the subject of intense exploration, with an emphasis on the common mechanism of the defect formation: locally uniform symmetry breaking in separate parts of the system which cannot communicate in a finite time, and which thus form to be globally nonuniform to a degree set by the speed of the phase transition (the quench rate). The main difference between the

KZ transition and pattern forming in nonequilibrium systems is that in the former, it is assumed that the system is driven out of equilibrium only in the vicinity of the phase transition [98]. In spite of extensive research on both the KZ transition and on pattern formation in a wide variety of nonequilibrium systems, questions remain regarding the nature of the cross-over between the two mechanisms, and regarding the types of the defects that they can result in. Numerical experiments regarding the rate of *polarization* defect formation between quasi-1D spinor polariton condensates formed in chains of microcavities have been performed [105], but to our knowledge no proposal of this kind of study has been made in regard to uniform polariton condensates formed on ordinary GaAs samples, or in regard to phase defects.

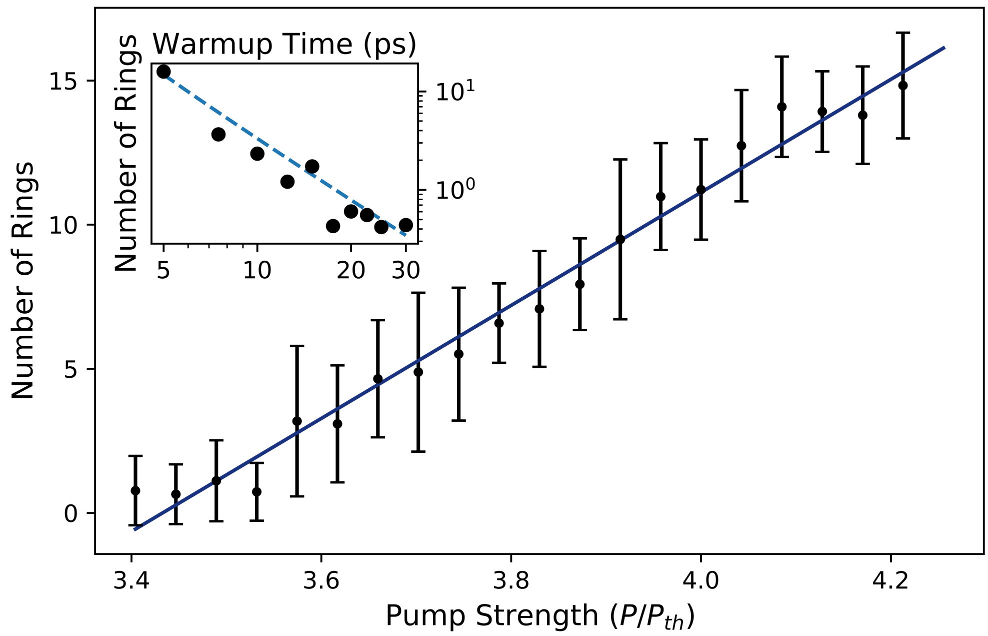

Fig. 2.5 Number of rings in the quasistationary state as a function of pump strength ($P = \bar{P} = \text{const}$), in units of the threshold pump strength P_{th}. Results are averaged over 10 random iterations of initial noise and potential disorder. Ring solitons were counted algorithmically, using built-in computer vision tools in Mathematica to detect nested circular edges. A linear fit is shown in blue. The inset shows a log-log plot of the number of rings in the quasistationary state as a function of warmup-time, defined as the time over which the pumps are increased to a fixed amplitude ($P = \bar{P} = 4.2P_{th}$). A dashed blue line shows the power law t^{-2}.

We investigate this relationship by counting the number of quasistationary rings formed spontaneously from random initial noise in the presence of a small sample disorder, modelled by setting V_{ext} to a randomly distributed set of needle-like potentials, with Gaussian profile and width much smaller than the healing length of the condensate. This disorder does not hamper the formation of rings, but rather acts like sandpaper, resisting their movement across its surface. Fig. 2.5 shows the resulting linear, positive correlation between pump power and ring soliton density. To elucidate the effect of the quenching time on the defect formation, we repeated our simulations linearly increasing the pumps from zero to $P = \bar{P}$ over different timescales. The results, shown in the inset of Fig. 2.5, reveals a t^{-2} power law. We note that recent theoretical work on nonequilibrium holographic superfluids have shown qualitatively similar results: a linear dependence of excitation strength (temperature in that context) on defect (vortex) density, and a power law dependence of quench time on defect density [106]. Due to the unclear relationship between quench rate and the parameters tuned here, it is not clear how the power law exponent itself compares to theory. Here it is more important to show that there is *any* power law, which is highly suggestive of having probed the physics of interest here [94, 107]: the purpose of this section is to serve as a proposal to open the door to Kibble-Zurek type experimental probes of scalar polariton condensates, as had been thought impossible[105].

In conclusion, we have theoretically predicted the spontaneous formation of stable breathing ring solitons in exciton-polariton condensates. The proposed experimental realisation for such novel topological defects is well within the current experimental conditions and properties of existing microcavities. These structures represent the first fundamental solitonic breather and the first stable ring soliton in any quantum hydrodynamical system, and are made possible by the polariton condensates' unique combination of inherent nonequilibriation with the existence of a hot exciton reservoir which scatters particles into the condensate while repulsively interacting with condensed particles. We have shown how combining resonant and nonresonant forcing can be used to suppress the snake instability, and have discussed how the robust stability of breathing ring solitons can be exploited to study nonequilibrium defect formation statistics, and thus to probe the fundamentals of nonequilibrium phase transitions. Further, we have proposed an experimental scheme by which these statistics could be probed over the continuous crossover between equilibrium and nonequilibrium phase transitions. This work highlights the exceptional promise of exciton-polariton condensates in the highly interdisciplinary field of nonlinear pattern formation.

2.4 Polygonal Breathers

Polygon Breathers - One of the powers of polaritonic systems is that pumping can take on any optically feasible profile. We can thus consider the interesting case of spatially dependent resonant forcing, so that the degree to which the phase is symmetry broken can vary spatially.

We thus consider the scenario of a large disk-shaped region of uniform non-resonant pumping, with a resonant pump of Gaussian profile $\bar{P}\exp(-\alpha r^2)$ at the centre of that region, with α characterizing the inverse width of the pump, so that the degree of the symmetry breaking of the phase depends on the radial distance from the center of the pump. This is the most extreme when $\bar{P}$ and α are chosen such that the condensate wavefunction is forced into the phase locked regime at the centre, but can be seen to transition into the regime in which the symmetry breaking is negligible. With direct numerical integration of Eqs. 2.1-2.2, we simulate this geometry. For large α (small spot), density oscillations are driven around the center at the radius at which the condensate is in the breathing regime, forming a breathing ring.

For larger resonant pump spots however, the behavior changes drastically: as the pump spot width is increased (keeping $\bar{P}$ constant), the radius of the dark ring increases, and existing out of the bistable regime, reaches the circumference at which the ring becomes unstable to the “snake-instability", the well known phenomenon in which azimuthal modes of the annular defect shatter the dark soliton into an integer number of chiral defects [108, 14, 109]. This instability can be understood by computing the Bogoliubov modes of the dark soliton solution in a finite 2D domain: a soliton shorter than the lengthscale of a healing length has only real frequency modes, whereas for a soliton of increased length there appear a countable number of complex eigenmodes, with each corresponding to a point where a vortex antivortex nucleation will appear [108]. This instability thus naturally quantizes the number of vortex-antivortex pairs produced as a function of the ring radius. This quantization is demonstrated in Fig. 2.6, which shows the dependence of the emergent polygonal symmetry as a function of the Gaussian half-width in units of healing lengths, as determined from numerical experiments.

Once the rotational symmetry breaks after a finite number of oscillation cycles, the symmetry remains broken, and a new dynamically stable structure is formed which, though evolving dynamically, is at every time symmetric under transformations of the dihedral group D_m (the group of symmetry transformations of the polygon of degree m). Fig. 2.7 shows density profiles of two polygonal breathers at several times during their evolutions. The bottom panel of that figure shows the inner product $|\langle\psi_0|\psi_t\rangle|$ (denoting the wavefunction at time t as ψ_t) of the $m = 4$ (square-symmetric) breather, where we arbitrarily set ψ_0 to the wavefunction at the time shown in (a). This shows that the wavefunction indeed forms a closed periodic cycle once the symmetry has broken, despite the rotational symmetry of the physical system. We note that the periodicity of the breather is almost exactly equal to twice the predicted periodicity of the density oscillations studied in 0D. This period doubling comes from the broken rotational symmetry in real space:

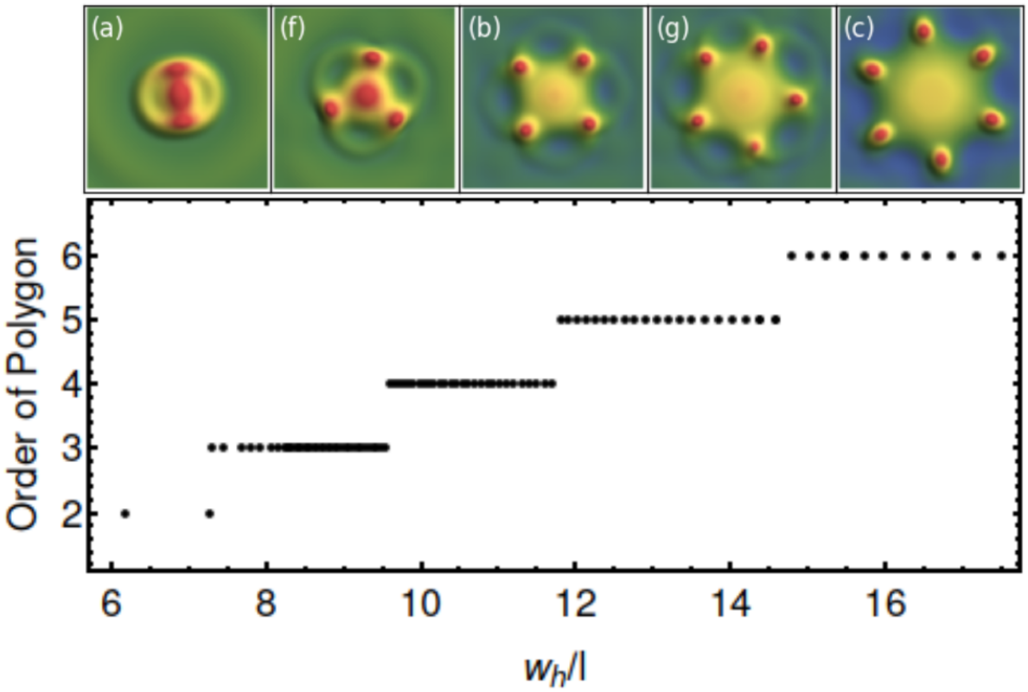

Fig. 2.6 Top: From direct numerical integration of Eqs. 2.1-2.2, density profiles exhibiting $m = \{2..6\}$ spatial symmetry, adopted spontaneously for fixed homogenous nonresonant pump ($P = 2$) and $2^{nd}-$ order resonant pumping with Gaussian profile $\bar{P}\exp(-\alpha r^2)$ at fixed strength ($\bar{P} = 15$) and varying width parameter α. Here red represents high density, while blue represents low density. Bottom: Corresponding dependence of spontaneously adopted symmetry order m on the Gaussian half-width in units of the healing length.

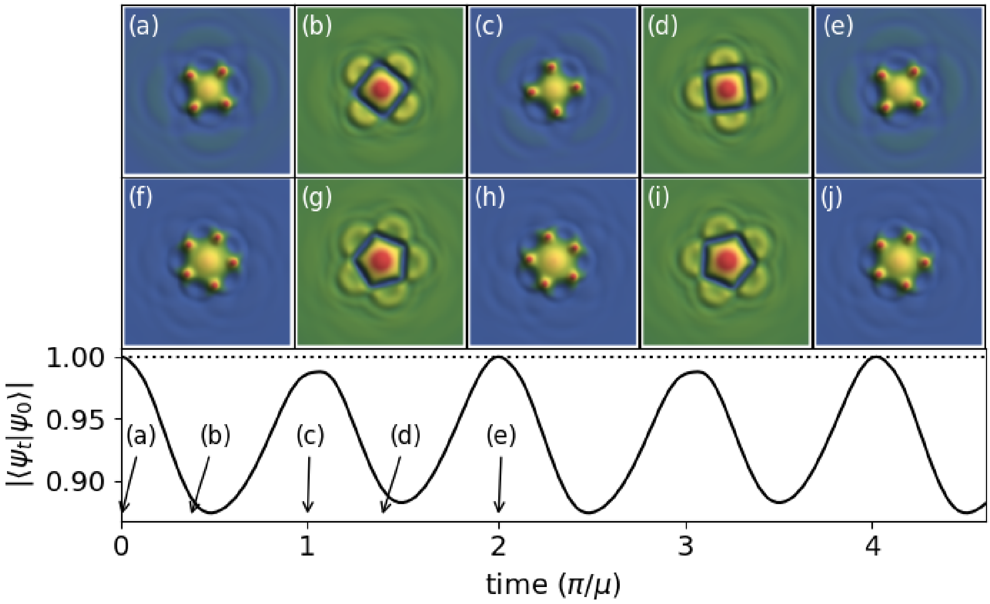

Fig. 2.7 From direct numerical integration of Eqs. 2.1-2.2, density profiles over the evolution of two breathing structures exhibiting different degress of quantized spatial symmetry breaking, under uniform nonresonant pumping $P = 2$ and a Gaussian $n = 2$ resonant pump of the form $\bar{P}\exp(-\alpha r^2)$, with $\bar{P} = 10$. (a)-(e) shows the dynamics of the breather formed when $\alpha = 0.05$, which spontaneously adopts degree-4 polygonal symmetry, and then evolves in a closed cycle: the bottom panel shows the inner product of the condensate wavefunction over time with that shown in (a), showing that the wavefunction perfectly repeats periodically (as at (e). (f)-(j) show the evolution of a degree-5 symmetric breather, formed spontaneously when $\alpha = 0.03$.

the period of the polygonal breather is $2\pi/\mu$, but up to a rotation of real space, the period is π/μ.

Orientation Glass - While these spontaneously polygon-symmetric excitations are translationally fixed by the location of a Gaussian resonant pump, they do posses a rotational degree of freedom. As breathers, the polygonal structures radiate density oscillations through the condensate, and these radiation patterns possess the polygonal symmetry of their source. We might thus imagine the emergence of orientational order in a lattice of polygonal breathers. Fig. 2.8 shows the direct numerical simulation of a condensate forced by uniform nonresonant pumping and by a square lattice of Gaussian pumps with width parameter α. When

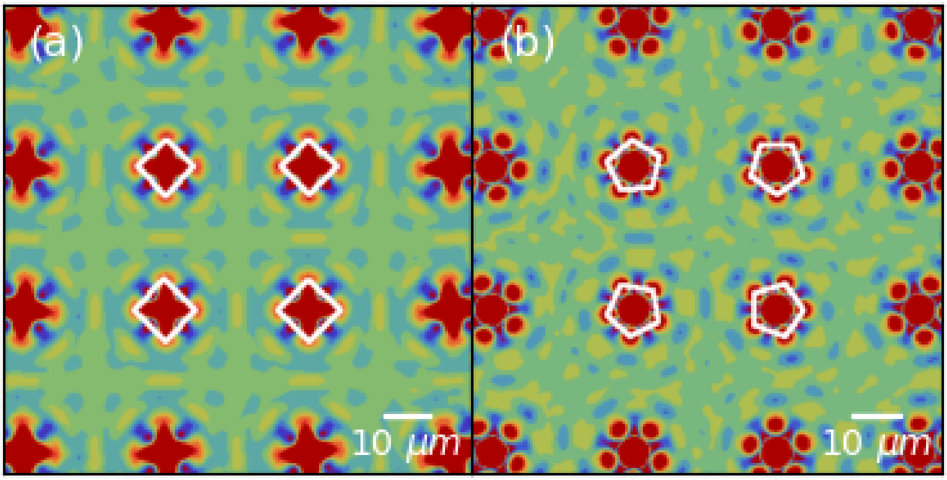

Fig. 2.8 Detail of condensate under uniform nonresonant pumping, simultaneously pumped by a square lattice of resonant pumps with Gaussian profile $\bar{P}\exp(-\alpha r^2)$. Orientations of central lattice site excitations highlighted in white. (a) Spontaneous orientational order emerges when α is chosen such that the lattice site excitations match the symmetry of the lattice. (b) A glassy ordering emerges instead when α is chosen such that the symmetry of the lattice site excitations is incommensurate with that of the lattice. $P = 1.5$ and $\bar{P} = 10$. $\alpha = 0.1$ in (a) and $\alpha = 0.075$ for (b). Lattice length is set at $35\mu m$, with periodic boundaries.

α is chosen such that the lattice sites exhibit square-symmetric excitations, the symmetries of the excitations and the lattice are commensurate and spontaneously align (a). When α is instead chosen such that the lattice sites exhibit pentagonal symmetry, the symmetries of the lattice and the lattice sites are incommensurate, causing geometric frustration resulting in a glassy state. These are the analogues of the ferromagnetic and spin glass states, but where the spin degree of freedom (parameterized by $\mathbb{Z}_n$ for discrete spins) is replaced by the polygonal orientation degree of freedom (parameterized by D_m).

2.5 Closing Remarks

In conclusion, we have introduced a generic mechanism of breather formation in nonequilibirum condensates forced by simultaneous resonant and nonresonant pumping. In the case of 2^{nd}-order resonant pumping, we have shown that this mechanism can lead to highly nontrivial dynamical behaviour, including the spontaneous adoption of unusual spatial symmetries and emergent order. I hope that the result sparks interest in the physics of condensates forced by multiple driving frequencies, and that it sheds some light on the importance of the underlying symmetries imposed by those forces, especially on emergent spatial symmetries.

Chapter 3

Multiply Charged Vortices

3.1 Introduction

From their macroscopic coherence it follows that Bose Einstein condensates (BECs) may only support rotational flow in the form of quantized vortices [110]. These vortices are thus topological in nature, and are characterized by a phase rotation of integer (ℓ) steps of 2π around a phase singularity. However, while in principle quantized vortices may take on any topological charge, in practice it is understood that only vortices of charge $\ell = \pm 1$ are dynamically stable: higher order vortices quickly shatter into constellations of unit vortices due to the energetics of the system. This shattering process has been detailed theoretically and observed experimentally in the context of stationary, harmonically trapped atomic BECs [19–21].

The case is somewhat different for superharmonically trapped, rapidly rotated condensates, for which there exists a critical rotation rate above which the vorticity of the system becomes concentrated within a single effective core. This state, in which all vorticity is within a single effective core, has been called the *giant vortex* state by its first experimental observers [23], the theoretical framework of which was then built by [24]. However, while this approach does theoretically result in the collection of vorticity into a single vortex core, such *complete* concentration of vorticity has not yet been achieved in experiments, which instead see the a giant vortex in the centre of a lattice of unit strength vortices. This precludes the study of the giant vortex in isolation, a significant blow to hopes of studying the structures in the context of analogue gravity [111]. Further, the very nature of the mechanism of vorticity concentration generates its own limitation. It is the centrifugal force from the rotation which leads to the buildup of density at the potential walls, and by extension to the low density region in the condensate centre in which the vortex cores may then merge due to their increased core size (the effect of the local density reduction) [24]. The mechanism is therefore to exert, via the same rotation which imparts vorticity, a Mexican hat potential, which in the extreme results in an annular condensate, in which the requirement for topological charge to result in a singularity at all disappears. This approach, even when performed in theory, has two issues. The first is somewhat ironic: to concentrate vorticity requires high rotation rates, producing more vortices! This essentially precludes the formation of what are potentially the most interesting objects, the stable multiply charged vortex of low or moderate vorticity, for example a doubly or triply charged vortex. The second issue is perhaps somewhat aesthetic: concentrating vorticity in the lowest density region feels like cheating!

The difficulty of forming any higher-than-unit vortex in a BEC thus remains difficult at best, and it remains an open problem to see the stability of a multiply charged vortex in isolation, or in the high-density region of a condensate, or at low (but higher-than-unit) vorticities. However, in this chapter I will show that in all of these open problems sort themselves out naturally in the polaritonic BEC, due explicitly to its nonconservation of particles.

Such giant vortex is, therefore, different from a state in which there is a single point singularity with topological charge magnitude greater than one – *multiply charged* vortex, however, in practice it is often impossible to distinguish between the two. On the one hand, the density in the vortex core is negligible, which hinders the resolution of singularity. On the other hand, the structure of interest is hydrodynamical, and thus only has meaning up to the length scales for which the hydrodynamical treatment applies. The classical field description being a long wavelength approximation of something which is in reality granular and nonclassical, the hydrodynamic description only applies down to the healing length. Singularities of like charge which are bound to within a healing length are thus, to any probe in the hydrodynamical regime, indiscernible from the theoretical *multiply charged vortex*. Thus from here on we find it useful to call all such vortex structures *multiply charged*.

In our study we focus on a BEC away from the thermodynamical equilibrium supported by continuous gain and dissipation such as polariton [40], photon [112] or magnon [113, 114] condensates. To be more specific we will use the example of polariton condensate however the results reported may be relevant to other nonequilibrium condensates.

While a polariton condensate may settle into a *steady state* (a state in which the wavefunction is time invariant up to a global phase shift), such a state is one in which dissipation is balanced by particle gain. The corollary is that steady state flows are possible. It is well understood that that the pattern forming capabilities of nonequilibrium, nonconservative systems is richer than those of equilibrium, conservative systems [115], making the polariton condensate a fascinating object with which to explore the possibility of novel quantum hydrodynamical behaviors [3].

In this chapter, we show theoretically that multiply charged vortex states can appear spontaneously and remain throughout the coherence time in a BEC of exciton-polariton quasiparticles excited by a ring-shaped laser profile, without the application of any external rotation, trapping potentials, or stirring. Previously, the spontaneous formation of multiply charged vortices of a given charge has been theoretically proposed and experimentally realised in polariton condensates by pumping in an odd number of spots around a circle [116], or by the engineering of helical pumping geometries [117]. In the first case the central vortex in this geometry is created driven by the antiferromagnetic coupling of the neighboring condensates and the frustration arising from their odd number. In the second case the helical patterns are engineered so that the condensate is pumped explicitly with orbital angular momentum. Another recent proposal has shown that phase imprinted vorticity might remain concentrated at a localized mirror defect [118], in contrast to another recent work in which nonresonant pumping with a higher-order Laguerre-Gaussian beam resulted in the clear transfer of total vorticity, while failing to form a multiply charged vortex structure [119]. Yet other works have exploited the lack of simple connectedness of condensates confined to annular traps, both in equilibrium [31] and exciton-polariton condensates [120]; in an annular condensate, rotation does not necessitate a vortex defect. Interestingly, a central multi-charged vortex was observed in a numerical study of polariton-condensates under the *weak* Mexican hat-type pump (see supplemental material of [121]). There, the particle fluxes exist from the center outwards as the pumping profile peaks at the center. As the pumping intensity increases the central vortex of small multiplicity (three in that case) breaks into the clusters of single-charge vortices trapped by the minima of the pumping potential. The multiply charged vortices we discuss in here differ from these works in the geometry considered (ring-pumped trapped condensates, long coherence times), formation mechanism (probabilistic and spontaneous during condensation, away from the hot reservoir) and the vortex properties (vortices exist on the maximum density background and so are truly nonlinear in nature). We describe their formation, stability, and dynamics. The dynamics of two and more interacting multiply charged vortices are also studied. We find that our results apply for a wide range of possible experimental parameters, suggesting that these structures are general to ring-pumped trapped polariton BECs in the strong coupling regime.

The dynamics of the polariton BEC in the mean field are described by the complex Ginzburg-Landau equation (cGLE) coupled to a real reservoir equation representing the bath of hot excitons in the sample, restated for this chapter as:

$$i\partial_t \psi = -(1 - i\eta N_R)\nabla^2\psi + |\psi|^2\psi + gN_R\psi + i(N_R - \gamma)\psi \tag{3.1}$$

$$\partial_t N_R = P - (b_0 + b_1|\psi|^2)N_R, \tag{3.2}$$

3.2 Spontaneous Formation

Polaritons can be confined all-optically by shaping the excitation laser beam. By using spatial light modulators to shape the optical excitation, ring shaped confinements were generated with condensates forming inside the ring [92, 122], and have been predicted to support the spontaneous formation of unit vortices [123]. Long-lifetime polaritons in ring traps are emerging as a platform for studies of fundamental properties of polariton condensation largely decoupled from the excitonic reservoir and, therefore, having significantly larger coherence times [124–127]. We represent the profile of the ring pump by a Gaussian annulus of the form $P(r,\theta,t) = Pe^{-\alpha(r-r_0)^2}$ with inverse width α and radius r_0, which excites local quasiparticles which then flow outward. The closed-loop pump geometry has two major implications. The first is that the condensation threshold is first achieved not where the sample is pumped, but *within* the borders of the pumping ring. This results in the effective spatial separation of Eqs. (3.1-3.2), which makes the parameters related to the excitonic reservoirs such as b_0, b_1, and g irrelevant to the condensate dynamics up to a change of pump strength. The second and most critical implication of the ring pump geometry is the existence of constant fluxes towards the centre of the ring. Such fluxes carry the matter together with spontaneously formed vortices and force vortices to coalesce.

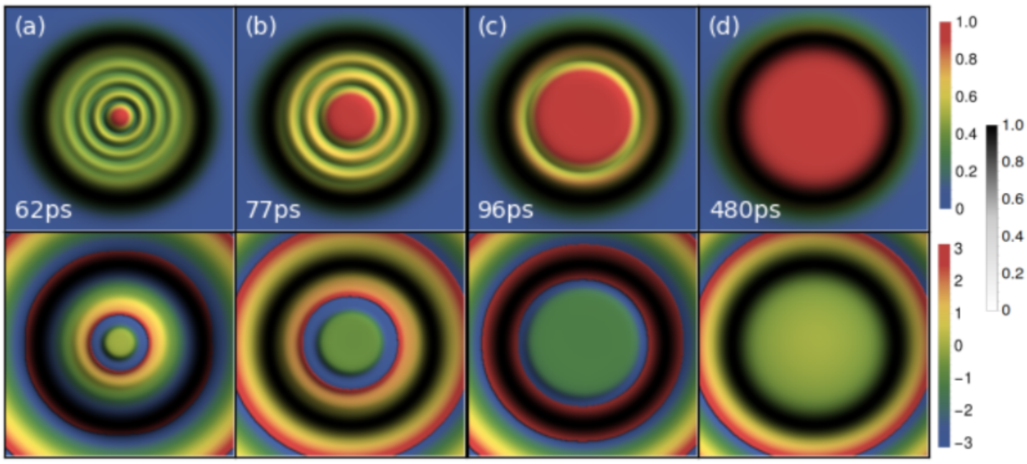

Fig. 3.1 Formation of a non-vortical, flat-disk shaped condensate within a ring pump, from numerical integration of Eqs. (3.1-3.2). Density (top row) and phase (bottom row) snapshots are shown at various stages of the condensate formation. For clarity, each density profile is rescaled to unit maxima. The pumping profiles are superposed in black (in units of P), showing the spatial separation between the pump and the condensate. At the beginning of the condensate formation; due to the pump geometry, matter wave interference leads to annular zeros in the wavefunction (a). These ring singularities are theoretically unstable to dynamical instabilities, but here they extend to the condensate boundary before instabilities take over (b,c), and a nearly uniform condensate fills the region circumscribed by the ring pump (d). Here $P = 5$ and $r_0 = 10\mu m$. In this chapter all simulations use zero boundary conditions, and are calculated with 4th order extrinsic Runge Kutta methods, in which mesh size is set to be at least several times smaller than the healing length.

It is well known that vortices can form during the rapid condensation of a Bose gas, via the Kibble-Zurek mechanism [96–98, 95, 94, 99–102, 104]. However, in our system there exist a different mechanism of spontaneous defect generation in our system, which requires a relatively *slow* condensate formation. Due to the inward flow of particles in our system, the condensation threshold is reached first in the center of the system. Assuming a large enough ratio of new particle flow to dissipation, this young condensate will grow into a relatively uniform disk within the boundary of the pump. However, in between these two stages, radial matter wave interference is to be expected, with higher frequency during the early stages of condensation. The zeros of the radial interference pattern are well studied under a different name: the dark ring soliton [87, 115, 65]. As has been shown previously, these dark solitons are unstable to transverse (‘snake’) perturbations, and break apart into pairs of unit vortices of opposite charge [109, 128]. Thus for a slowly condensing system, it is reasonable to expect that these solitons have enough time to break down to produce a chaotic array of vortex singularities. This process resembles a two-dimensional case of the collapsing bubble mechanism of vortex nucleation [129]. As the condensation process completes and the vortex turbulence decays, there is some finite chance of the condensate being left with a net topological charge, as vortex pairs may unbind near the boundary and one or the other may leave to annihilate with its image. These like-charged vortices would then coalesce in the center of the condensate.

Direct numerical integration of Eqs. (3.1-3.2) not only confirms that this process can take place, but that for low pump power, the condensate takes on a net topological charge more often than not [1]. We reiterate that this coalescence of vortices is despite the lack of external rotation, or sample nonuniformity. Repeating the numerical experiment with many iterations of random initial wavefunction noise, we find multiply charged vortex states of stochastic sign and magnitude. The average topological charge magnitude is found to depend significantly on the radius of the pump ring, increasing for larger radii. An example of these dynamics is presented in Fig. 3.2, which shows the main steps in the process by which the condensate spontaneously adopts a topological charge of two: the formation of a central condensate surrounded by annular discontinuities in Fig. 3.2(a), the breakdown of an annular discontinuity into vortex pairs in Fig. 3.2(b), vortex turbulence in Fig. 3.2(c), and the final bound vortex state Fig. 3.2(d). For Fig. 3.2 we use the system parameters $\eta = 0.3$, $\gamma = 0.05$, $g = 1$, $b_0 = 1$,

[1] The initial wavefunction is set to a profile of low amplitude random noise. All simulations are repeated for many of these profiles.

$b_1 = 6$, but the result was found not to depend sensitively on these choices; up to a rescaling of pump strength this behavior was reconfirmed for a large range of sample parameters: $g \in [0.1-2]$, $b_0 \in [0.01-10]$, for $\gamma \in [0.05-0.1]$, and for all reasonably physical values of η (including $\eta = 0$.)

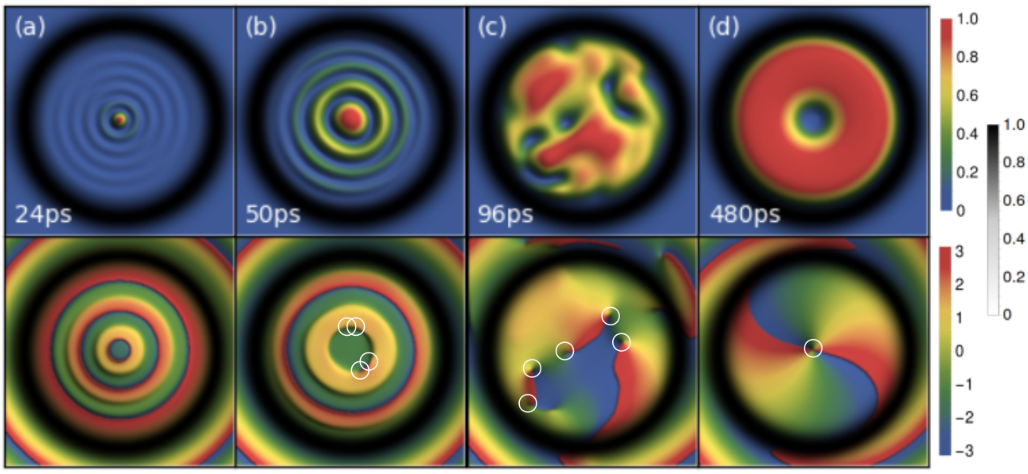

Fig. 3.2 Spontaneous formation of a multiply charged quantum vortex in a ring pumped polariton condensate by numerical integration of Eqs. (3.1-3.2). Density (top row) and phase (bottom row) snapshots are shown at various stages of the condensate formation. For clarity, each density profile is rescaled to unit maxima. The pumping profiles are superposed in black (in units of P), showing the spatial separation between the pump and the condensate. At the beginning of the condensate formation; due to the pump geometry, matter wave interference leads to annular zeros in the wavefunction (a). These ring singularities are unstable to dynamical instability, become asymmetrical (b) and can be observed to break into more stable unit vortices (locations marked with white circles) in as the condensate continues to develop. The condensate fills a disk shaped region with near uniformity within the ring pump, but remaining vortices interact chaotically in (c). The vortex turbulence eventually decays, leaving a net topological charge [130, 131]. The vortex charge is equal to the number of 2π phase windings around the singularity; here the final vortex has charge two. Repeating these simulations with different random initial conditions, the magnitude and sign of the final vorticity varies. Here $P = 5$ and $r_0 = 10\mu m$.

An advantage of the spatial separation of the condensate from the reservoir in ring pumped geometry is in the enhanced coherence time that exceeds the individual particle lifetime by three orders of magnitude [132]. Therefore, spontaneously created multiply charged vortices might soon be observable in single shot experiments within one condensate realisation. However, for now only the average wavefunctions of many iterations of the stochastic condensate formation are observable in experiment. In a perfectly uniform sample, one would expect an equal chance of the stochastic formation of vortex charges of either handedness, which would cancel in the experimentally observable mean wavefunction. However, it has been established in experiments that the slight inhomogeneities inherently present in all physical samples act to favor one handedness over the other [116]. Thus the only experimental observable is the mean *magnitude* of the vorticity distribution. This magnitude is well above zero for a wide range of parameters [2] , making the experimental observation of this effect highly feasible within the current state of the art.

3.3 Stability and Form

Another way to study the multiply charged vortices is to imprint them explicitly upon a fully formed, uniform condensate [53]. This allows for the study of the structure and dynamics of carefully controlled systems of vortices. To model the result of experimental pulsed phase imprinting, we first model the formation of fully developed non-singular condensate disks. To prevent the spontaneous formation of vortices by the process described above, a relatively strong pump amplitude is used, so that the condensate forms too quickly for the decay of ring-singularities into vortices. After the background condensate is formed, phase singularities are imprinted instantaneously and their dynamics is observed. To first understand the structure of isolated multiply charged vortices, we imprint a series of condensates with different topological charges, and allow these structures to form steady states. When imprinted in equilibrium BEC, multiply charged vortices quickly break into vortices of a single unit of quantization [133].

[2]For example: mean vorticity amplitudes determined from direct simulations of Eqs. (3.1-3.2) for pump radius $12\mu m$ tends linearly from 2.5 to 4.9 as the pump strength is decreased from $P = 9$ to $P = 5$.

From the spatial separation of the condensate and the reservoir, the reservoir density is negligible near the central core of the multiply charged vortex, so that Eq. (3.1) takes the familiar form of the damped nonlinear Schrödinger equation (dNLSE): $i\partial_t\psi = -\nabla^2\psi + |\psi|^2\psi - i\gamma\psi$.

Under the Madelung transformation $\psi = \mathscr{A}\exp[iS - i\mu t]$ where μ is the chemical potential, the velocity is the gradient of the phase S: $\mathbf{u} = \nabla S$ and the density is $\rho(r) = \mathscr{A}^2$, the imaginary part of the dNLSE yields $\nabla\cdot(\rho\mathbf{u}) = -\gamma\rho$. Except for a narrow spatial region where the density heals itself from zero to the density of the vortex free state the density is almost a constant, so the radial component of the velocity becomes $u_r = -\gamma r$. The real part of the dNLSE reads

$$\partial_r^2\mathscr{A} + \partial_r\mathscr{A}/r + (\mu - \mathbf{u}^2 - \mathscr{A}^2)\mathscr{A} = 0, \tag{3.3}$$

which coincides with the corresponding steady state equation for the equilibrium condensates where velocity profile plays the role of the external potential. We therefore expect the structure of the vortices to be similar to those in equilibrium condensates with the external potential given by $\mathbf{u}^2$. Close to the centre of the condensate the velocity becomes $\mathbf{u} = -\gamma r\hat{r} + \frac{\ell}{r}\hat{\theta}$, where $\hat{r}$ and $\hat{\theta}$ are unit vectors in polar coordinates. When this expression for $\mathbf{u}$ is substituted into Eq. (3.3) it becomes the equation on the vortex amplitude in the centre of the harmonic trap, where γ characterises the frequency of the “trap." In the vortex core, for small r, the centrifugal velocity dominates the radial velocity, so the equation on the rescaled amplitude $A = \mathscr{A}/\sqrt{\mu}$ with $\tilde{r} = \sqrt{\mu}r$ becomes

$$\partial_{\tilde{r}^2}A + \partial_{\tilde{r}}A/\tilde{r} + \left(1 - \frac{\ell^2}{\tilde{r}^2} - A^2\right)A = 0. \tag{3.4}$$

The profiles A take the approximate form

$$A = \frac{\tilde{r}^{|\ell|}}{(\tilde{r}^n + w)^{|\ell|/n}}, \tag{3.5}$$

with parameters w and n in which we incorporated the power expansion behaviour of the amplitude $A \sim \tilde{r}^{|\ell|}$ as $\tilde{r} \to 0$. Figure 3.3 shows the amplitude cross-section profiles of stable giant vortices with different topological charges $\ell \in \{1,2,...,10\}$ as the solutions of Eq. (3.4), along with Eq. (3.5) , showing a compelling fit between vortex profiles seen in the full numerical simulations of the coupled condensate-reservoir system (without an external trap) and those of the steady state solutions of an equilibrium condensate under harmonic trapping, as predicted by our theory.

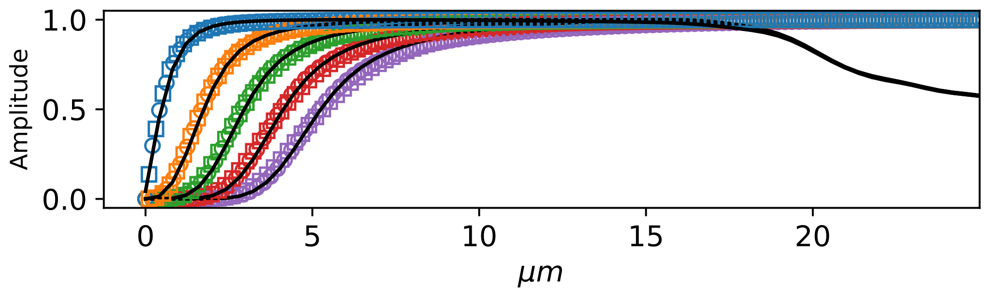

Fig. 3.3 Wavefunction amplitude cross sections $\sqrt{\rho(r)}$ of multiply charged vortices. For clarity, and without loss of generality, we show only odd topological charges less than $\ell = 10$. Profiles from the full numerical integration of Eqs. (3.1-3.2) (normalized) for $r_0 = 20\mu m$, $P = 12$, and $\gamma = 0.3$ are shown in black, and illustrate the decay of the condensate near the pump ring (outside shown frame, the condensate density continues to decay to zero). The numerical solutions of the reduced equation Eq. (3.4) are marked by circles colored by charge, and the corresponding fits to the ansatz Eq. (3.5) by squares with matching colors. From these fits, we can write the approximate parameterization of Eq. (3.4) as $n(\ell) = (1.1)\ell^{1.6} - 2.8$ and $w(\ell) = 2.3 + (0.6)ln(\ell))$.

We have shown above that the inward fluxes necessitated by the closed pumping geometry result in an effective trapping potential - independent from any effective trapping from the reservoir near the edge of the condensate - which drives the vortices closer together. Our analysis above, which shows that the forces from the inward fluid fluxes overcome the topological repulsion of like-signed vortices, applies when the condensate is nearly uniform, which is the case until the vortices begin to overlap. At this stage there is a further interaction between vortices: it has long been understood that in nonequilibrium systems the topological repulsion of like-signed vortices can be balances due to the nontopological force emerging from the effective variations in the supercriticality stemming from the density decrease surrounding the defects [18]. The variable-supercriticality force is negligible until the vortices are close enough for significant overlap between their associated density structures. In our system, the radial flux forces bring the vortices of like sign to within the regime at which they may bind to form a multiply-charged vortex.

3.4 Acoustic Properties of the Multiply Charged Vortex

Next we consider the arrangements of multiple multiply charged vortices imprinted away from the trap center and brought together by the radial fluxes. Fig. 3.4 shows two examples of the coalescence dynamics of imprinted phase defects. In the first case, three unit vortices coalesce while moving in inward spirals towards the center of the condensate, where there is no net lateral flow. In the second case, which shows the coalescence of two doubly charged vortices, it is observed that both doubly charged vortices hold together for a while before merging in the center to form a single vortex of multiplicity four. These results are found to be repeatable for a wide range of system parameters, suggesting that this behaviour is to be expected for any system parameters which allow the formation of the trapped condensate within a ring pump. We note that in this system, the center of the condensate corresponds to the location of maximum background fluid density, in stark contrast to systems designed to collect virtual vorticity into a low-density area [31].

As two (or more) vortices merge while spiralling around the center they excite density waves in the otherwise uniform background fluid. These acoustic excitations are long lived, and take on a frequency set by the angular frequency of the vortex spiral. For well separated vortices, this frequency increases consistently as time progresses and their separation shrinks. However, as the vortices begin to share a these dynamics become even more complicated and the new physics dominated by the processes in the vortex core emerges [134].

Figure 3.5 shows the relative amplitudes of the density waves radiated during the motion of two vortices of unit charge imprinted with a large initial separation. Density waves are sampled directly from densities in direct simulations, using sample regions near the condensate edge. The average frequency of ”acoustic”[3] radiation is found to increase with time at a fixed rate until the vortex cores begin to overlap (left vertical line). During this phase, the frequency distribution narrows and the average radiation frequency increases linearly at a much lower rate than in the well-separated vortex regime. This continues until the singularities within the core overlap within a healing length (right vertical line), after which a fixed narrow band of acoustic radiation is emitted. As shown in Fig. 3.5, the narrowband acoustic emission dominates the "surface wave" physics of the system.

Of course, multiply charged vortices may also collide: we find that from merger of two equal multiply charged vortices of increasing topological charge, the characteristic acoustic resonances have decreasing frequency, in the near-terahertz regime. This is because the effective mass of the vortex increases with topological charge, so that vortices of larger multiplicity orbit more slowly. As expected, we see that in contrast, when multiple singly charged vortices placed

[3]Here we use acoustic to refer to soundlike density oscillations.

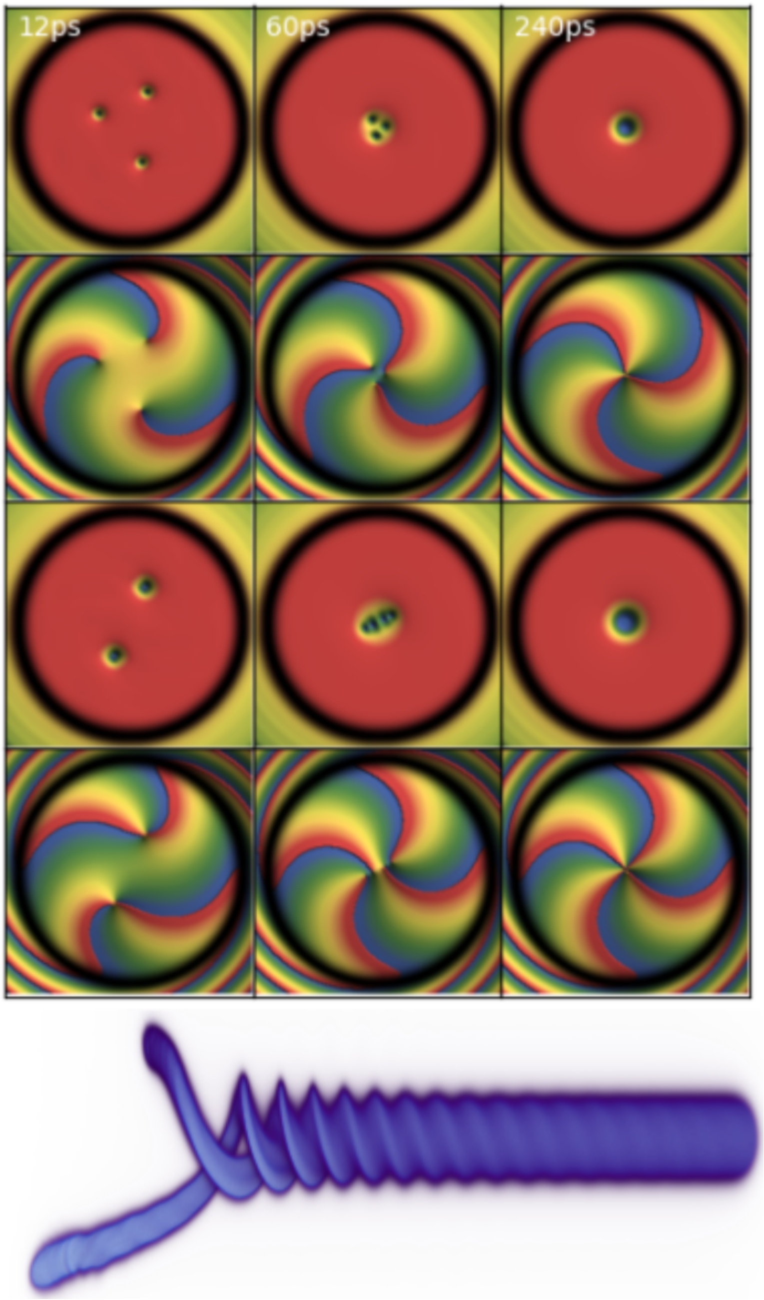

Fig. 3.4 From Top: Density (first row) and phase (second row) resolved dynamics of three unit vortices of like charge in a condensate formed within the boundary of an annular pump (green). Over time, the three vortices approach each other in an inward spiral, eventually merging to an inter-singularity length scale less than the healing length of the condensate. Density (3rd row) and phase (4th row) of two doubly charged vortices (each having topological charge $n = 2$), which over time merge into a single fourth-order vortex. Here $P = 10$ and $r_0 = 15\mu m$. Colour scales are the same as in Fig. 3.2. At bottom, a density isosurface of the two merging second-order vortices, with time shown along the horizontal axis , from 12 ps (left) to 240 ps (right).

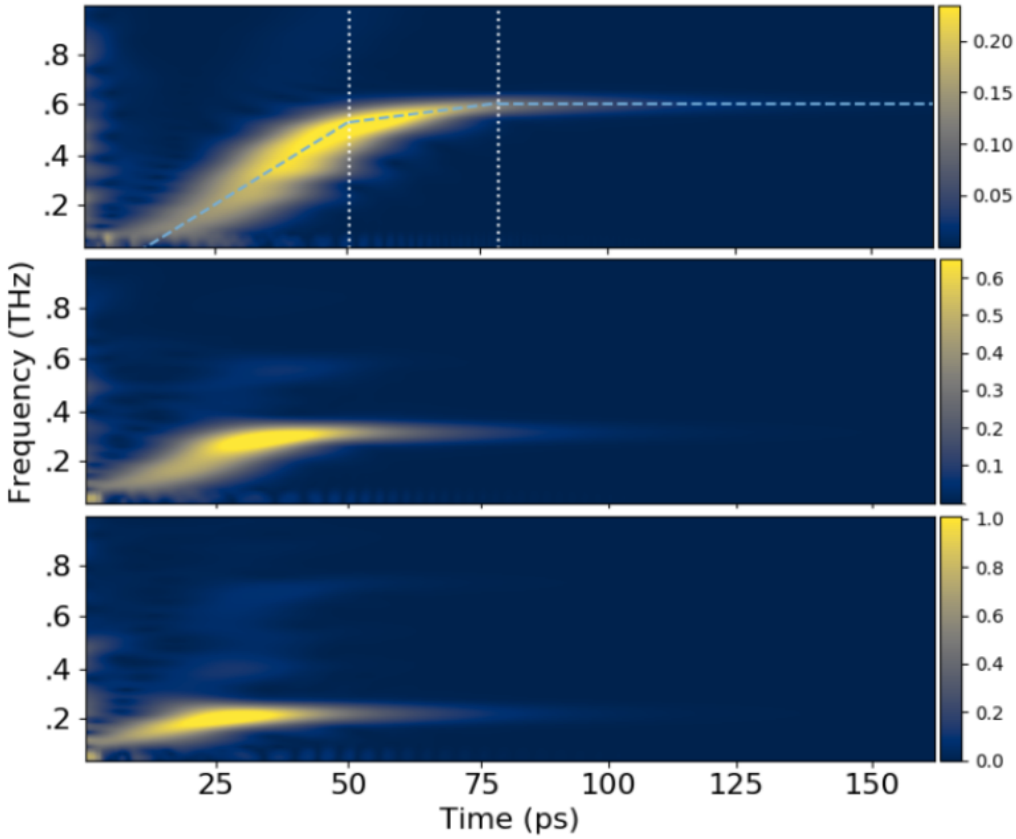

Fig. 3.5 Power spectral density of acoustic waves radiated by the approach and merger of two vortices, resolved in time-frequency space. Top panel shows the merger of two unit vortices, and vertical lines mark the time of transition from well separated vortices to vortices sharing a common low-density core (left) and the time at which the singularities have merged to within a healing length (right). Middle and bottom panels show the acoustic spectra of two merging doubly charged vortices (middle) and two merging triply charged vortices (bottom). The ring pump radius is $20\mu m$. In the case of two single vortices, one vortex is imprinted at the condensate center, and the other at a distance of $18\mu m$ from the center. In the cases of two multiply charged vortices, both vortices are imprinted $18\mu m$ from the center.

evenly about a common radius merge, they emit higher frequency radiation as the number of unit vortices is increased. Once the multiply charged vortex has formed and is allowed to settle, low energy density perturbations can be applied to the condensate. To model this, we simulate the effect of a small Gaussian laser pump pulse centered on the vortex. The observed effect is the emission of an acoustic energy pulse at the characteristic frequency of the vortex, as is seen in from the merger of the equivalent number of unit vortices. As in any physical system there exist many small perturbations due to intrinsic disorder, it is likely that multiply charged vortices in a real system are regularly being excited and emitting acoustic radiation. The amplitude of these density oscillations were found to start on the order of 1% of the density, decreasing exponentially over time. This makes experimental observation, while certainly not easy, not out of the realm of possibility.

3.5 Nonconservative Kelvin-Helmholtz Instability

Next we will establish the limit on the vortex multiplicity that the trapped condensate can support. This limit is set by the maximum counterflow velocity that can be supported between the condensate and the reservoir, therefore, is determined by the onset of a Kelvin-Helmholtz instability (KHI). KHI is the dynamical instability at the interface of two fluids when the counterflow velocity exceeds a criticality. It appears in variety of disparate systems, both classical and quantum, but has never been discussed in the context of the polaritonic systems. In quantum fluids KHI manifests itself via nucleation of vortices at a counterflow velocity exceeding the local speed of sound $v_c = \sqrt{\frac{U_0 \rho}{m}}$. It has been extensively studied for the interface between different phases of ^{3}He [135], two components in atomic BECs [136] or for the relative motion of superfluid and normal components of ^{4}He [137, 138]. In trapped condensates considered here, the counterflow is that between the con-

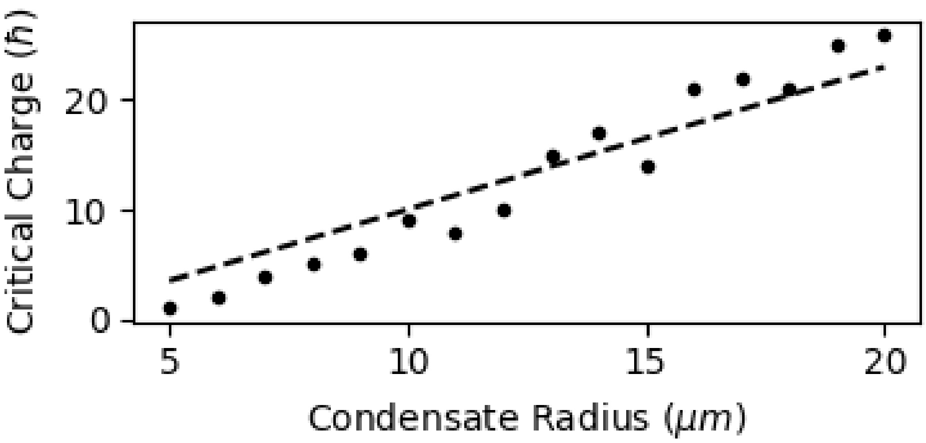

Fig. 3.6 Plotted is the critical topological charge at which the KHI sets in, as a function of pump radius. This is obtained by the direct numerical simulations of Eqs. (3.1-3.2). The dashed line represents the theoretical expectation of Eq. 3.6.

densate of radius R (which rotates with velocity $\frac{\hbar}{m}\frac{|\ell|}{R}$ at the boundary), and the reservoir particles along the ring, that are stationary. Thus it is expected that KHI should be initiated when the topological charge of the multiply charged vortex state is high enough so that the velocity of condensate particles at the ring pump radius reach v_c. Thus the maximum topological charge ℓ_c allowed is set by

$$|\ell_c| = \frac{\sqrt{R^2 m U_0 \rho}}{\hbar}. \tag{3.6}$$

Fig. 3.6 shows Eq. 3.6 (dashed line) along with the critical topological charges found by direct numerical integration of Eqs. (3.1-3.2) (dots). In these numerical experiments, we begin with a fully developed, vortex-free condensate. A unit topological charge is imprinted in the center of the condensate, and the system is allowed to settle, before another unit charge is added. This process is repeated until the onset of the KHI leads to the vortex nucleation followed by annihilation of vortex pairs and, therefore, by the reduction in the topological charge of the system. This dynamical process is shown in Fig. 3.7. We note that the question of the critical velocity in superfluids is always a subtle one. Even in the simplest case of a homogeneous, zero-temperature, equilibrium superflow around a 2D disk as first studied in [139], both numerical and experimental data fluctuate significantly around the analytical prediction of criticality [140]. Thirty years later, there has not been a significantly better analytical estimate. Still, though we have a much more complicated nonequilibrium system on a nonuniform background with a nonuniform reservoir, our numerical data as compared to the analytical estimate is rather accurate and shows the correct trend. Thus while there are certainly higher order corrections to make to the analytical treatment of this system (as they remain to be made in simpler equilibrium systems), the result presented here has shown substantial evidence that the simple underlying physics of the instability are the same in a nonequilibrium system. Further, we have shown that this fundamental instability can not only be engineered to appear in polariton condensates, but that it serves as a basic mechanism of capping vorticity.

In conclusion, we have shown that exciton-polariton condensates excited by an annular pump can spontaneously rotate despite a uniform sample and no angular momentum applied, forming multiply charged vortices. The formation, dynamics and structure of these vortices were studied. We would like to emphasise that the Kelvin-Helmholtz instability mechanism is quite specific to the ring-like pumping configuration we considered. In the gain-dissipative condensate systems, the particle fluxes exist even in the steady state connecting the regions where they are predominantly created to the regions where they are predominantly dissipated. With the ring-like pumping, the fluxes are oriented strictly towards the center stabilizing the multiply-charged vortex while preventing the formation of localised vortex clusters elsewhere. When other pumping profiles are considered, a more complicated flux distribution emerges. In some localised parts of the sample radial fluxes may exist similar to our ring-like pumping but much weaker and less controllable. This may create conditions for the formation of multiply-charged vortices, but of rather small multiplicity and that are quickly destroyed by the

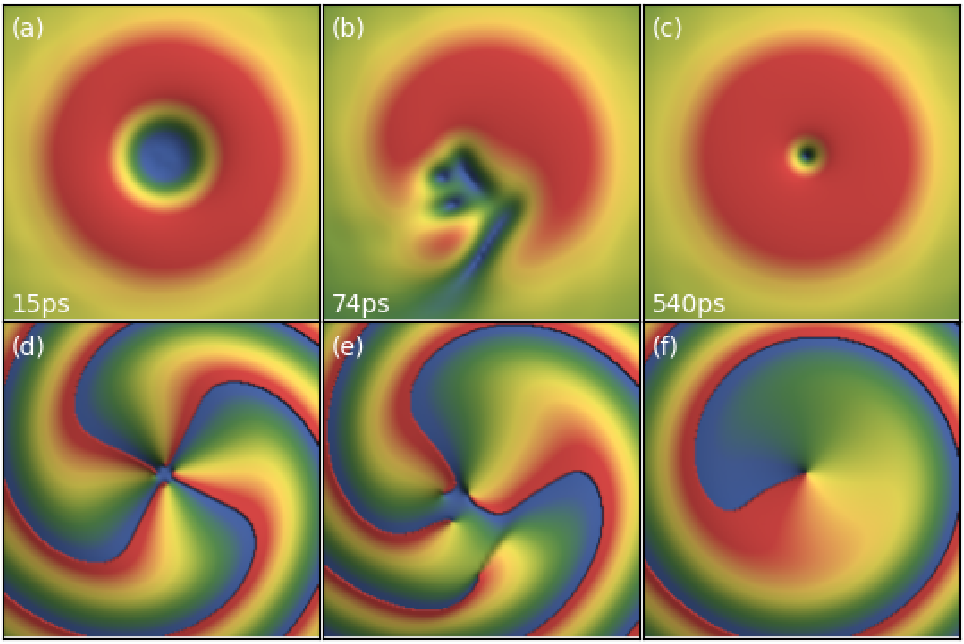

Fig. 3.7 For a great enough topological charge (compared to the size of the condensate), the rotational flow at the boundary of the condensate reaches the critical velocity for the Kelvin-Helmholtz instability to set in, which results in the reduction of topological charge via the nucleation of new vortices, with charges opposite to that of the multiply charged vortex and further pair annihilation. Shown are density profiles from a direct simulation of Eqs. Eqs. (3.1-3.2) exhibiting this process (radius $7\mu m$,$P = 10$). The initial topological charge is imprinted one quanta at a time, and the dynamics observed. After the fourth quanta of rotation is imprinted, the system loses stability and expels some rotation through the KHI mechanism, ending with unit topological charge.

small changes in parameters (e.g. pumping intensity or the pumping spot size). For instance, a Mexican hat pumping profile in [121] gives rise to the outward particle fluxes from the center in addition to the inward fluxes from the annular pump, so a vortex of small multiplicity (two or three) is destroyed as the pumping intensity is increased, instead bringing about clusters of vortices stabilized where the fluxes from the center meet the radially inward fluxes. This destruction of the multiply-charged vortices in this and similar cases can not be attributed to the Kelvin-Helmholtz instability.

Chapter 4

Nonconservative Turbulence

4.1 Introduction

The phenomenon of turbulence is ubiquitous in nature, but its quantitative understanding is a notoriously difficult problem. Turbulence occurs in many everyday fluids as well as in exotic systems such as plasmas and quantum fluids. The quantization of vorticity in the latter leads to significant differences between the dynamics of quantum and classical turbulence. However, at large Reynolds numbers the motion of well–separated vortices in incompressible classical flows can have similar features to superfluid turbulence: in this case the turbulent vortex dynamics of superfluids are nearly classical, being well described by the classical Biot-Savart law. As such, the behavior of superfluid turbulence has been extensively studied [141]. However, polaritonic systems hold promise of a distinct form of quantum turbulence, in which the particle number of the condensate is itself changing chaotically as a feature of its turbulent dynamics: unlike other quantum fluid systems which see turbulence decay and which must see continued stirring or other energy input to sustain turbulence, here the fluid itself is decaying and must be replaced, and as I will show, sustained turbulence may be a self-generated state.

Further, superfluid turbulence is not the only type of turbulent behavior seen in quantum fluidic systems. It has been shown somewhat recently that by introducing an external oscillatory perturbation to a trapped atomic Bose-Einstein condensate (BEC), it becomes possible to obtain a large number of disordered vortices [76], the dynamics of which differed dramatically from the vortex dynamics observed in both classical *and* superfluid turbulence. In that system, the characteristic distance between vortices is comparable to the size of its core; because of this, the chaotic behaviour of the system extends down to the length scale of single vortices which are therefore not well structured and thus do not obey the Biot-Savart law for intervortex interactions (which severely complicates the treatment of interactions; for one, compressibility can no longer be neglected). Together with the system of [76] being in a strongly non-equilibriated state, this represented a novel and highly nontrivial regime of turbulent behavior, called *strong* turbulence.

As with other nonlinear systems such as plasmas, classical fluids and nonlinear optics, there exists, beyond the regime of strong turbulence, the regime of *weak* turbulence, in which the dynamical structure of the system extends to *beneath* the length scale of single vortices, so that the phase structure of the complex wavefunction is effectively destroyed, becoming essentially random. Weak turbulence is thought to play an important role in the kinetics of Bose-Einstein condensation, with it having been shown that a strongly non-equilibrium Bose gas evolves from the regime of weak turbulence to that of superfluid turbulence, via states of strong turbulence in the long-wavelength region of energy space [103].

Recently all three regimes (superfluid, strong, and weak turbulence) were observed at different temperatures in 2D cold atomic gases, showing a universal scaling [142]. It has, however, remained an important open question whether it is possible to force a condensate system to pass through these stages in a reverse order. The purpose of this short chapter is to demonstrate that polariton condensates, given their inherent far-from-equilibrium nature, allow for just this:

we will see that the mean inter-vortex spacing, in units of healing length, can be tuned *continuously* from the well separated vortices of the superfluid regime, to the regimes of strong and then weak turbulence.

Towards Polaritonic Turbulence

The mechanisms of vortex generation and turbulence in equilibrium condensates are quite well known: examples include the energy exchanges between rarefaction pulses [143], the supercritical flow past barriers [139], and the modulational instabilities of density variations such as with the breakdown of dark solitons into vortices [144–146, 129, 109], and some of these mechanisms are known to produce vortices in polariton condensates as well. For instance, the flow of exciton-polaritons about a spatially extended defect can produce vortex pairs of opposite circulation depending on the flow velocity [147]. In the third chapter of this thesis, we showed that vorticity can also be spontaneously generated via the breakdown of dark solitons [4]. However, by nature of being permanently out-of-equilibrium and thus being characterised by persistent particle fluxes, polariton condensates can form vortices by *distinct* mechanisms as well. For instance, an inhomogeneity of the pump or the potential can form steady currents which can produce vortices through a pattern forming symmetry breaking mechanism [45].

As discussed already in the preliminary chapter, the formation of vortices in polariton condensates has been demonstrated in a number of experiments, and via various mechanisms. However, the observation of polaritonic turbulence has remained elusive. Various pump geometries have been used to experimentally generate vortices in polariton condensates [148, 149], and with four pumping spots arranged in a square grid it was observed that the vortex locations fluctuate, but remain very close to stationary pinning points [148]. A more disordered formation of vortices was experimentally demonstrated by the pumping of a cavity sample which possessed a random potential [52].

A fundamental issue in any experiment involving polaritonic turbulence is that chaotic dynamics are not resolvable in time with current technology: dynamical evolutions of polaritonic systems are observed in experiment by repeating the experiment many times, each time recording single-time data at slightly later moments in the dynamics. In this way the dynamics of a repeatable process are time resolved. For a behaviour as chaotic as turbulence, this is not possible, and experimentalists are restricted to measuring time-integrated wavefunctions. Thus, even when a turbulent state may exist in polariton condensate systems, it is not obvious how one might demonstrate the signatures of that turbulent state.

4.2 Modeling Experiments

Recently the Advanced Photonics Lab in Lecce, headed by Dr. Daniele Sanvitto, performed experiments which recorded the time-integrated wavefunctions of a polariton condensate fed by a single Gaussian pump, on a semiconductor sample with a naturally inhomegeneous surface structure. Intuitively, we should expect the nucleation of vortices from a large enough flow past the disordered potential barriers/wells, and for a larger flow might expect turbulence.

The Lecce group has shared their unpublished experimental results with us, and has kindly allowed me to discuss it here. In this section I will repeat their physical experiment in the form of a numerical experiment, and will show that their data is consistent with having recorded the time-integrated wavefunctions of polaritonic turbulence. As it stands, the experimental data that I discuss here is the only of its kind, and is thus the only experimental data point with which to ground our theories.

We begin by modeling the Lecce experiment geometry: we consider a single Gaussian pump of the form $P = P_0 \exp(-wr^2)$, where w is a width parameter, and introduce a disordered potential in a region displaced from the central pump spot. Our disordered potential is composed of a sum of many randomly parameterized Gaussian potentials, the locations of which are randomly distributed about square lattice positions, so as to prevent the overlap of randomly placed inhomogeneities; the parameters of the disordered potential (for example the distribution of inhomogenuity widths) are chosen to approximately match the experimental sample. For convenience we restate our model as

$$\begin{aligned} i\partial_t \psi &= -(1 - i\eta N_R)\nabla^2 \psi + |\psi|^2 \psi + g N_R \psi + i(N_R - \gamma)\psi, && (4.1) \\ \partial_t N_R &= P - (b_0 + b_1 |\psi|^2) N_R, && (4.2) \end{aligned}$$

with all quantities defined to match the experimental parameters of the Lecce experiments [1].

The behavior of the system depends critically on pump strength. For low pump strengths, we observe the formation of vortices which are pinned to the local minima of the potential and remain stationary, as in the experimental work of Lagoudakis et al. [52]. As the pump strength is increased, the positions of these vortices begin to fluctuate, as was seen in the experiments of Tosi et al. [148] (though for a different system geometry). As the pump strength is further increased, vortex fluctuations become great enough that the vortices are freed from the local minima of the potential where they had been trapped, and interact chaotically; this represents the creation of a turbulent state of the polariton condensate.

The behaviour we see in our numerical simulations is consistent with the experimental results. The experimental images (necessarily time-averaged) are

[1] In this chapter, the parameter values in our simulations are fixed to $g = 1.1$, $b_0 = 1$, $b_1 = 6$, $\gamma = 0.01$, and $\eta = 0.3$

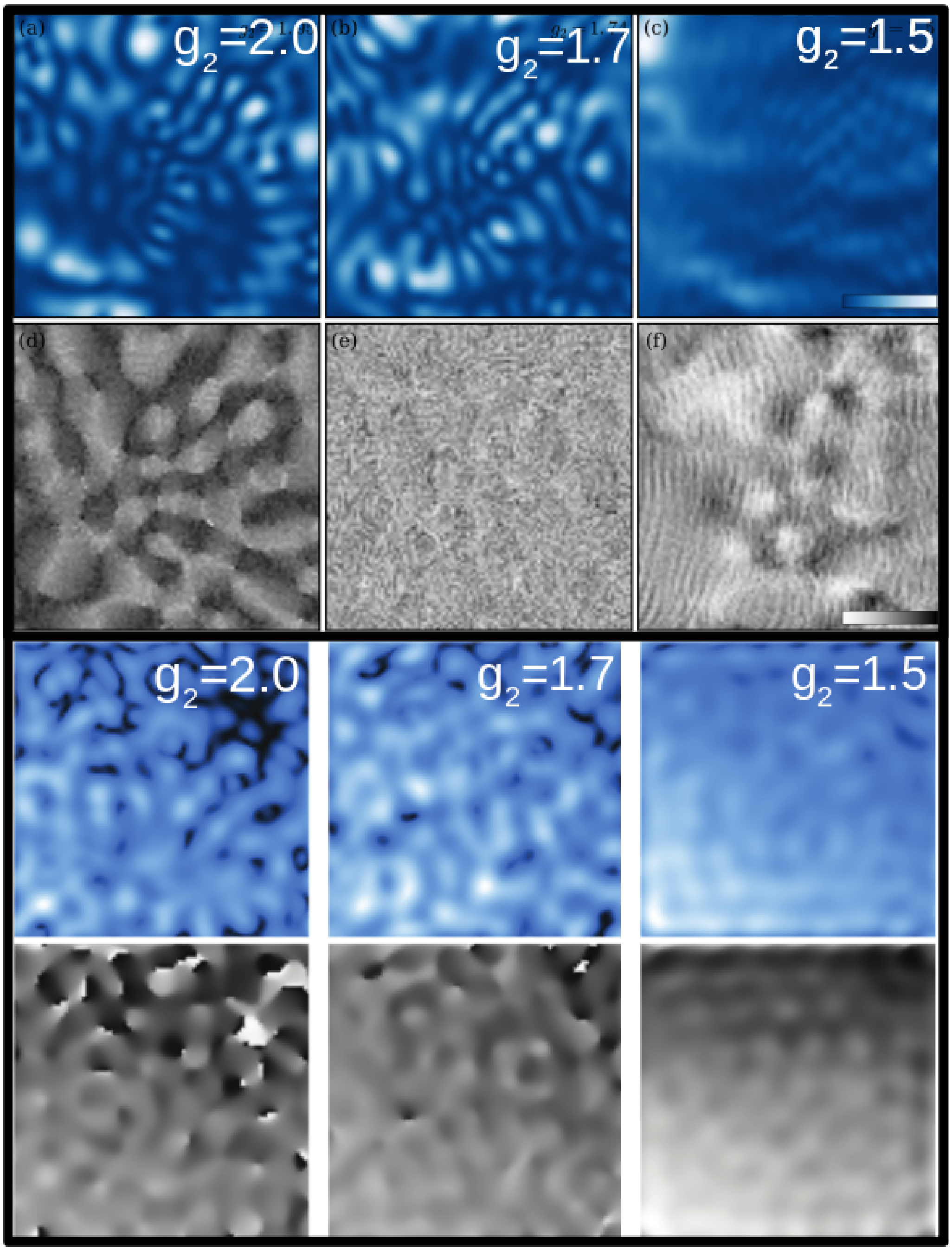

Fig. 4.1 Top two rows: Numerically simulated time-averaged amplitude (bluescale) and phase (greyscale) of a polariton condensate pumped by a single Gaussian spot (outside the image frame, to the left) in the presence of a disordered potential. Lower two rows: corresponding experimental images. Each column represents the result of a different pump strength, which increase to the right. The numerical frames show the time averaged states which were stationary ($g^{(2)}$=2.0), nonstationary ($g^{(2)}$=1.7), and turbulent ($g^{(2)}$=1.5), which had second-order correlations consistent with the experimental images. Experimental images courtesy of Dr. Daniele Sanvitto and the Advanced Photonics Lab, Lecce, Italy.

shown for several pump intensities in Fig. 4.1. As in our numerical results, we see that as the pump strength is increased, the time-averaged images become blurrier and blurrier, as would be expected given increased motion: disordered motions should "average out" in the integrated image, while stationary disorder should remain sharply disordered. To quantify this we introduce the correlation function $g_2 = \langle|\psi|^4\rangle/\langle|\psi|^2\rangle^2$. This function, borrowed from quantum optics, represents a measurement of the relative order of a complex wavefunction. For a very disordered system, the function approaches $g^{(2)} = 2$, while for a uniform wavefunction it approaches $g^{(2)} = 1$. Measuring $g^{(2)}$ of the intrinsically time-averaged experimental data and of the explicitly time-averaged numerical simulations, we see a strong quantitative match, as shown in Figs. 4.1, with an inverse dependence of $g^{(2)}$ on pump intensity.

This dependence, again, comes from the high degree of spatial disorder in *stationary* state (left column): in the case of low pump strength, states are stationary and thus time-averaged images fully resolve that disorder, resulting in a high value of $g^{(2)}$. As the pump strength increases and vortices become nonstationary and eventually turbulent, the time-averaged images become blurrier and more uniform, resulting in lower values of $g^{(2)}$. As expected, the value of $g^{(2)}$ remains high when calculated for non-time-averaged numerical data, for all pump strengths.

While our numerical modelling has demonstrated that the Lecce experiment is *consistent* with representing a transition to turbulence, it does not prove the existence of any such transition. However, with current experimental apparatuses, there is simply no way to *directly* observe turbulence, so all we may hope for is a signature. This will be discussed again at the end of this chapter.

4.3 Generating Turbulence without Extrinsic Disorder

Again, there are many ways one might approach the generation of a turbulent state in a polariton condensate. Very recently a numerical study considered the generation of turbulence in polariton condensates using "spoon stirring" with a laser, or with many stirrers obeys Brownian motion [150]. This is not dissimilar in approach to the system of [52], where the flows past physical inhomogeneities in the sample are relied upon for the nucleation of vorticity - this is still essentially nuleation via flow past external obstacle - with the disorder imposed externally. However, such proposals are quite complicated, in that it requires external drivers of turbulence with their own particularities. Moreover, these approaches squander the ability of polariton condensates to exhibit *self-driving* turbulence, a property I will demonstrate now.

We will do this by first introducing our pumping geometry, which actually matches that of the experiment of [52], which did not observe signs of turbulence, except for one key difference: unlike that experiment which required sample disorder to nucleate and trap vortices, we will consider the more general scenario of a uniform sample. We thus consider the system pumped nonresonantly by four Gaussian pump spots arranged in an even grid, with the distance between nearest pump spots denoted as d. With such a setup, our degrees of freedom are the pump strengths, and the pump spot distance d (for simplicity we will say that the spots are pumped evenly, and we will fix their Gaussian width as that variable turns out to be redundant). We thus perform numerical experiments for various choices of these variables, and again find that for suitably high pump strength turbulent states are generated. An example of such a state is shown in Fig. 4.2, which shows a snapshot of the condensate density (in the plane), and also shows

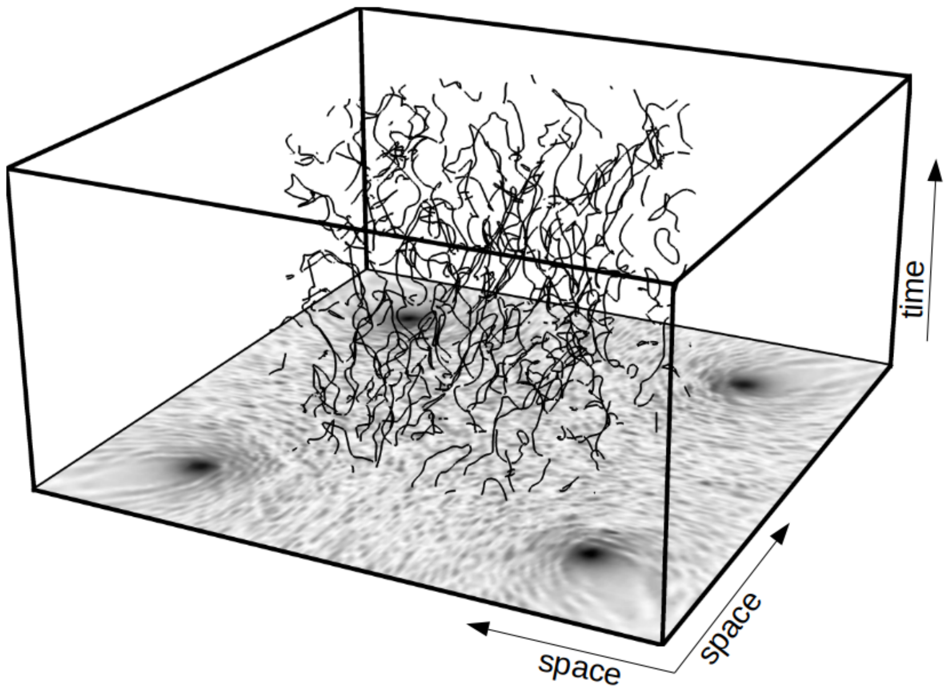

Fig. 4.2 A visual representation of a 2D nonconservative quantum turbulence. In the plane, the densities of the BEC at a snapshot in time are plotted; the turbulence is initiated and sustained from the flow of particles from the four pump spots with grid spacing $50\mu m$ (dark spots). The black lines represent the paths of central vortex points over time (out of plane axis). Both the in and out-of-plane structures are the results of direct numerical simulations, but do not match in scale.

the paths of vortices over the time evolution of the condensate (out of the plane). Vortex paths are determined by marking the intersections of real and imaginary zero-crossing lines at each time-slice. Paths of individual vortices are separately marked by a depth-first search of nearest-neighbor vortices in consecutive time frames, where which the vortex line is determined to start/end when there is not a correspondingly close neighbor in the preceding/proceeding frame.

4.4 Strong and Weak Regimes

So far we have demonstrated that polariton condensates can self-generate sustained turbulence without requiring the explicitly imposed disorder of a randomly structured sample. This is itself not really new, having been demonstrated already (though for a simpler model) more than a decade ago in the unpublished preprint of Berloff [151]. However, we have set out to demonstrate something more interesting: that depending on the pump geometry, we can observe not only superfluid turbulence, but also strong and weak turbulence.

Thus we need to quantify the concentration of vorticity in our system. It is possible to mark the locations of vortices throughout the computed wavefunction at each timestep, which can be done precisely by finding the intersections of the real and imaginary zero-surfaces. In this way, the vortex number density can be determined. However, it is important to note that achieving strong or weak turbulence is not quite as conceptually simple as increasing the pump strength: doing so *does* increase the number of vortices seen, but also increases the background condensate density and correspondingly shortens the healing length. As the regimes of interest are defined relative to that lengthscale, this strategy is fruitless.

Instead, we will opt for what I will contend is the *second* most intuitive strategy: increasing the pump spot separation. The intuition behind this is as follows: as the pump spots are separated further, the density of interference fringes arising from their interacting particle fluxes increases relative to the density of the condensate (more fringes, less condensate). The regular grid of density zeros associated with the four-wave interference pattern are necessarily vortices, arranged in an unstable lattice. Obviously keeping the pump strength constant while increasing the area of inward particle fluxes results in a lower condensate density in that region.

This idea is confirmed with direct numerical simulation, from which we measure the vortex density (vortices per square healing length unit cell) of the turbulent flow for different distances between pump and potential (with healing length measured separately for each separation difference). The result is shown in Fig. 4.3. As expected, as the distance increases between the pump spots and the region of interest, the average number of vortices found per healing length

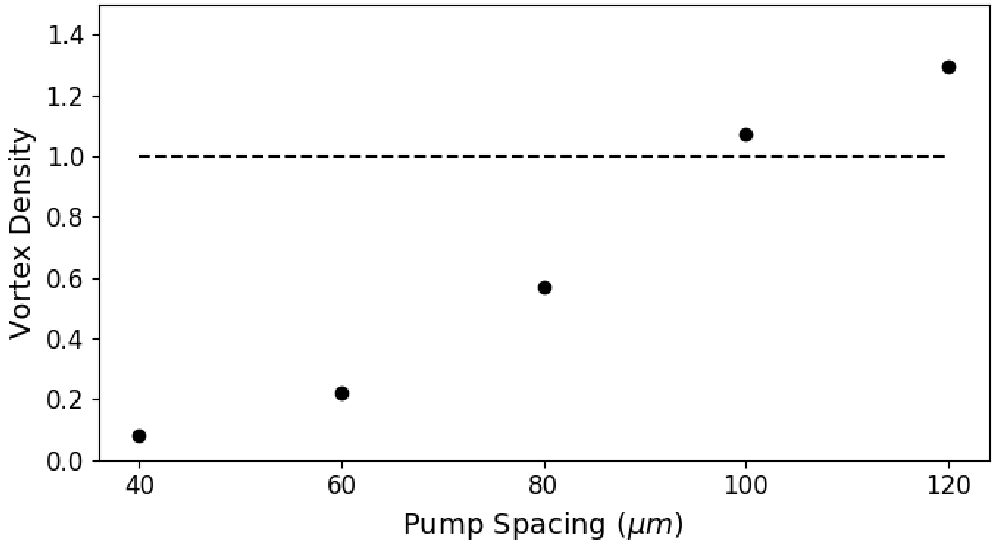

Fig. 4.3 Vortex density, scaled nondimensionally as the vortices per square healing length unit-cell, plotted several distances between pump spots and the disordered potential (where the vortex densities are sampled). As this distance increases, the vortex density increases. The range of vortex densities shown here represents a transition from superfluid (vortex density<1) to strong (≈ 1) to weak (>1) turbulent states as this distance is increased.

increases. This shows directly that our system exhibits a smooth transition between regimes of quantum turbulence, here showing such a transition from superfluid turbulence (vortex density<1) through the strong turbulent state (vortex density ≈ 1), and into the regime of weak turbulence (vortex density>1). Fig. 4.4 shows corresponding snapshots of density and phase for turbulent states formed with different distances between the four pump spots. It shows clearly that as the lattice spacing increases from left to right, so does the absolute vortex density. Of course as the pump spots are moved apart the wavefunction density in the central region also decreases, which increases the healing length.

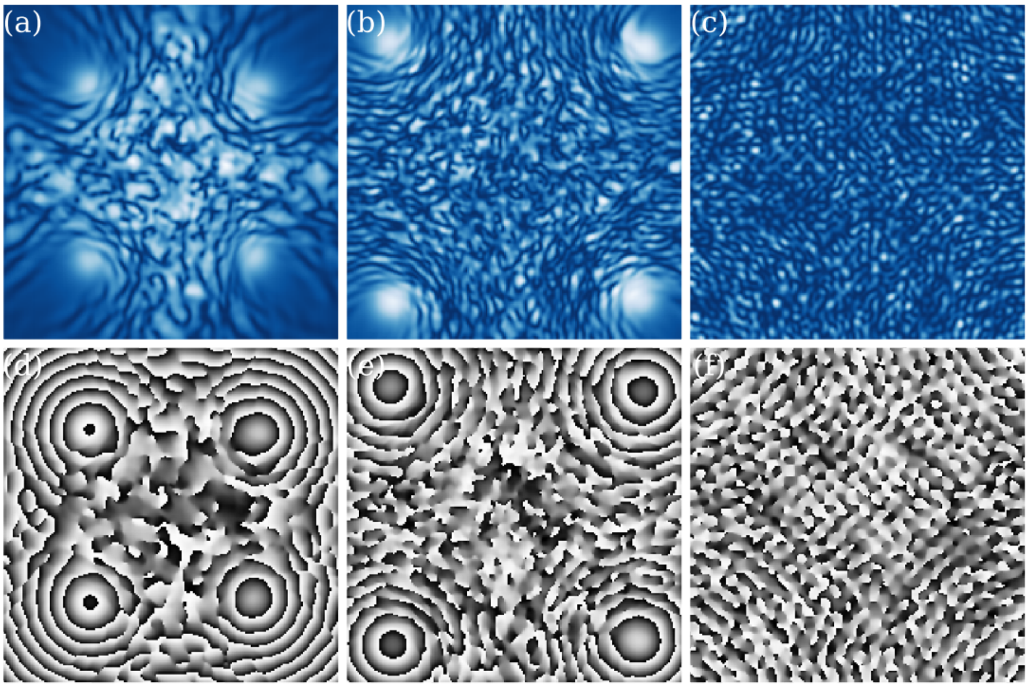

Fig. 4.4 Density (bluescale) and phase (greyscale) snapshots (top) of simulated polariton turbulence, formed by the four-spot system. From left to right, the distance between pump spots increases (the spots are out of the frame in the far right column). The bottom rows show time-averaged images of the same simulations. The time averaged phase images show order on finer and finer length scales as the vortex density increases (left to right). From left to right, inter-pump distances d are $40\mu m$, $60\mu m$, and $100\mu m$.

4.5 Turbulent Structure

Wavenumber Spectra

To better understand the nature of the turbulence that we observe, we calculate the wavenumber spectra of these states. The spectra of turbulent states with varying vortex density are shown in Fig. 4.5. From that figure it is clear that the spectra shown are all nearly identical and fit a k^{-3} dependence. In two-dimensional equilibrium Bose-Einstein condensates, this dependence is associated with *acoustic* turbulence, which was derived from the assumption of weakly nonlinear random excitations, and is conceptually similar to weak turbulence [152]. It is not clear why the polaritonic turbulence appears to fit to this spectrum regardless of vortex density. Regardless, the spectrum does not survive the time-averaging process; we find that the spectra of time-averaged data no longer fits to k^{-3} (dashed), but rather fits to k^{-2} which is consistent with the (necessarily time-averaged) Lecce data, although the reason for this particular relationship is not immediately clear.

Fractality

The study of random laser scatter has revealed that the vortices which naturally appear in such fields trace out complicated paths through the propagation axis, and have fractal dimension $d = 2$ (matching that of paths characteristic of Brownian motion) [153]. Representing a completely linear random wave limit, the optical scatter in a sense represents a "weaker than weak turbulence", and might thus help us understand how vortex propagation lines are to be structured when nonlinearity is not a dominating component of their dynamics (as would be consistent with the acoustic-like wavenumber spectrum).

Taking time as our propagation axis, we track the vortex lines from our direct numerical simulations of polaritonic turbulence, algorithmically separating indi-

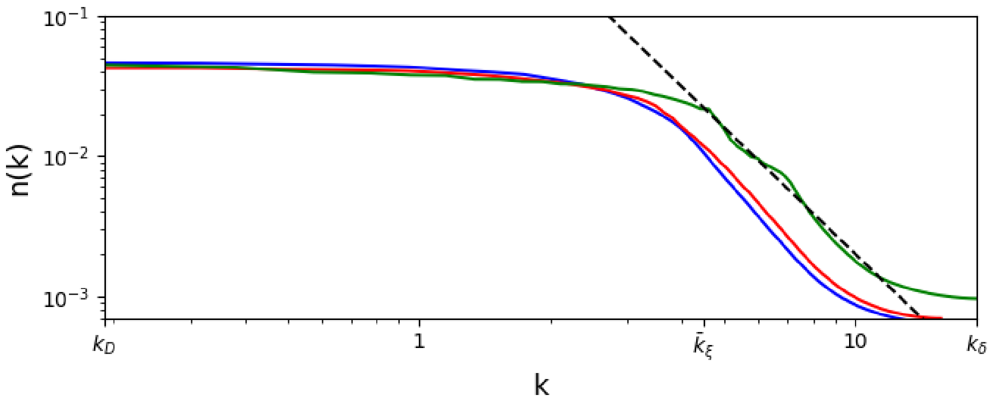

Fig. 4.5 Wavenumber spectrum of the fully time-resolved turbulent states, plotted along with k^{-3} (dashed). States correspond to those in Fig. 4.4, with pump spacings of $40\mu m$ (blue), $60\mu m$ (red), and $100\mu m$ (green). Marked are the wavenumbers $k_D = 2\pi/D$ (where D is the size of the studied area), $k_\delta = 2\pi/\delta$ (where δ is the mesh size), and $\bar{k}_\xi = 2\pi/\xi$, which is the wavenumber corresponding to the average healing length. Not shown are the wavenumbers k_ℓ, which correspond to the typical intervortex lengthscale. These are 1.1, 2.6, and 5.9 for each plotted spectrum, respectively. In other two-dimensional quantum turbulent systems this spectral dependence is associated with what is known as acoustic turbulence [152].

vidual vortex lines from each other and analyzed. In this setup, the line structure represents more than a snapshot of the condensate structure, but rather includes the entire dynamics: any fractality of such a line, as in the paths of Brownian particles, encodes information about how the velocity of the vortex changes over time and in space.

The fractal dimension is at its most fundamental a measure of complexity, and a system described by a single fractal dimension over a range of length scales can formally said to be self similarly complicated over those length scales. There are many definitions of the fractal dimension (Hausdorff, packing, box-counting, etc), but we will use that of Mandelbrot in his treatment of random walks, in which the fractal dimension $d = log(N)/log(L)$, where N and L are the path integrated and Pythagorean distances between points along the path, respectively [154].

What is found is that regardless of vortex density, the vortex lines in our simulations are self similar with fractal dimension $d \approx 2$ for lower lengthscales. Fig.

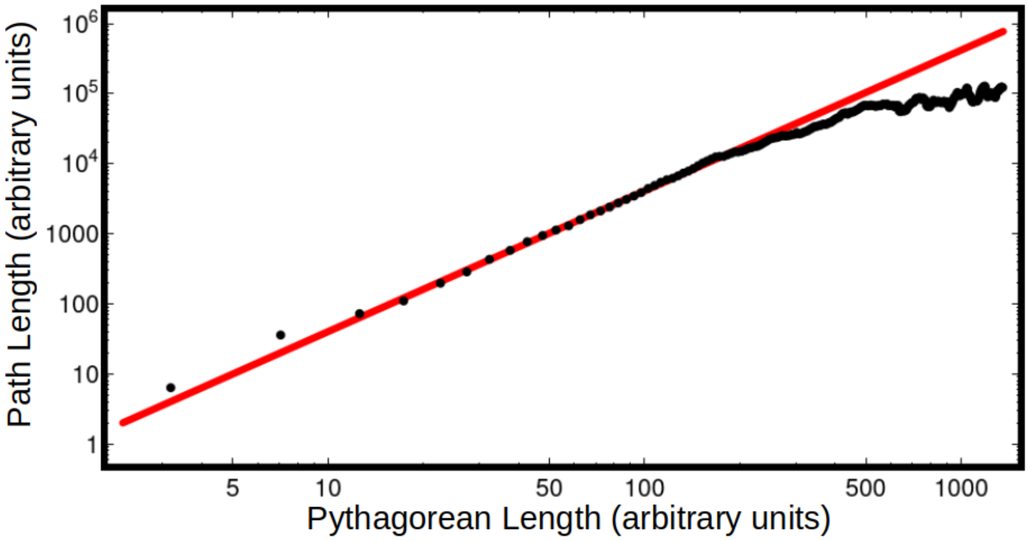

Fig. 4.6 Path integrated distance vs point-to-point distance between points along many vortex paths from a direct numerical simulation of quantum turbulence in the superfluid regime (corresponding to spot separation $40\mu m$ in Fig. 4.4). In this space, linearity indicates self similarity, and the slope indicates the fractal dimension: that corresponding to $d = 2$ is shown in red. The dropoff of fractal dimension at higher lengthscales is thought to come from the effects of the maximum system lengthscale: the turbulence is only approximately isotropic at lengthscales smaller than that of the pump lattice.

4.6 shows the vortex line path distance as a function of Pythagorean distance for a characteristic simulation of polaritonic turbulence in the regime of well separated vortices. Thus at least at lower lengthscales, the fractal structure is consistent with that of vortex lines propagating in a linear random wave system. Combined with the finding that our simulations yield wavenumber spectra consistent with that of weakly nonlinear random wave (acoustic) turbulence, it appears that our numerical probes consistently suggest that the turbulent states we are probing, regardless of vortex density, are surprisingly similar in structure to weakly nonlinear disordered systems.

4.6 Closing Remarks

This chapter has discussed the topic of polaritonic turbulence, a subject about which very little is understood; in this chapter I have reported on new ideas, but have admittedly not come to any clear conclusions. In the first part of the chapter I discussed the possibility that the Lecce group has already observed the signatures of polaritonic turbulence. However, while I showed that their results are *consistent* with turbulent states, there was no smoking gun. One possibility I have proposed is to look for the scars of rogue waves (rare non-Gaussian amplitude spikes) which are associated with turbulence in nonlinear-Schrodinger type equations. Due to their non-Gaussian statistics, these would appear as heavier-than-Gaussian tails (kurtosis higher than three) in the amplitude distributions of the time integrated data. Early data from the Lecce group appears to find this sudden change in the tail-heaviness, and is being probed further. As for developing an understanding of the structure of polaritonic turbulence, we simply need further study. My work here has been entirely numerical, and this has been useful to gain some intuition as to what is going on. However, an analytical theory of polaritonic turbulence is clearly as necessary as it is difficult to realize.

Chapter 5

Conclusion

Over the course of this work, we have investigated the fundamental dynamics of nonconservative quantum fluids, composed of condensed exciton-polariton quasiparticles. In doing so, we have demonstrated how fundamentally distinct the behaviours of such systems are from their equilibrium counterparts. Equilibrium condensates do not allow for spatially localized breathers or for stable vortices of higher-than-unit topological charge, yet here we have shown that in the nonconservative condensate both structures emerge naturally. Clearly, the structural and dynamical limitations of equilibrium systems no longer apply far from equilibrium, but the ways in which this manifests itself is not always so clear; beyond introducing and probing new quantum hydrodynamical structures, a main result of this thesis is simply that the hydrodynamics of nonconservative quantum fluids are quite far from being fully understood. In this thesis I have looked for some of the *most* fundamental structures, - vortices and the fundamental excitations of dual-forcing - but surely more interesting structures remain undiscovered. Thus while I conclude this thesis with many questions remaining, knowing that even the structures discussed here are in possession of more secrets to yield, my hope is that this work provides a sense of intuition and direction which helps, in some small way, to orient this new field of nonconservative quantum hydrodynamics towards a deeper and more coherent understanding.

References

[1] Immanuel Bloch, Jean Dalibard, and Sylvain Nascimbene. Quantum simulations with ultracold quantum gases. *Nature Physics*, 8(4):267, 2012.

[2] Jeff Steinhauer. Observation of self-amplifying Hawking radiation in an analogue black-hole laser. *Nature Physics*, 10(11):864, 2014.

[3] Samuel N Alperin and Natalia G Berloff. Formation and dynamics of quantum hydrodynamical breathing-ring solitons. *Physical Review A*, 102 (3):031304, 2020.

[4] Samuel N Alperin and Natalia G Berloff. Emergence and ordering of polygonal breathers in polariton condensates. *arXiv preprint arXiv:2105.04439*, 2021.

[5] Samuel N Alperin and Natalia G Berloff. Multiply charged vortex states of polariton condensates. *Optica*, 8(3):301–307, 2021.

[6] Christopher J Pethick and Henrik Smith. *Bose–Einstein condensation in dilute gases*. Cambridge university press, 2008.

[7] Elliott H Lieb, Robert Seiringer, and Jakob Yngvason. Bosons in a trap: A rigorous derivation of the Gross-Pitaevskii energy functional. In *The Stability of Matter: From Atoms to Stars*, pages 685–697. Springer, 2001.

[8] Anthony J Leggett. Bec: The alkali gases from the perspective of research on liquid helium. In *AIP Conference Proceedings*, volume 477, pages 154–169. American Institute of Physics, 1999.

[9] Brian J Cantwell. *Introduction to symmetry analysis*. Cambridge university press, 2002.

[10] Toshio Tsuzuki. Nonlinear waves in the pitaevskii-gross equation. *Journal of Low Temperature Physics*, 4(4):441–457, 1971.

[11] PO Fedichev and GV Shlyapnikov. Dissipative dynamics of a vortex state in a trapped Bose-condensed gas. *Physical Review A*, 60(3):R1779, 1999.

[12] Lauren M Aycock, Hilary M Hurst, Dmitry K Efimkin, Dina Genkina, Hsin-I Lu, Victor M Galitski, and IB Spielman. Brownian motion of solitons in a bose–einstein condensate. *Proceedings of the National Academy of Sciences*, 114(10):2503–2508, 2017.

[13] Th Busch and JR Anglin. Motion of dark solitons in trapped Bose-Einstein condensates. *Physical Review Letters*, 84(11):2298, 2000.

[14] G Theocharis, DJ Frantzeskakis, PG Kevrekidis, Boris A Malomed, and Yuri S Kivshar. Ring dark solitons and vortex necklaces in Bose-Einstein condensates. *Physical Review Letters*, 90(12):120403, 2003.

[15] Paul H Roberts and Natalia G Berloff. The nonlinear schrödinger equation as a model of superfluidity. In *Quantized vortex dynamics and superfluid turbulence*, pages 235–257. Springer, 2001.

[16] Natalia G Berloff. Padé approximations of solitary wave solutions of the Gross–Pitaevskii equation. *Journal of Physics A: Mathematical and General*, 37(5):1617, 2004.

[17] Lev Pitaevskii and Sandro Stringari. *bose-Einstein condensation and superfluidity*, volume 164. Oxford University Press, 2016.

[18] Len M Pismen and Len M Pismen. *Vortices in nonlinear fields: from liquid crystals to superfluids, from non-equilibrium patterns to cosmic strings*, volume 100. Oxford University Press, 1999.

[19] S Inouye, S Gupta, T Rosenband, AP Chikkatur, A Görlitz, TL Gustavson, AE Leanhardt, DE Pritchard, and W Ketterle. Observation of vortex phase singularities in Bose-Einstein condensates. *Physical Review Letters*, 87(8): 080402, 2001.

[20] Yong-il Shin, Michele Saba, Mukund Vengalattore, TA Pasquini, Christian Sanner, AE Leanhardt, Mara Prentiss, DE Pritchard, and Wolfgang Ketterle. Dynamical instability of a doubly quantized vortex in a Bose-Einstein condensate. *Physical Review Letters*, 93(16):160406, 2004.

[21] Peter Engels, I Coddington, PC Haljan, Volker Schweikhard, and Eric A Cornell. Observation of long-lived vortex aggregates in rapidly rotating Bose-Einstein condensates. *Physical Review Letters*, 90(17):170405, 2003.

[22] Jamil R Abo-Shaeer, Chandra Raman, Johnny M Vogels, and Wolfgang Ketterle. Observation of vortex lattices in Bose-Einstein condensates. *Science*, 292(5516):476–479, 2001.

[23] Uwe R Fischer and Gordon Baym. Vortex states of rapidly rotating dilute Bose-Einstein condensates. *Physical Review Letters*, 90(14):140402, 2003.

[24] Alexander L Fetter, B Jackson, and S Stringari. Rapid rotation of a Bose-Einstein condensate in a harmonic plus quartic trap. *Physical Review A*, 71 (1):013605, 2005.

[25] Guillaume Gauthier, Matthew T Reeves, Xiaoquan Yu, Ashton S Bradley, Mark A Baker, Thomas A Bell, Halina Rubinsztein-Dunlop, Matthew J Davis, and Tyler W Neely. Giant vortex clusters in a two-dimensional quantum fluid. *Science*, 364(6447):1264–1267, 2019.

[26] Peter Engels, Collin Atherton, and MA Hoefer. Observation of faraday waves in a Bose-Einstein condensate. *Physical Review Letters*, 98(9): 095301, 2007.

[27] Kenichi Kasamatsu, Makoto Tsubota, and Masahito Ueda. Giant hole and circular superflow in a fast rotating Bose-Einstein condensate. *Physical Review A*, 66(5):053606, 2002.

[28] Amandine Aftalion and Ionut Danaila. Giant vortices in combined harmonic and quartic traps. *Physical Review A*, 69(3):033608, 2004.

[29] Alexander L Fetter. Rotating trapped Bose-Einstein condensates. *Reviews of Modern Physics*, 81(2):647, 2009.

[30] Vincent Bretin, Sabine Stock, Yannick Seurin, and Jean Dalibard. Fast rotation of a Bose-Einstein condensate. *Physical Review Letters*, 92(5): 050403, 2004.

[31] Marco Cozzini, B Jackson, and S Stringari. Vortex signatures in annular Bose-Einstein condensates. *Physical Review A*, 73(1):013603, 2006.

[32] Raphaël Saint-Jalm, Patricia CM Castilho, Édouard Le Cerf, Brice Bakkali-Hassani, J-L Ville, Sylvain Nascimbene, Jérôme Beugnon, and Jean Dalibard. Dynamical symmetry and breathers in a two-dimensional Bose gas. *Physical Review X*, 9(2):021035, 2019.

[33] Jeff Steinhauer. Observation of quantum Hawking radiation and its entanglement in an analogue black hole. *Nature Physics*, 12(10):959–965, 2016.

[34] Michael D Fraser. Coherent exciton-polariton devices. *Semiconductor Science and Technology*, 32(9):093003, 2017.

[35] M Gurioli, F Bogani, L Cavigli, H Gibbs, Galina Khitrova, and DS Wiersma. Weak localization of light in a disordered microcavity. *Physical Review Letters*, 94(18):183901, 2005.

[36] David Snoke and Peter Littlewood. Polariton condensates. *Physics Today*, 63(8):42–47, 2010.

[37] Tim Byrnes, Na Young Kim, and Yoshihisa Yamamoto. Exciton–polariton condensates. *Nature Physics*, 10(11):803–813, 2014.

[38] Hui Deng, Glenn S Solomon, Rudolf Hey, Klaus H Ploog, and Yoshihisa Yamamoto. Spatial coherence of a polariton condensate. *Physical Review Letters*, 99(12):126403, 2007.

[39] Hamid Ohadi, Y del Valle-Inclan Redondo, A Dreismann, YG Rubo, F Pinsker, SI Tsintzos, Z Hatzopoulos, PG Savvidis, and JJ Baumberg. Tunable magnetic alignment between trapped exciton-polariton condensates. *Physical Review Letters*, 116(10):106403, 2016.

[40] Jacek Kasprzak, M Richard, S Kundermann, A Baas, P Jeambrun, JMJ Keeling, FM Marchetti, MH Szymańska, R André, JL Staehli, et al. Bose–Einstein condensation of exciton polaritons. *Nature*, 443(7110):409, 2006.

[41] N David Mermin and Herbert Wagner. Absence of ferromagnetism or antiferromagnetism in one-or two-dimensional isotropic heisenberg models. *Physical Review Letters*, 17(22):1133, 1966.

[42] Pierre C Hohenberg. Existence of long-range order in one and two dimensions. *Physical Review*, 158(2):383, 1967.

[43] Sidney Coleman. There are no goldstone bosons in two dimensions. *Communications in Mathematical Physics*, 31(4):259–264, 1973.

[44] Anna Posazhennikova. Colloquium: Weakly interacting, dilute Bose gases in 2d. *Reviews of modern physics*, 78(4):1111, 2006.

[45] Jonathan Keeling and Natalia G Berloff. Spontaneous rotating vortex lattices in a pumped decaying condensate. *Physical Review Letters*, 100 (25):250401, 2008.

[46] NG Berloff and J Keeling. Universality in modelling non-equilibrium pattern formation in polariton condensates. In *Physics of Quantum Fluids*, pages 19–38. Springer, 2013.

[47] Iacopo Carusotto and Cristiano Ciuti. Quantum fluids of light. *Reviews of Modern Physics*, 85(1):299, 2013.

[48] David W Snoke and Jonathan Keeling. The new era of polariton condensates. *Phys. Today*, 70(10):54–60, 2017.

[49] Konstantinos G Lagoudakis, Francesco Manni, Barbara Pietka, Michiel Wouters, Timothy Chi Hin Liew, Vincenzo Savona, Alexey V Kavokin, Régis André, and Benoit Deveaud-Plédran. Probing the dynamics of spontaneous quantum vortices in polariton superfluids. *Physical Review Letters*, 106(11):115301, 2011.

[50] Iacopo Carusotto. Sorting superfluidity from bose-Einstein condensation in atomic gases. *Physics*, 3:5, 2010.

[51] Anthony J Leggett. Superfluidity. *Reviews of Modern Physics*, 71(2):S318, 1999.

[52] Konstantinos G Lagoudakis, Michiel Wouters, Maxime Richard, Augustin Baas, Iacopo Carusotto, Regis André, Le Si Dang, and B Deveaud-Plédran. Quantized vortices in an exciton–polariton condensate. *Nature Physics*, 4 (9):706, 2008.

[53] A Amo, D Sanvitto, FP Laussy, D Ballarini, E Del Valle, MD Martin, A Lemaitre, J Bloch, DN Krizhanovskii, MS Skolnick, et al. Collective fluid dynamics of a polariton condensate in a semiconductor microcavity. *Nature*, 457(7227):291–295, 2009.

[54] S Utsunomiya, L Tian, G Roumpos, CW Lai, N Kumada, T Fujisawa, M Kuwata-Gonokami, A Löffler, S Höfling, A Forchel, et al. Observation of Bogoliubov excitations in exciton-polariton condensates. *Nature Physics*, 4(9):700–705, 2008.

[55] Iacopo Carusotto and Cristiano Ciuti. Probing microcavity polariton superfluidity through resonant rayleigh scattering. *Physical Review Letters*, 93 (16):166401, 2004.

[56] Alberto Amo, Jérôme Lefrère, Simon Pigeon, Claire Adrados, Cristiano Ciuti, Iacopo Carusotto, Romuald Houdré, Elisabeth Giacobino, and Alberto Bramati. Superfluidity of polaritons in semiconductor microcavities. *Nature Physics*, 5(11):805–810, 2009.

[57] Alberto Amo, S Pigeon, D Sanvitto, VG Sala, R Hivet, Iacopo Carusotto, F Pisanello, G Leménager, R Houdré, E Giacobino, et al. Polariton superfluids reveal quantum hydrodynamic solitons. *Science*, 332(6034):1167–1170, 2011.

[58] Giovanni Lerario, Antonio Fieramosca, Fábio Barachati, Dario Ballarini, Konstantinos S Daskalakis, Lorenzo Dominici, Milena De Giorgi, Stefan A Maier, Giuseppe Gigli, Stéphane Kéna-Cohen, et al. Room-temperature superfluidity in a polariton condensate. *Nature Physics*, 13(9):837–841, 2017.

[59] F Tassone, C Piermarocchi, V Savona, A Quattropani, and P Schwendimann. Bottleneck effects in the relaxation and photoluminescence of microcavity polaritons. *Physical Review B*, 56(12):7554, 1997.

[60] MH Szymańska, J Keeling, and PB Littlewood. Nonequilibrium quantum condensation in an incoherently pumped dissipative system. *Physical Review Letters*, 96(23):230602, 2006.

[61] Stefano Giovanazzi, Augusto Smerzi, and Stefano Fantoni. Josephson effects in dilute Bose-Einstein condensates. *Physical Review Letters*, 84 (20):4521, 2000.

[62] M Wouters, TCH Liew, and V Savona. Energy relaxation in one-dimensional polariton condensates. *Physical Review B*, 82(24):245315, 2010.

[63] Michiel Wouters and Iacopo Carusotto. Excitations in a nonequilibrium Bose-Einstein condensate of exciton polaritons. *Physical Review Letters*, 99(14):140402, 2007.

[64] Kirill P Kalinin and Natalia G Berloff. Simulating ising and n-state planar potts models and external fields with nonequilibrium condensates. *Physical Review Letters*, 121(23):235302, 2018.

[65] Igor S Aranson and Lorenz Kramer. The world of the complex Ginzburg-Landau equation. *Reviews of Modern Physics*, 74(1):99, 2002.

[66] Mark C Cross and Pierre C Hohenberg. Pattern formation outside of equilibrium. *Reviews of Modern Physics*, 65(3):851, 1993.

[67] Samuel N Alperin and Mark E Siemens. Angular momentum of topologically structured darkness. *Physical Review Letters*, 119(20):203902, 2017.

[68] Victor M Perez-Garcia, Humberto Michinel, JI Cirac, M Lewenstein, and P Zoller. Dynamics of Bose-Einstein condensates: Variational solutions of the Gross-Pitaevskii equations. *Physical Review A*, 56(2):1424, 1997.

[69] Michael Robin Matthews, Brian P Anderson, PC Haljan, DS Hall, CE Wieman, and Eric A Cornell. Vortices in a Bose-Einstein condensate. *Physical Review Letters*, 83(13):2498, 1999.

[70] KW Madison, F Chevy, W Wohlleben, and Jl Dalibard. Vortex formation in a stirred Bose-Einstein condensate. *Physical Review Letters*, 84(5):806, 2000.

[71] J Denschlag, Je E Simsarian, Dl L Feder, Charles W Clark, La A Collins, J Cubizolles, Lu Deng, Edward W Hagley, Kristian Helmerson, William P Reinhardt, et al. Generating solitons by phase engineering of a Bose-Einstein condensate. *Science*, 287(5450):97–101, 2000.

[72] BP Anderson, PC Haljan, CA Regal, DL Feder, LA Collins, Charles W Clark, and Eric A Cornell. Watching dark solitons decay into vortex rings in a Bose-Einstein condensate. *Physical Review Letters*, 86(14):2926, 2001.

[73] Zachary Dutton, Michael Budde, Christopher Slowe, and Lene Vestergaard Hau. Observation of quantum shock waves created with ultra-compressed slow light pulses in a Bose-Einstein condensate. *Science*, 293(5530):663–668, 2001.

[74] AA Penckwitt, RJ Ballagh, and CW Gardiner. Nucleation, growth, and stabilization of Bose-Einstein condensate vortex lattices. *Physical Review Letters*, 89(26):260402, 2002.

[75] Oliver Morsch and Markus Oberthaler. Dynamics of Bose-Einstein condensates in optical lattices. *Reviews of Modern Physics*, 78(1):179, 2006.

[76] EAL Henn, JA Seman, G Roati, KMF Magalhaes, and VS Bagnato. Emergence of turbulence in an oscillating Bose-Einstein condensate. *Physical Review Letters*, 103(4):045301, 2009.

[77] Nir Navon, Alexander L Gaunt, Robert P Smith, and Zoran Hadzibabic. Emergence of a turbulent cascade in a quantum gas. *Nature*, 539(7627):72–75, 2016.

[78] Andrea Trombettoni and Augusto Smerzi. Discrete solitons and breathers with dilute Bose-Einstein condensates. *Physical Review Letters*, 86(11):2353, 2001.

[79] Michal Matuszewski, E Infeld, Boris A Malomed, and Marek Trippenbach. Fully three dimensional breather solitons can be created using feshbach resonances. *Physical Review Letters*, 95(5):050403, 2005.

[80] LP Pitaevskii and A Rosch. Breathing modes and hidden symmetry of trapped atoms in two dimensions. *Physical Review A*, 55(2):R853, 1997.

[81] Frédéric Chevy, Vincent Bretin, Peter Rosenbusch, KW Madison, and Jean Dalibard. Transverse breathing mode of an elongated Bose-Einstein condensate. *Physical Review Letters*, 88(25):250402, 2002.

[82] Chenwei Lv, Ren Zhang, and Qi Zhou. S u (1, 1) echoes for breathers in quantum gases. *Physical Review Letters*, 125(25):253002, 2020.

[83] Zhe-Yu Shi, Chao Gao, and Hui Zhai. Idealized hydrodynamics. *arXiv preprint arXiv:2011.01415*, 2020.

[84] Pierre Coullet and Kjartan Emilsson. Strong resonances of spatially distributed oscillators: a laboratory to study patterns and defects. *Physica D: Nonlinear Phenomena*, 61(1-4):119–131, 1992.

[85] Jonathan Keeling and Natalia G Berloff. Exciton–polariton condensation. *Contemporary Physics*, 52(2):131–151, 2011.

[86] Michiel Wouters. Energy relaxation in the mean-field description of polariton condensates. *New Journal of Physics*, 14(7):075020, 2012.

[87] Kestutis Staliunas and Victor J Sanchez-Morcillo. *Transverse patterns in nonlinear optical resonators*, volume 183. Springer Science & Business Media, 2003.

[88] Bryan Nelsen, Gangqiang Liu, Mark Steger, David W Snoke, Ryan Balili, Ken West, and Loren Pfeiffer. Dissipationless flow and sharp threshold of a polariton condensate with long lifetime. *Physical Review X*, 3(4):041015, 2013.

[89] Kirill P Kalinin and Natalia G Berloff. Polaritonic network as a paradigm for dynamics of coupled oscillators. *Physical Review B*, 100(24):245306, 2019.

[90] Natalia G Berloff, Matteo Silva, Kirill Kalinin, Alexis Askitopoulos, Julian D Töpfer, Pasquale Cilibrizzi, Wolfgang Langbein, and Pavlos G Lagoudakis. Realizing the classical xy hamiltonian in polariton simulators. *Nature Materials*, 16(11):1120, 2017.

[91] F Manni, KG Lagoudakis, Régis André, M Wouters, and B Deveaud. Penrose-Onsager criterion validation in a one-dimensional polariton condensate. *Physical Review Letters*, 109(15):150409, 2012.

[92] P Cristofolini, A Dreismann, G Christmann, G Franchetti, NG Berloff, P Tsotsis, Z Hatzopoulos, PG Savvidis, and JJ Baumberg. Optical superfluid phase transitions and trapping of polariton condensates. *Physical Review Letters*, 110(18):186403, 2013.

[93] Ch Schneider, K Winkler, MD Fraser, M Kamp, Y Yamamoto, EA Ostrovskaya, and Sven Höfling. Exciton-polariton trapping and potential landscape engineering. *Reports on Progress in Physics*, 80(1):016503, 2016.

[94] Bogdan Damski and Wojciech H Zurek. Soliton creation during a bose-einstein condensation. *Physical review letters*, 104(16):160404, 2010.

[95] Wojciech H Zurek. Cosmological experiments in condensed matter systems. *Physics Reports*, 276(4):177–221, 1996.

[96] Thomas WB Kibble. Topology of cosmic domains and strings. *Journal of Physics A: Mathematical and General*, 9(8):1387, 1976.

[97] Tom WB Kibble. Some implications of a cosmological phase transition. *Physics Reports*, 67(1):183–199, 1980.

[98] Wojciech H Zurek. Cosmological experiments in superfluid helium? *Nature*, 317(6037):505, 1985.

[99] C Bäuerle, Yu M Bunkov, SN Fisher, H Godfrin, and GR Pickett. Laboratory simulation of cosmic string formation in the early universe using superfluid 3He. *Nature*, 382(6589):332, 1996.

[100] VMH Ruutu, VB Eltsov, AJ Gill, TWB Kibble, M Krusius, Yu G Makhlin, B Placais, GE Volovik, and Wen Xu. Vortex formation in neutron-irradiated superfluid 3He as an analogue of cosmological defect formation. *Nature*, 382(6589):334, 1996.

[101] Mark J Bowick, L Chandar, Eric A Schiff, and Ajit M Srivastava. The cosmological Kibble mechanism in the laboratory: string formation in liquid crystals. *Science*, 263(5149):943–945, 1994.

[102] A Maniv, E Polturak, and G Koren. Observation of magnetic flux generated spontaneously during a rapid quench of superconducting films. *Physical Review Letters*, 91(19):197001, 2003.

[103] Natalia G Berloff and Boris V Svistunov. Scenario of strongly nonequilibrated Bose-Einstein condensation. *Physical Review A*, 66(1):013603, 2002.

[104] Chad N Weiler, Tyler W Neely, David R Scherer, Ashton S Bradley, Matthew J Davis, and Brian P Anderson. Spontaneous vortices in the formation of Bose–Einstein condensates. *Nature*, 455(7215):948, 2008.

[105] DD Solnyshkov, AV Nalitov, and G Malpuech. Kibble-Zurek mechanism in topologically nontrivial zigzag chains of polariton micropillars. *Physical Review Letters*, 116(4):046402, 2016.

[106] Paul M Chesler, Antonio M García-García, and Hong Liu. Defect formation beyond Kibble-Zurek mechanism and holography. *Physical Review X*, 5(2): 021015, 2015.

[107] Adolfo Del Campo. Universal statistics of topological defects formed in a quantum phase transition. *Physical review letters*, 121(20):200601, 2018.

[108] Joachim Brand and William P Reinhardt. Solitonic vortices and the fundamental modes of the “snake instability”: Possibility of observation in the gaseous bose-einstein condensate. *Physical Review A*, 65(4):043612, 2002.

[109] LD Carr and Charles W Clark. Vortices and ring solitons in Bose-Einstein condensates. *Physical Review A*, 74(4):043613, 2006.

[110] Richard P Feynman. Chapter II application of quantum mechanics to liquid helium. In *Progress in low temperature physics*, volume 1, pages 17–53. Elsevier, 1955.

[111] Mário Novello, Matt Visser, and Grigory E Volovik. *Artificial black holes*. World Scientific, 2002.

[112] Jan Klaers, Julian Schmitt, Frank Vewinger, and Martin Weitz. Bose–Einstein condensation of photons in an optical microcavity. *Nature*, 468 (7323):545, 2010.

[113] VE Demidov, O Dzyapko, SO Demokritov, GA Melkov, and AN Slavin. Observation of spontaneous coherence in Bose-Einstein condensate of magnons. *Physical Review Letters*, 100(4):047205, 2008.

[114] P Nowik-Boltyk, O Dzyapko, VE Demidov, NG Berloff, and SO Demokritov. Spatially non-uniform ground state and quantized vortices in a two-component Bose-Einstein condensate of magnons. *Scientific Reports*, 2: 482, 2012.

[115] Len M Pismen. *Patterns and interfaces in dissipative dynamics*. Springer Science & Business Media, 2006.

[116] Kirill Kalinin, Matteo Silva, Julian D Töpfer, Wolfgang Langbein, Natalia G Berloff, and Pavlos G Lagoudakis. Giant vortices of controlled multiplicity in polariton lattices. *arXiv preprint arXiv:1710.03451*, 2017.

[117] Robert Dall, Michael D Fraser, Anton S Desyatnikov, Guangyao Li, Sebastian Brodbeck, Martin Kamp, Christian Schneider, Sven Höfling, and Elena A Ostrovskaya. Creation of orbital angular momentum states with chiral polaritonic lenses. *Physical Review Letters*, 113(20):200404, 2014.

[118] DD Solnyshkov, C Leblanc, SV Koniakhin, O Bleu, and G Malpuech. Quantum analogue of a Kerr black hole and the Penrose effect in a Bose-Einstein condensate. *Physical Review B*, 99(21):214511, 2019.

[119] Min-Sik Kwon, Byoung Yong Oh, Su-Hyun Gong, Je-Hyung Kim, Hang Kyu Kang, Sooseok Kang, Jin Dong Song, Hyoungsoon Choi, and Yong-Hoon Cho. Direct transfer of light's orbital angular momentum onto a nonresonantly excited polariton superfluid. *Physical Review Letters*, 122 (4):045302, 2019.

[120] VA Lukoshkin, VK Kalevich, MM Afanasiev, KV Kavokin, Z Hatzopoulos, PG Savvidis, ES Sedov, and AV Kavokin. Persistent circular currents of exciton-polaritons in cylindrical pillar microcavities. *Physical Review B*, 97(19):195149, 2018.

[121] F Manni, Timothy Chi Hin Liew, KG Lagoudakis, C Ouellet-Plamondon, Régis André, V Savona, and B Deveaud. Spontaneous self-ordered states of vortex-antivortex pairs in a polariton condensate. *Physical Review B*, 88 (20):201303, 2013.

[122] A Askitopoulos, H Ohadi, AV Kavokin, Z Hatzopoulos, PG Savvidis, and PG Lagoudakis. Polariton condensation in an optically induced two-dimensional potential. *Physical Review B*, 88(4):041308, 2013.

[123] Alexey V Yulin, Anton S Desyatnikov, and Elena A Ostrovskaya. Spontaneous formation and synchronization of vortex modes in optically induced traps for exciton-polariton condensates. *Physical Review B*, 94(13):134310, 2016.

[124] Yongbao Sun, Patrick Wen, Yoseob Yoon, Gangqiang Liu, Mark Steger, Loren N Pfeiffer, Ken West, David W Snoke, and Keith A Nelson. Bose-Einstein condensation of long-lifetime polaritons in thermal equilibrium. *Physical Review Letters*, 118(1):016602, 2017.

[125] Alexis Askitopoulos, Kirill Kalinin, Timothy Chi Hin Liew, Pasquale Cilibrizzi, Zacharias Hatzopoulos, Pavlos G Savvidis, Natalia G Berloff, and Pavlos G Lagoudakis. Nonresonant optical control of a spinor polariton condensate. *Physical Review B*, 93(20):205307, 2016.

[126] Lucy Pickup, Kirill Kalinin, A Askitopoulos, Zacharias Hatzopoulos, PG Savvidis, Natalia G Berloff, and PG Lagoudakis. Optical bistability under nonresonant excitation in spinor polariton condensates. *Physical Review Letters*, 120(22):225301, 2018.

[127] Sergey Alyatkin, Julian D Töpfer, Alexis Askitopoulos, Helgi Sigurdsson, and Pavlos G Lagoudakis. Optical control of synchronous phases in a programmable polariton cell. *arXiv preprint arXiv:1907.08580*, 2019.

[128] Panayotis G Kevrekidis, Dimitri J Frantzeskakis, and Ricardo Carretero-González. *Emergent nonlinear phenomena in Bose-Einstein condensates: theory and experiment*, volume 45. Springer Science & Business Media, 2007.

[129] Natalia G Berloff and Carlo F Barenghi. Vortex nucleation by collapsing bubbles in Bose-Einstein condensates. *Physical Review Letters*, 93(9): 090401, 2004.

[130] Vladimir N Gladilin and Michiel Wouters. Multivortex states and dynamics in nonequilibrium polariton condensates. *Journal of Physics A: Mathematical and Theoretical*, 52(39):395303, 2019.

[131] Vladimir N Gladilin and Michiel Wouters. Interaction and motion of vortices in nonequilibrium quantum fluids. *New Journal of Physics*, 19(10): 105005, 2017.

[132] Alexis Askitopoulos, Lucy Pickup, Sergey Alyatkin, Anton Zasedatelev, Konstantinos G Lagoudakis, Wolfgang Langbein, and Pavlos G Lagoudakis. Giant increase of temporal coherence in optically trapped polariton condensate. *arXiv preprint arXiv:1911.08981*, 2019.

[133] Yuki Kawaguchi and Tetsuo Ohmi. Splitting instability of a multiply charged vortex in a Bose-Einstein condensate. *Physical Review A*, 70(4): 043610, 2004.

[134] Natalia Berloff and Boris V Svistunov. The turbulent matter field of ultra-cold atoms. *Physics*, 2:61, 2009.

[135] Grigorii Efimovich Volovik. On the Kelvin-Helmholtz instability in superfluids. *Journal of Experimental and Theoretical Physics Letters*, 75(8): 418–422, 2002.

[136] Hiromitsu Takeuchi, Naoya Suzuki, Kenichi Kasamatsu, Hiroki Saito, and Makoto Tsubota. Quantum Kelvin-Helmholtz instability in phase-separated two-component Bose-Einstein condensates. *Physical Review B*, 81(9): 094517, 2010.

[137] Risto Hänninen and Andrew W Baggaley. Vortex filament method as a tool for computational visualization of quantum turbulence. *Proceedings of the National Academy of Sciences*, 111(Supplement 1):4667–4674, 2014.

[138] Pavel M Lushnikov and Nikolay M Zubarev. Exact solutions for nonlinear development of a Kelvin-Helmholtz instability for the counterflow of superfluid and normal components of helium ii. *Physical Review Letters*, 120 (20):204504, 2018.

[139] Th Frisch, Yves Pomeau, and Sergio Rica. Transition to dissipation in a model of superflow. *Physical Review Letters*, 69(11):1644, 1992.

[140] M Leadbeater, T Winiecki, and CS Adams. Effect of condensate depletion on the critical velocity for vortex nucleation in quantum fluids. *Journal of Physics B: Atomic, Molecular and Optical Physics*, 36(8):L143, 2003.

[141] Carlo F Barenghi, Russell J Donnelly, and WF Vinen. *Quantized vortex dynamics and superfluid turbulence*, volume 571. Springer Science & Business Media, 2001.

[142] Chen-Lung Hung, Xibo Zhang, Nathan Gemelke, and Cheng Chin. Observation of scale invariance and universality in two-dimensional Bose gases. *Nature*, 470(7333):236–239, 2011.

[143] Natalia G Berloff and Paul H Roberts. Motions in a Bose condensate: X. new results on the stability of axisymmetric solitary waves of the gross–pitaevskii equation. *Journal of Physics A: Mathematical and General*, 37 (47):11333, 2004.

[144] EA Kuznetsov and SK Turitsyn. Instability and collapse of solitons in media with a defocusing nonlinearity. *Zh. Eksp. Teor. Fiz*, 94:129, 1988.

[145] EA Kuznetsov and J Juul Rasmussen. Instability of two-dimensional solitons and vortices in defocusing media. *Physical Review E*, 51(5):4479, 1995.

[146] Naomi S Ginsberg, Joachim Brand, and Lene Vestergaard Hau. Observation of hybrid soliton vortex-ring structures in Bose-Einstein condensates. *Physical Review Retters*, 94(4):040403, 2005.

[147] Simon Pigeon, Iacopo Carusotto, and Cristiano Ciuti. Hydrodynamic nucleation of vortices and solitons in a resonantly excited polariton superfluid. *Physical Review B*, 83(14):144513, 2011.

[148] G Tosi, G Christmann, NG Berloff, P Tsotsis, Tingge Gao, Z Hatzopoulos, PG Savvidis, and JJ Baumberg. Geometrically locked vortex lattices in semiconductor quantum fluids. *Nature Communications*, 3(1):1–5, 2012.

[149] G Tosi, G Christmann, NG Berloff, P Tsotsis, T Gao, Z Hatzopoulos, PG Savvidis, and JJ Baumberg. Sculpting oscillators with light within a nonlinear quantum fluid. *Nature Physics*, 8(3):190–194, 2012.

[150] S.V. Koniakhin, O. Bleu, G. Malpuech, and D.D. Solnyshkov. 2d quantum turbulence in a polariton quantum fluid. *Chaos, Solitons Fractals*, 132:109574, 2020. ISSN 0960-0779. doi: https://doi.org/10.1016/j.chaos.2019.109574. URL https://www.sciencedirect.com/science/article/pii/S0960077919305314.

[151] Natalia G Berloff. Turbulence in exciton-polariton condensates. *arXiv preprint arXiv:1010.5225*, 2010.

[152] S Khlebnikov. Strong acoustic turbulence and the speed of Bose-Einstein condensation. *Physical Review A*, 66(6):063606, 2002.

[153] Kevin O'Holleran, Mark R Dennis, Florian Flossmann, and Miles J Padgett. Fractality of light's darkness. *Physical Review Letters*, 100(5):053902, 2008.

[154] D Stauffer, A Aharony, and BB Mandelbrot. Self-similarity and covered neighborhoods of fractals: A random walk test. *Physica A: Statistical Mechanics and its Applications*, 196(1):1–5, 1993.